TABLE OF CONTENTS

LIST OF TABLES

LIST OF FIGURES

NOTATION AND SYMBOLS

a	random function of time
a_y	lateral acceleration (right, positive), ft/sec^2
a_z	vertical acceleration (down, positive), ft/sec^2
b	wingspan, ft; also a random function of time
c	wing chord, ft; also a random function of time
C_{uu}	autocorrelation of random process $u(t)$
$\tilde{C}_{uu}$	$= \dfrac{C_{uu}}{\sigma_u^2}$, normalized autocorrelation
C_{uv}	cross correlation of random processes $u(t)$ and $v(t)$
$\tilde{C}_{uv}$	$= \dfrac{C_{uv}}{\sigma_u \sigma_v}$, normalized cross correlation
d	random function of time
f	frequency, hertz
g	standard acceleration, ft/sec^2
K_o	modified Bessel function of second type, order zero
L	scale-length of atmospheric turbulence, ft
n	integer
p	roll rate (right wing down, positive), rad/sec
Δp	differential pressure, psi
P	probability density function
q	pitch rate, (nose-up, positive), rad/sec also dynamic pressure
r	yaw rate, (nose right, positive), rad/sec

R $\left(= \dfrac{\sigma_c}{\sigma_d}\right)$, ratio of standard deviations

s Laplace transform variable

S wing area, ft^2

t time, sec

T total time history length, sec. also temperature in the atmosphere, °F

$\overline{U}$ velocity of the mean wind ft/sec

u_o reference flight speed, ft/sec

(u, v, w) x, y and z-components of aircraft velocity with respect to still air, ft/sec

(u_m, v_m, w_n) x, y and z-components of the gust velocities measured at the probeheads, ft/sec

(u_p, v_p, w_p) x, y and z-components of the velocity of the probe-head with respect to an aircraft centered inertial axis system, ft/sec

x , y distances of the probeheads to the aircraft center of gravity, ft

x, y, z aerodynamic forces on the aircraft in x, y and z direction.

z height above sealevel

α aircraft angle of attack, rad

α_p probe angle of attack, rad

β aircraft sideslip angle, rad

β_p probe sideslip angle, rad

γ $\left(= -\dfrac{dT}{dz}\right)$, lapse rate, °F/1000 ft

Γ adiabatic lapse rate, °F/1000 ft

η Gaussian white noise

σ standard deviation

ρ atmospheric density

ϕ aircraft roll angle, rad

τ time lag, sec

$\Phi_i(f)$ power spectral density of the variable i, in (units of the variable i)^2/hertz

$\Phi_{ij}(f)$ cross spectral density of the variables i and j, in (units of variable i) (units of variable j)/hertz

SUBSCRIPTS

u, v, w denotes u, v, or w gust component

$(\quad)_o$ = value at reference flight condition

COMPLETED

ORIGINAL

ANALYSIS OF LOW ALTITUDE ATMOSPHERIC TURBULENCE DATA MEASURED IN FLIGHT

Victor M. Ganzer, Robert G. Joppa,
and Gerrit van der Wees

1. Report No. NASA CR-2886	2. Government Accession No.	3. Recipient's Catalog No.
4. Title and Subtitle "Analysis of Low Altitude Atmospheric Turbulence Data Measured in Flight"		5. Report Date September 1977
		6. Performing Organization Code
7. Author(s) Victor M. Ganzer, Robert G. Joppa and Gerrit van der Wees		8. Performing Organization Report No.
		10. Work Unit No.
9. Performing Organization Name and Address University of Washington Department of Aeronautics & Astronautics Seattle, Washington 98195		11. Contract or Grant No. NASA NGR-48-002-085
		13. Type of Report and Period Covered
12. Sponsoring Agency Name and Address National Aeronautics & Space Administration Washington, DC 20546		14. Sponsoring Agency Code

15. Supplementary Notes

16. Abstract

All three components of turbulence were measured simultaneously in flight at each wing tip of a Beech D-18 aircraft. The flights were conducted at low altitude, 30.5 - 61.0 meters (100-200 ft.), over water in the presence of wind driven turbulence.

Statistical properties of flight measured turbulence are compared with Gaussian and non-Gaussian turbulence models. Spatial characteristics of turbulence models. Spatial characteristics of turbulence were analyzed using the data from flight perpendicular and parallel to the wind. The probability density distributions of the vertical gusts show distinctly non-Gaussian characteristics. The distributions of the longitudinal and lateral gusts are generally Gaussian.

The power spectra compare in the inertial subrange at some points better with the Dryden spectrum, while at other points the von Karman spectrum is a better approximation. In the low frequency range the data show peaks or dips in the power spectral density.

The cross spectra between vertical gusts in the direction of the mean wind for the present data are compared with a matched non-Gaussian model. The real component of the cross spectrum is in general close to the non-Gaussian model. The imaginary component, however, indicates a larger phase shift between these two gust components than was found in previous research.

17. Key Words (Suggested by Author(s)) Aircraft Atmospheric Turbulence Atmospheric Turbulence Modeling Flight Measurement of Turbulence Gusts Turbulence		18. Distribution Statement UNCLASSIFIED-UNLIMITED STAR Category 05	
19. Security Classif. (of this report) UNCLASSIFIED	20. Security Classif. (of this page) UNCLASSIFIED	21. No. of Pages 108	22. Price* $5.50

FOREWORD

ANALYSIS OF LOW ALTITUDE ATMOSPHERIC

TURBULENCE DATA MEASURED IN FLIGHT

SUMMARY

This report presents the results of the research performed on the statistical characteristics of atmospheric turbulence encountered by an aircraft flying at low altitudes.

The dependence of several statistical properties of the turbulence on the direction of the flight with respect to the mean wind was evaluated. The turbulence velocities in longitudinal, lateral, and vertical direction were measured at the wingtips of the aircraft.

Estimates were made of the probability density, the power spectra, and the cross spectra of gust time histories measured in runs parallel and perpendicular to the wind direction. The probability density distributions of the vertical gusts show distinctly non-Gaussian characteristics. The distributions of the longitudinal and lateral gusts are generally Gaussian.

The power spectra compare in the inertial subrange at some points better with the Dryden spectrum, while at other points the von Karman spectrum is a better approximation. In the low frequency range the data show peaks or dips in the power spectral density.

The cross spectra between vertical gusts in the direction of the mean wind for the present data are compared with a matched non-Gaussian model. The real component of the cross spectrum is in general close to the non-Gaussian model. The imaginary component, however, indicates a larger phase shift between these two gust components than was found in previous research.

The spatial characteristics of turbulence were analyzed by comparing autocorrelations with the cross correlations between the appropriate gusts at the two wingtips and by estimating the integral scale lengths of the longitudinal and lateral gust time histories.

The above results must be regarded to be of a tentative nature, as the data were obtained in only two flights. More data is required if more definite conclusions are to be drawn.

1

1. INTRODUCTION

This chapter gives an introduction to the general area of interest in this research program. A review is given of some of the past research on characteristic properties of atmospheric turbulence at low altitude. Furthermore, an explanation of the purpose of the present study and the reasoning behind the selection of the approach for this study are presented.

1.1 Background of Past Research

Random processes are usually characterized by the probability of the occurrence of a certain event, e.g. a gust with a certain magnitude. This probabilistic character is expressed in the probability density distribution, which is defined as

$$Probability\ density = P_u(x)dx = Probability\ that\ x < u \leq x + dx$$

The most commonly known probability density distribution is the Gaussian distribution

$$P_u(x) = \frac{1}{\sigma_u \sqrt{2\pi}} \quad exp \quad -\frac{1}{2}\left(\frac{x - \bar{u}^2}{u}\right) \tag{1.1.1}$$

This distribution is generally used as a model for atmospheric turbulence in the fatigue testing of aircraft wings.

Recent research showed distinct non-Gaussian characteristics in atmospheric turbulence encountered by aircraft, particularly in the vertical direction. Reeves, et al. [1] and [2] developed a non-Gaussian model, which consists basically of the addition of Gaussian and Modified Bessel processes. A schematic representation of this system is shown in figure 1.

The probability distribution and patchy character of a random process $U(t)$ generated in the manner described above for the non-Gaussian model are a function of the ratio of the standard deviations

$$R = \frac{\sigma_c}{\sigma_d} \tag{1.1.2}$$

where $d(t)$ is a Gaussian process and $c(t)$ is a Modified
Bessel process generated by multiplication of two Gaussian
processes $a(t)$ and $b(t)$.

Reeves indicated that the non-Gaussian model with a value
for the standard deviation ratio R in the order of unity would
give a good match with measured data. In the present research
a comparison is made between the measured data and both the
Gaussian model and the non-Gaussian model for $R = 1$.

Another very important statistical property of atmospheric
turbulence is described by the power spectral density .
The power spectrum provides information on the average contri-
bution to the random process from the frequency components
which make it up. Research by Burns [3] showed indications
that the shape of the power spectra was influenced considerably
by the direction of flight with respect to the mean wind. It
showed particularly that the power spectral density of the
vertical component at low frequencies was considerably lower
during the crosswind runs. In the present research the shape
of the power spectra is evaluated for data runs both parallel
to the wind and crosswind.

Several analytical expressions have been suggested to
represent the power spectral density of the three turbulence
gust components. The most commonly used representations are
those of Dryden [4] and von Karman [5]. Chapter 4.1   presents
the algebraic formulations of these models. In the results of
the present research a comparison is made between the spectra
of the measured data and the Dryden and von Karman models.

A topic of particular interest to atmospheric scientists
is the shear flow in the boundary layer of the atmosphere.
When a mass of air moves over the surface of the earth,
the wind velocity at higher altitudes will be higher than
at lower altitudes due to the friction in the boundary
layer. This difference in horizontal velocity produces
rotation in the flow and thus turbulence. In the
statistical analysis of the turbulence this phenomena can best
be analyzed by determining the cross spectral density of the
gust component in the direction of the mean wind correlated
with the vertical gust component. Elderkin [6] determined
these cross spectra for data measured at altitudes up to

3

87 meters. Reeves, et al.[1,2] developed a non-Gaussian model based on Elderkin's tower measurements. In the present research a comparison is made between the cross spectra of the measured turbulence and this non-Gaussian model.

1.2 Purpose of the Present Study

The purpose of this research is to attempt to determine if the statistical properties of turbulence are independent of the direction of the flight path with respect to the mean wind. The statistical properties which are to be evaluated in this context are:

probability density distribution

power spectral density and the corresponding autocorrelation

cross spectral density and the corresponding cross correlation

integral scale length.

The probability density distributions and the power spectra are compared for runs parallel to the wind and crosswind. An estimate is made of the integral scale lengths of the turbulence in order to determine the elongation of the turbulence eddies.

An important aspect of the purpose of the present study is the evaluation of the spatial distribution of atmospheric turbulence. The main tools in this evaluation are the autocorrelations of the measured gust time histories at a value of the time lag τ_1 where τ_1 is the time it takes the aircraft to fly a distance equal to the span of the aircraft. These autocorrelations are then compared with the cross correlation between measured turbulence velocities at two separate points in space, the two wingtips of the aircraft. This comparison should provide an indication whether time correlation of a gust signal with itself is equivalent to spatial correlation of two gust signals measured at two separate points.

4

2. THE TEST AIRCRAFT AND INSTRUMENTATION

This chapter presents a short description of the aircraft, a twin-engine Beechcraft D-18S, and gives some characteristics such as stability derivatives. The modifications of the aircraft which were necessary to perform the test program are described. Furthermore a general description of the instrumentation is given.

2.1 Description of the Aircraft

The Beechcraft D-18S is a low wing all metal semi-monocoque aircraft with fully retractable conventional landing gear (Fig. 2). The aircraft used in this research program, N-4545, is powered by two Pratt and Whitney Model R985-14B radial engines, each rated at 450 horsepower.

The principal dimensions and geometry of the aircraft are given in Table 1.

At several points in the analysis of the data it will be necessary to know the characteristics of the natural modes of the aircraft. Sandusky [7] did a study on the stability derivatives and the natural modes of the Beechcraft D-18S. Table 2 presents some estimates from this study.

2.2 Modifications

In this section some details are given relating to the necessary modifications of the aircraft, particularly with respect to the installation of the gust booms and probes on the wingtips and the installation of equipment in the cabin of the aircraft.

The gust booms were attached to the pods at the wingtips of the aircraft (Fig. 2). These gust booms were designed such that the probeheads were positioned far in front of the wing. The effect of the airflow about the wing on the data measurement was thereby minimized. The upflow in front of the wing at constant angle of attack is accounted for through

the probehead constant C_{p_α} , which was obtained from wind-
tunnel tests.

Vibration tests on the gust booms showed their natural
frequency well above ten cycles per second, which is the
highest frequency of interest in this program.

The probeheads were designed to carry the pressure trans-
ducers, which were connected to the pressure ports on the
hemispherical front of the probeheads. The probeheads were
fitted on the front end of the booms. A more detailed
description of the probeheads is given in appendix A1.

In the cabin of the aircraft some modifications were made
to facilitate the installation of data recording equipment.
In the right front corner of the cabin, against the bulkhead
dividing the cockpit and the cabin, a panel was installed with
instruments such as airspeed indicator, altimeter, outside
air temperature indicator and rpm and manifold pressure indi-
cators for both engines. This instrument panel, being located
near the c.g. of the aircraft, also contained the vertical and
lateral accelerometers.

The left front cabin chair was removed and in its place
an Ampex FR 1300 14 channel FM taperecorder was installed.
Just above the taperecorder, a Tektronix 561 oscilloscope was
fitted on a shelf which in turn was fixed to the cabin bulk-
head.

2.3 Instrumentation

The Beechcraft D-18S test aircraft was instrumented to
measure and record the variables necessary for the calculation
of the turbulence velocities in longitudinal, lateral and
vertical direction at the wingtips of the aircraft. The lay-
out of the instrumentation is shown in Fig. 3 .   A detailed
description of the instrumentation and the calibration of the
instrumentation is presented in appendix A.

Each wingtip probe contained three differential pressure
transducers connected to appropriate pressure ports on the
hemispherical head of the probe with short lengths of 3/16"
i.d. plastic tubing (Fig. 4).

The probehead constants for vertical and lateral gust
velocities were obtained from wind tunnel tests of the actual

6

probes in the Venturi wind tunnel of the Department of
Aeronautics and Astronautics, as well as from tests of a 1/8
scale model of the Beech D-18, including probes, in the
F. K. Kirsten 8' x 12' wind tunnel to get the effects of flow
angles induced by the aircraft.

The resulting constants were:

$$\frac{\Delta p}{q\alpha_p} = 5.45/rad \quad \text{for vertical velocities}$$

$$\frac{\Delta p}{q\beta_p} = 4.7/rad \quad \text{for lateral velocities}$$

where Δp = pressure difference between the $\pm 45^o$ orifices.

       q = dynamic pressure

    α_p & β_p = angles of attack of the probehead in radians

These values compare favorably with the value of
$\frac{\Delta p}{q\alpha} = 4.5/rad$ obtained from the theoretical calculation of
flow of a perfect fluid about a sphere.

Longitudinal velocities were measured as described in
appendix A.3.

In order to determine the gust velocities actually
occurring in the atmosphere it was necessary to remove the
motions of the aircraft from the gust velocity signals
measured by the pressure transducers. This was achieved by
measuring the motions of the aircraft with the following
instrumentation system:

       roll rate gyro

       pitch rate gyro

       yaw rate gyro

       lateral accelerometer

vertical accelerometer

vertical gyro   (measuring the roll angle)

The motions of the probeheads were calculated from these
signals in computer program GUST (appendix B.3). The dif-
ferences between these computed probe velocities and the
velocities measured by the probes were then the gust velocities
occurring in the atmosphere.

3. DATA ACQUISITION

The data were acquired in a series of flights with
Beechcraft D-18S N4545, above open water in the area of the
Straits of Juan de Fuca, south of Victoria, B. C.

This chapter presents some aspects of the flight planning,
the in-flight instrument operation checks, and gives a
description of the atmospheric conditions during the test
flights as well as a description of the physical features of
the area surrounding the test area.

3.1 Flight Planning

For each one of the flights, a flight plan was set up
giving all the test items that were to be performed, and de-
scribing the procedures and test conditions for each test item.
Before each flight it was ascertained that all instruments and
the recording equipment were operating properly. The instru-
mentation was calibrated regularly as described in appendix A.2.

Test item #1 consisted of the in-flight instrument opera-
tion verification, usually performed en route from Seattle to
the test area. It constituted pilot-induced motions of the
aircraft, preferably in still air. The signals of the appro-
priate instruments were monitored at the output of the recorder
and checked for correspondence with the motion.

In section 3.2 a description of the instrument operation
checks, both on the ground and in-flight, is given.

Test item #2 consisted of a sequence of motions at alti-
tude. The signals from the instruments were recorded for use
in checking of computer program GUST. A further discussion of
this test item is given in section 3.2 of this report.

After it was ascertained that all instruments operated
properly and the motions at altitude had been carried out, the
aircraft descended to the appropriate altitude for test item
#3, the atmospheric turbulence data runs. These runs were
usually made in the area of the Straits of Juan de Fuca,
although on several occasions, when no full data runs were
required, an area closer to Seattle, such as Hood Canal was
selected.

9

Table 3   gives a listing of the flights performed with Beechcraft D-18S N4545 in this research program. Flights #1 through #5 were mainly concerned with checking out the gust probe booms, the electrical power supplies and the instrumentation installed in the aircraft for this program.

Flights # 15 and # 16 were the data flights which gave data suitable for analysis. The results of this analysis are presented in this report.

3.2   Instrument Operation Checks

Table 4   presents a listing of the data instruments which were checked for proper operation before each flight and in flight under test item #1: In-flight Instrument Operation Verification.

On The Ground Checks.-The pressure transducers were checked by putting a pressure load on one side of the pressure transducers. The magnitude of the pressure was monitored on a manometer. In appendix A.2, calibration of the data instruments, a description of this system is given.

The rate gyros were checked by positioning them on a specially designed rocker table, which produced a sinusoidal oscillation. Appendix A.2 also gives a full description of this calibration technique.

The accelerometers were fixed on a platform which could be leveled and then rotated about a horizontal axis. The acceleration measured by the accelerometers varied sinusoidally with the angle of rotation of the platform.

The roll angle was measured by the vertical gyro, positioned in the nose of the aircraft which could be rotated about an axis parallel to the aircraft's roll axis.

All the output signals from the above instruments were checked at the output of the 14 channel tape recorder, in order to insure that all segments of the data measuring and recording equipment worked properly.

In-Flight Checks.-Operation of the instrumentation was

verified as the first test item of each flight. This checking usually took place while en route from Seattle to the test area. The pilot induced aircraft motions and the appropriate signals were monitored, again at the output of the tape recorder.

By rolling the aircraft the vertical pressure transducers, the roll rate gyro and vertical gyro could be checked. Yawing and sideslipping provided an opportunity to verify proper operation of the yaw rate gyro, the lateral pressure transducers, the lateral accelerometer and the longitudinal pressure transducers. By making the aircraft go through a short period pitching motion, it was possible to check the signal of the pitch gyro and the vertical accelerometer.

Motions at Altitude.-This test item, #2 of the flight plan, was usually performed after it was verified that all data instruments operated properly. These motions, rolling, short period pitching, yawing and a coordinated turn, were made in quick succession. The records from these motions were used to check computer program GUST, which was designed to compute gust time histories from the pressure signals. A detailed description of computer program GUST is given in appendix B.3.

3.3 Data Runs

Figure 5   gives a general idea of the area where the data runs were made. Forty miles to the southwest of the center of the test area was Mt. Olympus, 7965 ft. high, the highest point of the Olympic Peninsula. To the northwest was Vancouver Island, where mountains in the vicinity of the Straits of Juan de Fuca reach heights of approximately 3600 ft.

The prevailing wind flows between these two mountain masses from the Pacific Ocean, through the Straits of Juan de Fuca toward the Cascade Mountain Range, 80 miles east of the test area.

During each of the flights which gave a full set of data, four runs were made, the first run into the wind, the second run with tailwind, followed by two crosswind runs. Data were taken for about 4 to 5 minutes during each run.

Figures 6   and   7   present the patterns that were flown during flight #15 and #16 respectively. The prevailing surface wind during the test period is also indicated.

11

Tables 5 and 6 give the basic conditions of the four data runs of flights #15 and #16. These are the flights for which the recorded data could be fully reduced to statistical properties of the turbulence.

3.4   Atmospheric Conditions

For proper evaluation of the statistic properties of the atmospheric turbulence data, it is necessary to know the conditions of the atmosphere at the time the data were taken. In particular, it is important to know how the decrease of temperature with height, the lapse rate $\left(\gamma = -\frac{dT}{dZ}\right)$, compares with the adiabatic lapse rate Γ $(\Gamma \approx 1^{\circ}C/100 M$ or $5.5^{\circ}F/1000 ft)$.

In a hydrostatically unstable atmosphere $\gamma > \Gamma$. Under these conditions a volume of air which has been displaced upward will experience an additional force upward. In the case that $\gamma < \Gamma$ a volume of air which has been displaced upward will be at a lower temperature than its environment and thus experience a downward force. An atmosphere having these characteristics is classified stable.

If the lapse rate γ is approximately equal to the dry adiabatic lapse rate Γ the atmosphere is classified neutral.

Turbulence in the atmosphere is affected both by the above mentioned hydrostatic condition of the atmosphere and by the mean horizontal flow of air from which it derives energy through the Reynolds Stress. This "mechanical" turbulence is then dependent on whether the rate of energy supply from the mean flow exceeds the rate of work to be done in the earth's gravity field in moving air in vertical direction. The parameter relating buoyant production to stress production in a useful manner is the gradient Richardson number

$$Ri = \frac{g\left(\frac{\partial\theta}{\partial Z}\right)}{\theta\left(\frac{\partial\bar{u}}{\partial Z}\right)^2} \tag{3.4.1}$$

12

where θ is the potential temperature

           Z the height above the surface

           g the gravity constant, and

           $\bar{u}$ the velocity of the mean flow.

For an ideal gas the gradient Richardson number can be expressed as, reference [8]

$$Ri = \frac{g(\Gamma - \gamma)}{T\left(\frac{\partial u}{\partial Z}\right)^2}$$

Unstable air corresponds to $Ri < 0$. If $Ri \sim 0$ the air is classified as neutral. Under these conditions the turbulence is purely driven by the mean flow.

For stable conditions, $Ri > 0$, two regions can be distinguished; one when $\sim 0 < Ri < \sim 0.25$, under which conditions mechanical turbulence is damped by the thermal stability of the atmosphere, and the other when $0.25 \sim < Ri$, when no turbulence in vertical direction can be maintained.

Figures 8 and 9 give the temperature as a function of altitude for flights #15 and #16, the two flights for which the data are reduced to probabilistic characteristics in this report. In these figures both temperatures measured in flight and those measured by the Quillayute weather observation station are presented.

From the temperature and the wind velocity information presented in the above figures a calculation was made of the gradient Richardson number. Table 7 gives this calculation and the resulting Richardson numbers, which then give an indication of the stability of the atmosphere during the time of the test flights.

The most desirable atmospheric condition for turbulence data collection is one where reasonably strong winds occur, which is the case for unstable air. Table 7 shows that the atmosphere was slightly unstable during both test flights.

4. ANALYSIS AND DISCUSSION OF THE RESULTS

This chapter presents an analysis of the gust time histories, the probability distributions, the power spectra, the cross spectra, and the spatial characteristics of the measured turbulence. The first section gives the theoretical background for the analysis.

The data reduction process which was followed in obtaining these results from the raw data is described in appendix B.

4.1 Theoretical Background

The function which is generally used to determine the measure of predictability of random processes is the cross correlation function, defined as

$$C_{uw}(\tau) = \lim_{T \to \infty} \frac{1}{2T} \int_{-T}^{T} u(t)\, w(t + \tau)\, dt \tag{4.1.1}$$

$u(t)$ and $w(t)$ are two random processes and this correlation is the measure of predictability of $\backslash$ w at a future time $(t + \tau)$ based on the knowledge of u at time t .

If a random process is correlated with itself, the function is called autocorrelation function

$$C_{uu}(\tau) = \lim_{T \to \infty} \frac{1}{2T} \int_{-T}^{T} u(t)\, u(t + \tau)\, dt \tag{4.1.2}$$

A parameter of particular interest is the integral scale length, defined as

14

$$L_u = \frac{u_o}{\sigma_u^2} \int_{-\infty}^{\infty} C_{uu}(\tau)\,d\tau \qquad (4.1.3)$$

which is a measure of the distance an aircraft flies through turbulence which is correlated with itself. It is therefore an indication of the average size of the turbulence eddies in the atmosphere.

Two very important statistical descriptions of atmospherical turbulence are given by the power spectral density and the cross spectral density. The power spectral density of a random process is defined as the Fourier transform of its auto-correlation function

$$\Phi_u(f) = \int_{-\infty}^{\infty} C_{uu}(\tau)\ exp\ (-i2\pi f\tau)d\tau \qquad (4.1.4)$$

where f = frequency in cycles/second. The cross spectral density of two random processes $u(t)$ and $w(t)$ is then the Fourier transform of their cross correlation

$$\Phi_{uw}(f) = \int_{-\infty}^{\infty} C_{uw}(\tau)\ exp\ (-i2\pi f\tau)d\tau \qquad (4.1.5)$$

These spectra are functions of both positive and negative frequency f only for mathematical convenience. Negative f does not have any physical significance.

It is noted that the power spectrum is always a real function, since it is the Fourier transform of the autocorrelation function, which contains no phase information. The cross spectrum however, is a complex function of the frequency. The real component is called the co-spectrum Φ_r while the imaginary component is called the quad-spectrum Φ_i. The latter component contains the information on the phase shift

15

between the two random processes.

Several mathematical models have been suggested to describe the power spectral density of the three turbulence gust components. The model suggested by von Karman [5] is generally considered the most accurate one. Dryden's model [4] is usually used in turbulence simulation, as the resulting spectra can be exactly matched using linear filters. Both models will be used in this report in a slightly modified form. The following changes are introduced: (1) instead of a single scale length L for all three gust components independent values for each gust component will be used. (2) The form of the lateral power spectrum will be changed to a form similar to that used for the longitudinal power spectrum. The algebraic form of the models to be used in this report are then

von Karman:

$$\phi_u(f) = \frac{\sigma_u^2 L_u}{u_o} \frac{2}{\left[1 + (1.34 \frac{2\pi L f}{u_o})^2\right]^{5/6}} \tag{4.1.6}$$

$$\phi_v(f) = \frac{\sigma_v^2 L_v}{u_o} \frac{2}{\left[1 + (1.34 \frac{2\pi L f}{u_o})^2\right]^{5/6}} \tag{4.1.7}$$

$$\phi_w(f) = \frac{\sigma_w^2 L_w}{u_o} \frac{\left[1 + \frac{8}{3}(1.34 \frac{2\pi L f}{u_o})^2\right]}{\left[1 + (1.34 \frac{2\pi L f}{u_o})^2\right]^{11/6}} \tag{4.1.8}$$

Dryden:

$$\phi_u(f) = \frac{\sigma_u^2 L_u}{u_o} \frac{2}{\left[1 + (\frac{2\pi L_u f}{u_o})^2\right]} \tag{4.1.9}$$

16

$$\phi_v(f) = \frac{\sigma_v^2 \, L_v}{u_o} \frac{2}{\left[1 + \left(\frac{2\pi L_v f}{u_o}\right)^2\right]} \tag{4.1.10}$$

$$\phi_w(f) = \frac{\sigma_w^2 L_w}{u_o} \frac{\left[1 + 3\left(\frac{2\pi L_w f}{u_o}\right)^2\right]}{\left[1 + \left(\frac{2\pi L_w f}{u_o}\right)^2\right]^2} \tag{4.1.11}$$

The cross spectral density (Eq. 4.1.5) provides information on the phase relationships of the frequency components of two random processes. In general little is known about the cross spectra of the gust components of atmospheric turbulence.

With respect to correlation between two gust components measured at one point, research by Elderkin [6] indicates a consistent low frequency cospectrum (real part ϕ_r of the cross spectral density) relating the gust velocity in the direction of the vertical gust component.

Reeves, et al. [1,2] used a mathematical model based on Elderkin's data.

$$\phi_{uw}(f) = \frac{-c_u \sigma_w \sqrt{2}}{R^2 + 1} \left\{ \frac{2R^2}{A^2} \left(\frac{L_w}{u_o}\right)^2 \left(\frac{L_u}{u_o}\right) \left[\frac{[1 + 3(\pi A f)^2] - i(2\pi A f)}{[1 + (\pi A f)^2]^2}\right] \right.$$

$$\left. + \sqrt{\frac{L_u L_w}{u_o^2}} \left[\frac{1 + i\sqrt{3}\left(2\pi \frac{L_w}{u_o} f\right)}{[1 + i\left(2\pi \frac{L_w}{u_o} f\right)][1 + (2\pi B f)^2]}\right] \right\} \tag{4.1.12}$$

A, B and R are parameters satisfying the following conditions

$$A > \frac{2L_w}{u_o} \qquad\qquad A > \frac{2L_u}{u_o}$$

$$B > \frac{L_w}{u_o} \qquad\qquad B > \frac{L_u}{u_o}$$

$$R \geq 0$$

where R is again the ratio of the standard deviations. In the comparison between the data from the present research program and the above model it should be realized that the aircraft coordinate system only coincides with the wind coordinate system during the downwind run. In the case of the headwind run the sign of the $u-w$ cross spectrum is inversed, while for the crosswind runs the $v-w$ cross spectrum is equivalent to $u-w$ in the above model.

With respect to the correlation between two gust components, in the same direction, measured at two separate points the following observations may be made:

- At high frequencies (small turbulence eddies) the random processes at the two points separated by distance b (the wingspan of the aircraft), will occur independently of each other. The cross spectrum will then be near zero.

- At low frequencies (large turbulence eddies) both sensors will measure a similar signal change and the correlation will be large.

- At intermediate frequencies (in the present data between $.2$ and 1 Hz) there will be some correlation and the power spectrum will have a normalized value $\frac{\phi_{ij}}{\sigma_i \sigma_j}$ between zero and approximately $.3$.

In order to analyze the spatial characteristics of the turbulence it is necessary to estimate the autocorrelation function of the gust time histories for a value of the time lag τ equal to the time it takes the aircraft to fly a distance equal to the wingspan. This estimate is found by

taking the inverse Fourier transform of the power spectral
density

$$C_{ii}(\tau_1) = \int_{-\infty}^{\infty} \Phi_i(f) \ exp \ (i2\pi f\tau_1)df \qquad (4.1.1?)$$

As the power spectrum is an even function this can be written
as

$$C_{ii}(\tau_1) = 2 \int_0^{\infty} \Phi_i(f) \ exp \ (i2\pi f\tau_1)df \qquad (4.1.14)$$

In order to compare data from different runs the correlation
functions are normalized to yield correlation coefficients

$$\tilde{C}_{ii}(\tau_1) = \frac{2}{\sigma_i^2} \int_0^{\infty} \Phi_i(f) \ exp \ (i2\pi f\tau_?)df \qquad (4.1.15)$$

As both the correlation function and the power spectral
density are real functions only the real part of the exponen-
tial function in the integral is used

$$\tilde{C}_{ii}(\tau_1) = \frac{2}{\sigma_i^2} \int_0^{\infty} \Phi_i(f) \ cos(2\pi f\tau_1)df \qquad (4.1.16)$$

The cross correlation function is determined from the
cross spectral density in the following manner

19

From Eq. 4.1.5

$$C_{ij}(\tau) = \int_{-\infty}^{\infty} \Phi_{ij}(f) \, exp \, (i2\pi f\tau) df \qquad (4.1.17)$$

which may be written as

$$C_{ij}(\tau) = \int_{-\infty}^{\infty} \Phi_{ij}(f) \left[cos \, 2\pi f\tau + i \, sin \, 2\pi f\tau \right] df \qquad (4.1.18)$$

As the two gust time histories are measured at exactly the same time the cross correlation becomes

$$C_{ij}(0) = \int_{-\infty}^{\infty} \Phi_{ij}(f) \, df \qquad (4.1.19)$$

The cross correlation is a real function, so only the real part of the complex cross spectrum is used. As this real part is even, the cross correlation may be written as

$$C_{ij}(0) = 2 \int_{0}^{\infty} \Phi_{ij}{}_{real}(f) \, df \qquad (4.1.20)$$

Normalization gives

$$\tilde{C}_{ij}(0) = \frac{2}{\sigma_i \sigma_j} \int_{0}^{\infty} \Phi_{ij}{}_{real}(f) \, df \qquad (4.1.21)$$

20

These expressions (Eqs. 4.1.16 and 4.1.21) are used in section 4.5 to calculate the normalized autocorrelation and cross correlation.

4.2   Probability Distributions

The probability density distributions of the gust components at both wingtips are presented in figs. 10 through 17. The data were measured in the following runs. Data showing 100 samples/sec were limited to about 150 seconds in length, while those reduced at 50 samples/sec could run to 300 seconds.

FLIGHT	RUN	
15	1	Upwind
	2	Downwind
	3	Crosswind, wind from the right
	4	Crosswind, wind from the left
16	1	Upwind
	2	Downwind
	3	Crosswind, wind from the left
	4	Crosswind, wind from the right

The probability density of the vertical gusts encountered by the aircraft shows distinctly non-Gaussian characteristics, particularly for the downwind and the crosswind runs (Fig. 11c , 12c , and 13c) .   For the upwind runs it is slightly less distinct, but still closer to the non-Gaussian model than to the Gaussian model (Fig. 10c and 14c) .

An example of a particularly non-Guassian probability density distribution is shown in Fig. 18 .   The gust time history was 170 seconds long and was sampled at 100 samples per second.   It is seen that the measured data match very well with the non-Gaussian model for $R = 1$.

Gusts in the direction of the mean wind are measured as longitudinal gusts in the up and downwind runs and as lateral

gusts in the crosswind runs. In general tnese gusts show Gaussian characteristics (Fig. 11a , 12b , 14a , 16b and 17a) although some cases show strong exception to this rule (Fig. 10a and 15a).

The gust component perpendicular to the mean wind is measured as lateral gust in the up and downwind runs and as longitudinal gust in the crosswind runs. The gust time histories of this component are in general also Gaussian (Fig. 10b , 12a , 16a), with, again, some non-Gaussian exceptions (Fig. 15a).

4.3 Power Spectra

The power spectral densities of the components of the gusts encountered at both wingtips of the aircraft are presented in Fig. 19 through 26 . Also presented in these graphs are the von Karman and Dryden spectra (Eqs. 4.1.6 through 4.1.11). The scale length L of these spectra is set such that the variance is equal to the variance of that particular gust time history.

The Longitudinal Gust Component.-Generally the power spectral density of the longitudinal gust component from flight #15 compares well with the Dryden spectrum, particularly for the downwind run (Figure 20a). The spectra of the crosswind runs show a significant reduction in the spectral density between $.3$ and $.4\ Hz$. (Fig. 21a and 22a). Run #3 shows more power at very low frequencies (below $.1\ Hz$) while run #4 shows much less power in this frequency range.

The power spectra of the longitudinal gust component from flight #16 show good correspondence with the von Karman spectra, particularly in the inertial subrange (the frequency range where energy transfer from lower to higher frequencies takes place without energy dissipation). However, in the low frequency range (below approximately $.2\ Hz$) the spectra of the measured data of the upwind and the downwind runs (Fig. 23a , 24a) and of one crosswind run (Fig. 26a) do not match the von Karman spectrum very well. There is no readily available explanation for this behavior.

The Lateral Gust Component.-The spectra of both the up-
wind and the downwind run of flight #15 show excellent cor-
respondence with the Dryden model (Figure 19b and
20b) .   The spectra of the lateral gusts measured at both
the left and the right wingtip during run #3 of flight #15
show a dip at approximately .2 Hz (Figure 21b) .
For run #4 the power spectral density shows good correspond-
ence with the von Karman model (Figure 22b) .

The data of flight #16 gave spectra which in general
corresponded well with the von Karman model. Below approxi-
mately .2 Hz,however, the power spectral density of the
measured turbulence falls below that of the von Karman
spectrum, and shows tendencies similar to those of the longi-
tudinal gusts. (Fig. 24b , 25b , and 26b) .

The Vertical Gust Component.-The data of flight #15 for
this component show an interesting phenomenon. The spectra
of the upwind and crosswind runs display a sharp peak at
approximately .2 Hz . (Figure 19c , 21c and
22c) .   The spectra of the downwind run show a
dip at this frequency (Fig.   20c) .   This char-
acteristic of the spectra is apparently due to a helical flow
pattern in the direction of the mean wind. This flow pattern
is described by Brown [9] and by LeMone [10]. It consists
basically of horizontal roll vortices in the direction of the
mean wind. Fig. 27   (from [10]) illustrates the flow model.

The peak in the power spectra of the data may then be
explained as follows: During the upwind run the aircraft
flew in the part of a roll vortex where strong up or down-
drafts occurred, which then resulted in high power at this
frequency. During the downwind run the aircraft flew in the
center part of a vortex, which gave relatively little power
in this frequency range of the power spectral density. Dur-
ing the crosswind runs the aircraft crossed a number of vor-
tices at right angles, experiencing alternately up and down-
drafts, which then resulted in higher power at this frequency.

The power spectra of the data of flight #16 show the
following characteristics: The spectra of the vertical gust
time histories of all four runs indicate higher power than
the von Karman or Dryden spectra above a frequency of
approximately 5 Hz (Figure 23c , 24c , 25c ,
and 26c) . No explanation for this behavior could be
found.

23

At the low frequency end the power spectra of the
vertical gust time histories displayed quite different char-
acteristics for different runs: The spectra of the upwind
run dropped sharply below approximately .15 Hz (Figure
23c) .   The spectra of the downwind run remained steady
below .5 Hz, but for the left wing the value was below the
level expected from the von Karman and Dryden spectra, while
for the right wing the spectra stayed above this level (Fig.
24c) .   The spectra of the crosswind runs showed
a sharp dip at approximately .2 Hz, similar to the dip
encountered in the spectra of the downwind run of flight #15
(Fig. 25c and 26c) .

Within the time available for the evaluation of the data
it was not possible to find an explanation for the character-
istics of the power spectra of the vertical gust time
histories measured in flight #16.

In general it can be concluded that in some cases the
von Karman spectra provide a good description of the turbu-
lence, while in other cases the Dryden spectra give a better
approximation. At low frequencies sharp peaks or dips occur,
which are approximated by neither model.

4.4 Cross Spectra

In this section two aspects of the cross spectra of the
measured data are considered.

(1) The Correlation Between the Component of the Gust
in the Direction of the Mean Wind and the Vertical Component.
- Figures 28 and 29   present these cross spectra for
the data of flight #15 and #16. As indicated in section 4.1
for the up and downwind runs the u-w spectrum should be
considered, while for the crosswind runs the v-w cross
spectrum should be considered. These graphs also show the
non-Gaussian model (Eq. 4.1.12) with the appropriate scale
lengths. It is seen that the co-spectrum (the real part of
the cross spectral density) of the non-Gaussian model in
general corresponds reasonably well with the co-spectrum
of the measured data (Fig. 28b , 28d , 29a) .   However,
the imaginary component, the quad-spectrum, of the present
data is usually larger than was assumed in the non-Gaussian
model   (Figures 28 and 29) .   This indicates a larger

24

phase shift between the gust component in the direction of the mean wind and the vertical gust component.

(2) The Correlation Between the Component of a Gust at the Left Wingtip and the Gust Component in the Same Direction at the Right Wingtip.-Fig. 30 through 32 present these cross spectra from the data of flight #15 and #16. These graphs show at which frequency the transition from no correlation (at high frequencies, small turbulence eddies) to full correlation (at low frequencies, large turbulence eddies) takes place. For the longitudinal gust component this occurs usually at approximately the same frequency, irrespective of the direction of the wind w.r.t. the flight path of the aircraft (Fig. 30) .

The lateral gusts are correlated up to higher frequencies for the crosswind runs (Fig. 31c , 31d , 31g , 31h) than is the case for the up and downwind runs (Fig. 31a, 31b , 31e , and 31f) .

For the vertical component no particular trend could be distinguished in this respect. However, for several runs the real and imaginary component of the cross spectrum were approximately equal and at low frequencies (.05 to .1 Hz) returned to zero correlation. This was particularly the case for the up and downwind runs of flight #15 (Fig. 32a , 32b) and for the upwind run of flight #16 (Fig. 32e) .

4.5 Spatial Characteristics

It is again emphasized that the results presented in this section are based on a limited amount of data, and the conclusions drawn are therefore of a tentative nature.

The analysis of the spatial characteristics is based on the following considerations.

(1) According to Taylor's Hypothesis [11] the time fluctuations of turbulence at a fixed point can be considered equal to the fluctuations caused at that point by the entire field, frozen at a particular instant and convected past the point. In this analysis an attempt is made to check the hypothesis by comparing the autocorrelation function at a time lag τ_1

$\left(\tau_1 = \frac{wingspan}{aircraft\ velocity}\right)$ with the cross correlation function

of the appropriate gusts at the two wingtips. E.g., the auto-
correlation of the longitudinal gust component for the up or
downwind run is compared with the v-v cross correlation of
the crosswind runs.

The correlations are calculated from the spectra in the
manner described in section 4.1. Table 8   presents the
normalized autocorrelations and cross correlations from flight
#15 for this comparison.

The results presented in Table 8   give no conclusive
evidence. The autocorrelation $\tilde{C}_u(\tau_1)$ of the downwind run
does not compare very well with the cross correlation $\tilde{C}_{vv}(0)$
of the crosswind runs. Similarly the autocorrelation
$\tilde{C}_v(\tau_1)$ of run #4 does not compare well with the cross correla-
tions $\tilde{C}_{uu}(0)$ of the up and downwind runs. It is noted
however that the autocorrelation $\tilde{C}_u(\tau_1)$ of the downwind run
is of approximately the same magnitude as the cross correlation
$\tilde{C}_{uu}(0)$ of the up and downwind runs. Similarly the autocor-
relation $\tilde{C}_v(\tau_1)$ of run #4 is approximately equal to $\tilde{C}_{vv}(0)$.

(2) The structure of the turbulence may also be analyzed
by comparing the autocorrelation of a particular gust compo-
nent at time lag τ_1 with the cross correlation between this
gust component and the component in the same direction at the
other wingtip. E.g., the autocorrelation of the vertical gust
is compared with the w-w cross correlation of the same data
run. Table 9   presents the results of this comparison.
These correlations are also computed from the spectra in the
manner described in section 4.1.

It is seen that the autocorrelations compare reasonably
well with the cross correlations, independent of the direction
of the mean wind w.r.t. the flightpath.

(3) A third aspect of the structure of atmospheric turbu-
lence which can be checked is the elongation of the turbulence
eddies. This is done by estimating the integral scale lengths
by matching the variance of the measured turbulence with the
variance of the longitudinal Dryden model. The resulting scale
lengths are an indication of the size of the eddies in the
direction of the flight of the aircraft. Table 10   presents
the scale lengths for the three components of the gusts at
both the left and right wingtips. As is seen in this table,
the vertical gust usually has the smallest scale length, while
the scale length of the longitudinal gust in any given run is
usually the largest. In virtually all cases the scale lengths

estimated for the gusts of the downwind run are larger than the scale lengths of the upwind run data.

5. CONCLUSIONS AND RECOMMENDATIONS

The analysis presented in chapter 4 centered on the examination of the following aspects:

- The characteristics of the probability density function.

- The characteristics of the power spectra and their dependence on the direction of the wind w.r.t. the flightpath.

- The properties of the cross spectra.

- The spatial distribution of atmospheric turbulence.

This chapter summarizes some of the major conclusions and presents recommendations for further study. It should be realized that these conclusions are based on a limited amount of data and are therefore of a tentative nature.

(1) It is concluded that the probability density functions of the vertical gusts show distinct non-Gaussian characteristics. The longitudinal and lateral gust time histories are generally Gaussian. No particular dependence on the direction of the mean wind w.r.t. the flightpath can be discovered.

(2) The power spectra do depend upon the direction of the mean wind w.r.t. the flightpath, particularly when there is a possibility that a helical secondary flow pattern as described in [9] and [10] is present.

(3) From the analysis of the cross spectra, representing the joint power and the phase shift between two gust time histories, the following conclusions may be drawn.

        (a) The co-spectrum of the gust component in the direction of the mean wind and the vertical gust component is in the same order of magnitude as the co-spectrum measured by Elderkin, indicating that the joint power is about the same as found in previous research. The quad-spectrum, however, is considerably larger which indicates a larger phase shift between these two gust components than was found in previous research.

(b) The data pertaining to the correlation between two gusts in the same direction, one at the left wingtip and one at the right wingtip, indicate that the transition between "no correlation" (high frequency) and "full correlation" (low frequency) normally occurs between .7 and 1.5 Hz . In some cases, particularly for the vertical component (w-w cross spectrum), the cross spectral density becomes very small again at low frequencies.

(4) From the analysis of the spatial characteristics the following conclusions may be drawn:

(a) The data presented for the confirmation of Taylor's Hypothesis (Table 9) give no conclusive evidence.

(b) From the comparison between the autocorrelation $\tilde{C}_w(\tau_1)$ and the cross correlation $\tilde{C}_{ww}(0)$ presented in Table 8 it is concluded that the time correlation of a vertical gust with itself is approximately equal to the space correlation between two vertical gusts (at a distance of 47 ft., the wingspan of the aircraft), independent of the direction of the flightpath w.r.t. the mean wind.

(c) The analysis of the structure of atmospheric turbulence by estimating the elongation of the turbulence eddies does not provide conclusive evidence.

In view of the above conclusions, the following recommendations for further research are made:

(1) Methods be developed to accurately measure gust spectra in the low frequency range

(2) Further research should be done to determine the character of the phase shift between the gusts in the direction of the wind and the vertical gusts. This is particularly important for better estimation of shear flows at low altitude.

(3) More autocorrelation and cross correlation data are required before further-reaching conclusions on the spatial characteristics can be made.

REFERENCES

1. Reeves, P. M., Campbell, G. S., Ganzer, V. M., and Joppa, R. G., "Development and Application of a Non-Gaussian Atmospheric Turbulence Model for Use in Flight Simulators," NASA Contractor Report CR-2451 (1974).

2. Reeves, P. M., Joppa, R. G., and Ganzer, V. M., "A Non-Gaussian Model of Continuous Atmospheric Turbulence for Use in Aircraft Design," NASA Contractor Report CR-2639 (1976).

3. Burns, A., "Power Spectra of Low Level Atmospheric Turbulence Measured from an Aircraft," Current Paper CP-733 (Aeronautical Research Council, London, 1964).

4. Dryden, H. L., "A Review of the Statistical Theory of Turbulence," in Turbulence.Classic Papers on Statistical Theory (Interscience Publishers, Inc., New York, 1961).

5. von Karman, T., "Progress in the Statistical Theory of Turbulence," in Turbulence.Classic Papers on Statistical Theory (Interscience Publishers, Inc., New York, 1961).

6. Elderkin, C. E., "Experimental Investigation of the Turbulence Structure in the Lower Atmosphere," Dissertation, Department of Atmospheric Sciences, University of Washington, Seattle (1966).

7. Sandusky, R. S., "A Comparison of Theoretically Estimated Stability Derivatives to Values Measured in Wind Tunnel and Flight Tests of the Beechcraft Model D18S," Thesis, Department of Aeronautics & Astronautics, University of Washington, Seattle (1971).

8. Teunissen, H. W., "Characteristics of the Mean Wind and Turbulence in the Planetary Boundary Layer," in Institute for Aerospace Studies Review No. 32, (University of Toronto, Toronto, Canada, 1970).

9. Brown, R. A., "A Secondary Flow Model for the Planetary Boundary Layer, etc.," J. Atmos. Sci. 27:742-757 (1970).

10. LeMone, M. A., "The Structure and Dynamics of Horizontal Roll Vortices in the Planetary Boundary Layer," J. Atmos. Sci. 30:1077-1091 (1973).

11. Taylor, G. I., "The Spectrum of Turbulence," in <u>Turbu-lence.</u> <u>Classic Papers on Statistical Theory</u> (Interscience Publishers, Inc., New York, 1961).

12. Jones, J. W., et al., "Low Altitude Atmospheric Turbulence, LO-LOCAT Phase III," Air Force Flight Dynamics Laboratory Technical Report AFFDL-TR-70-10 (1970).

BIBLIOGRAPHY

1. Blackman, R. B. and Tukey, J. W., The Measurements of Power Spectra (Dover Publications, Inc., New York, 1958).

2. Friedlander, S. K. and Topper, L., Turbulence,Classic Papers on Statistical Theory (Interscience Publishers, Inc., New York, 1961).

3. Gould, D. G. and MacPherson, J. I., "Measurement of the Statistical Properties of Atmospheric Turbulence at Atlitudes Below 1000 ft.," National Research Council of Canada Aeronautical Report LR-567 (National Research Council of Canada, Ottawa, 1973).

4. Lumley, J. L. and Panofsky, H. A., "The Structure of Atmospheric Turbulence," Monographs and Texts in Physics and Astronomy 12 (Interscience Publishers, Inc., New York, 1964).

5. Panofsky, H. A., "Determination of Stress from Wind and Temperature Measurements," Quarterly Journal of the Royal Meteorological Society 89:85-94 (1963).

6. Panchev, S., Random Functions and Turbulence (Pergamon Press, New York, 1971).

7. Plate, E. J., Aerodynamic Characteristics of Atmospheric Boundary Layers," Atomic Energy Commission, Critical Review Series (1971).

8. Tennekes, H. and Lumley, J. L., A First Course in Turbulence (The MIT Press, Cambridge, Mass., 1972).

	Wing	Horizontal Tail	Vertical Tail
Reference Area, ft^2	351.58	65.4*	33.58**
Span, ft	47.64	15.0	5.42
Mean Aerodynamic Chord, ft	8.06	5.16	NA

*   including elevator

**   total, both tails

TABLE 1.   BEECHCRAFT D-18S PRINCIPAL DIMENSIONS

Mode	Characteristic	Estimated Value		
		Theory	Windtunnel	Flight test
Phugoid	Roots: Real n Imaginary ω	− .016 + .166	− .016 + .163	− .010 .150
	Period T sec	37.9	38.6	42.0
	Time to Half Amplitude, sec	41.8	42.3	69.0
Short Period	Roots: Real n Imaginary ω	− 3.01 3.15	− 2.92 2.71	--- ---
	Period T, sec	1.99	2.32	
	Time to Half Amplitude, sec	.23	.24	
Spiral	Root n	+ .019	− .010	+ .059
	Time Constant τ	51.63	---	17.05
	Time to Double Amplitude, sec	35.79	---	11.8
Rolling Convergence	Root n	− 4.17	− 4.30	---
	Time Constant τ	.24	.23	---
	Time to Half Amplitude, sec	.17	.16	---
Dutch Roll	Roots: Real n Imaginary ω	−.28 2.4	−.22 2.2	--- ---
	Period T, sec	2.61	2.92	---
	Time to Half Amplitude, sec	2.43	3.19	---

TABLE   2.   CHARACTERISTICS OF THE NATURAL MODES OF THE BEECHCRAFT   D-18S.

Flight	Date	Winds	Instrument Op. Verification	Motions at Altitude	Data Runs	Area
			Test Items Performed			
1-5	Various Instrumentation Check Flights					
6	6/13/73	230/05			4	Straits of Juan de Fuca
7	8/9/73	225/10			1	Hood Canal
8	8/21/73	030/10G15			4	Straits of Juan de Fuca
9	7/25/74	210/05			5	Pt. Angeles
10	8/1/74	030/08			1	Hood Canal
11	8/15/74		Aborted due to malfunctioning pressure transducers.			
12	8/26/74	310/06			2	Straits of Juan de Fuca
13 A	9/6/74	310/06				Puget Sound
13 B	9/7/74	310/07				Puget Sound
14	10/18/74	250/07				Puget Sound
15	11/25/74	260/18G24			4	Straits of Juan de Fuca
16	12/17/74	080/06			4	Straits of Juan de Fuca

TABLE   3.   FLIGHTS PERFORMED WITH BEECHCRAFT D-18S N4545

Ch. No.	Measured Variable	Instrument	Make	Model	Range
1	$\Delta p_{x \text{ Left}}$	diff. pressure transducer	Statham	PM283TC	± .15 psid
2	$\Delta p_{y \text{ Left}}$	diff. pressure transducer	Statham	PM283TC	± .15 psid
3	$\Delta p_{z \text{ Left}}$	diff. pressure transducer	Statham	PM283TC	± .15 psid
4	$\Delta p_{x \text{ Right}}$	diff. pressure transducer	Statham	PM283TC	± .15 psid
5	$\Delta p_{y \text{ Right}}$	diff. pressure transducer	Statham	PM283TC	± .15 psid
6	$\Delta p_{z \text{ Right}}$	diff. pressure transducer	Statham	PM283TC	± .15 psid
7	roll rate p	rate gyro	Honeywell	JG7005A-11	± 6 deg/sec
8	pitch rate q	rate gyro	Honeywell	JG7005A-11	± 6 deg/sec
9	yaw rate r	rate gyro	Honeywell	JG7005A-11	± 6 deg/sec
10	lateral acceleration a_y	accelerometer	Statham	A301TC	± 1 g
11	vertical acceleration a_z	accelerometer	Statham	NA1 D47	± 3g
12	roll angle ϕ	vertical gyro	Honeywell	JG7044A-17	± 85°

TABLE 4.   DATA INSTRUMENTS.

FLIGHT 15/RUN 1 INITIAL CONDITIONS

```
TEST LOCATION                     STRAITS JUAN DE FUCA
LOCAL ALTIMETER SETTING                30.29   IN HG
WIND DIRECTION                           290   MAGNETIC
WIND VELOCITY                             20   KNOTS
DIRECTION OF FLIGHT                       290   MAGNETIC
RELATIVE WIND COMPONENTS
                        34   FPS, FROM AHEAD
                         0   FPS,

CALIBRATED AIRSPEED                      132   MPH
PRESSURE ALTITUDE                        200   FT
HEIGHT ABOVE SURFACE                     200   FT
OUTSIDE AIR TEMPERATURE                   48   DEG F
ATMOSPHERIC DENSITY (RO)             .002411   SL/CU FT
AIRCRAFT TRUE AIRSPEED                 192.2   FPS
DYNAMIC PRESSURE                       44.55   PSF
```

FLIGHT 15/RUN 2 INITIAL CONDITIONS

```
TEST LOCATION                     STRAITS JUAN DE FUCA
LOCAL ALTIMETER SETTING                30.29   IN HG
WIND DIRECTION            FROM          290   MAGNETIC
WIND VELOCITY                             20   KNOTS
DIRECTION OF FLIGHT                       115   MAGNETIC
RELATIVE WIND COMPONENTS
                        34   FPS, FRM BEHIND
                         3   FPS, FROM RIGHT

CALIBRATED AIRSPEED                      131   MPH
PRESSURE ALTITUDE                        200   FT
HEIGHT ABOVE SURFACE                     200   FT
OUTSIDE AIR TEMPERATURE                   48   DEG F
ATMOSPHERIC DENSITY (RO)             .002411   SL/CU FT
AIRCRAFT TRUE AIRSPEED                 190.8   FPS
DYNAMIC PRESSURE                       43.87   PSF
```

TABLE   5A.   FLIGHT CONDITIONS, FLIGHT #15
                 RUNS   1   AND   2.

FLIGHT 15/RUN 3 INITIAL CONDITIONS

```
TEST LOCATION                     STRAITS JUAN DE FUCA
LOCAL ALTIMETER SETTING                30.29   IN HG
WIND DIRECTION                           290   MAGNETIC
WIND VELOCITY                             20   KNOTS
DIRECTION OF FLIGHT                      220   MAGNETIC
RELATIVE WIND COMPONENTS
                          12   FPS, FROM AHEAD
                          32   FPS, FROM RIGHT

CALIBRATED AIRSPEED                      130   MPH
PRESSURE ALTITUDE                        200   FT
HEIGHT ABOVE SURFACE                     200   FT
OUTSIDE AIR TEMPERATURE                   48   DEG F
ATMOSPHERIC DENSITY (RO)             .002411   SL/CU FT
AIRCRAFT TRUE AIRSPEED                189.3   FPS
DYNAMIC PRESSURE                      43.21   PSF
```

FLIGHT 15/RUN 4 INITIAL CONDITIONS

```
TEST LOCATION                     STRAITS JUAN DE FUCA
LOCAL ALTIMETER SETTING                30.29   IN HG
WIND DIRECTION              FROM         290   MAGNETIC
WIND VELOCITY                             20   KNOTS
DIRECTION OF FLIGHT                       30   MAGNETIC
RELATIVE WIND COMPONENTS
                           6   FPS, FRM BEHIND
                          33   FPS, FROM LEFT

CALIBRATED AIRSPEED                      132   MPH
PRESSURE ALTITUDE                        200   FT
HEIGHT ABOVE SURFACE                     200   FT
OUTSIDE AIR TEMPERATURE                   48   DEG F
ATMOSPHERIC DENSITY (RO)             .002411   SL/CU FT
AIRCRAFT TRUE AIRSPEED                192.2   FPS
DYNAMIC PRESSURE                      44.55   PSF
```

TABLE   5B.   FLIGHT CONDITIONS, FLIGHT #15
                  RUNS   3   AND   4.

FLIGHT 16/RUN 1 INITIAL CONDITIONS

```
TEST LOCATION                 WEST OF SAN JUAN ISLANDS
LOCAL ALTIMETER SETTING            30.12  IN HG
WIND DIRECTION          FROM        255  MAGNETIC
WIND VELOCITY                        10  KNOTS
DIRECTION OF FLIGHT                  255  MAGNETIC
RELATIVE WIND COMPONENTS
                          17  FPS, FROM AHEAD
                           0  FPS,
```

```
CALIBRATED AIRSPEED                    132  MPH
PRESSURE ALTITUDE                      100  FT
HEIGHT ABOVE SURVACE                     95  FT
OUTSIDE AIR TEMPERATURE                  58  DEG F
ATMOSPHERIC DENSITY (RO)          .002373  SL/CU FT
AIRCRAFT TRUE AIRSPEED               193.8  FPS
DYNAMIC PRESSURE                     44.55  PSF
```

FLIGHT 16/RUN 2 INITIAL CONDITIONS

```
TEST LOCATION                 WEST OF SAN JUAN ISLANDS
LOCAL ALTIMETER SETTING            30.12  IN HG
WIND DIRECTION          FROM        255  MAGNETIC
WIND VELOCITY                        10  KNOTS
DIRECTION OF FLIGHT                   95  MAGNETIC
RELATIVE WIND COMPONENTS
                          16  FPS, FRM BEHIND
                           6  FPS, FROM RIGHT
```

```
CALIBRATED AIRSPEED                    132  MPH
PRESSURE ALTITUDE                      110  FT
HEIGHT ABOVE SURFACE                    105  FT
OUTSIDE AIR TEMPERATURE                  58  DEG F
ATMOSPHERIC DENSITY (RO)          .002372  SL/CU FT
AIRCRAFT TRUE AIRSPEED               193.8  FPS
DYNAMIC PRESSURE                     44.55  PSF
```

TABLE 6A.   FLIGHT CONDITIONS, FLIGHT #16
                  RUNS 1 AND 2.

FLIGHT 16/RUN 3 INITIAL CONDITIONS

```
TEST LOCATION                    WEST OF SAN JUAN ISLANDS
LOCAL ALTIMETER SETTING               30.12  IN HG
WIND DIRECTION           FROM           255  MAGNETIC
WIND VELOCITY                            10  KNOTS
DIRECTION OF FLIGHT                      350  MAGNETIC
RELATIVE WIND COMPONENTS
                           1  FPS, FRM BEHIND
                          17  FPS, FROM LEFT

CALIBRATED AIRSPEED                     133  MPH
PRESSURE ALTITUDE                       105  FT
HEIGHT ABOVE SURFACE                    100  FT
OUTSIDE AIR TEMPERATURE                  58  DEG F
ATMOSPHERIC DENSITY (RO)            .002373  SL/CU FT
AIRCRAFT TRUE AIRSPEED                195.2  FPS
DYNAMIC PRESSURE                      45.22  PSF
```

FLIGHT 16/RUN 4 INITIAL CONDITIONS

```
TEST LOCATION                    WEST OF SAN JUAN ISLANDS
LOCAL ALTIMETER SETTING               30.12  IN HG
WIND DIRECTION           FROM           255  MAGNETIC
WIND VELOCITY                            10  KNOTS
DIRECTION OF FLIGHT                     170  MAGNETIC
RELATIVE WIND COMPONENTS
                           1  FPS, FROM AHEAD
                          17  FPS, FROM RIGHT

CALIBRATED AIRSPEED                     130  MPH
PRESSURE ALTITUDE                       100  FT
HEIGHT ABOVE SURFACE                     95  FT
OUTSIDE AIR TEMPERATURE                  58  DEG F
ATMOSPHERIC DENSITY (RO)            .002373  SL/CU FT
AIRCRAFT TRUE AIRSPEED                190.8  FPS
DYNAMIC PRESSURE                      43.21  PSF
```

TABLE 6B.   FLIGHT CONDITIONS, FLIGHT #16
                 RUNS 3 AND 4.

Flight	γ $(^\circ C/100\ m)$	$\frac{\partial \bar{u}}{\partial z}$ $\left(\frac{m/sec}{100\ m}\right)$	T $(^\circ K)$	$R_i = \frac{g(\Gamma - \gamma)}{T\ \frac{\partial \bar{u}}{\partial z}^2}$
15	1.5	.5	282.5	- .069
16	1.2	.6	283.1	- .019

$$\Gamma = 1^\circ C/100\ m$$

$$g = 9.81\ m/sec^2$$

TABLE 7.   CALCULATION OF THE GRADIENT
RICHARDSON NUMBER FOR FLIGHT
15 AND #16.

Flight	Run		Auto Correlation $\tilde{C}_i(\tau_1)$ (left & right)		Run		Cross Correlation $\tilde{C}_{ii}(0)$	
	#	Direction	Component		#	Direction	Component	
15	2	down-wind	u_L	.98	3	cross-wind	$v_L - v_R$	.53
			u_R	.90	4	cross-wind	$v_L - v_R$	.71
	4	cross-wind	v_L	.62	1	upwind	$u_L - u_R$	.87
			v_R	.66	2	down-wind	$u_L - u_R$	.97

TABLE 8. COMPARISON BETWEEN THE AUTOCORRELATION AND THE CROSS CORRELATION OF LONGITUDINAL AND LATERAL GUSTS.

Flight	Run		Autocorrelation		Cross Correlation	
	#	Direction	Component	$\tilde{C}_i(\tau_1)$	Component	$\tilde{C}_{ii}(0)$
15	1	upwind	ω_L	.43	$\omega_L - \omega_R$	.51
			ω_R	.70		
	2	down-wind	ω_L	.13	$\omega_L - \omega_R$	.17
			ω_R	.18		
	3	cross-wind	ω_L	.32	$\omega_L - \omega_R$	.45
			ω_R	.34		
	4	cross-wind	ω_L	.82	$\omega_L - \omega_R$	.77
			ω_R	.75		

TABLE 9. COMPARISON BETWEEN THE AUTOCORRELATION AND THE CROSS CORRELATION OF VERTICAL GUSTS.

41

Flight	Run	Scale Length					
		L_{u_L}	L_{v_L}	L_{w_L}	L_{u_R}	L_{v_R}	L_{w_R}
15	upwind	205	113	53	234	125	51
	downwind	243	130	83	251	140	72
	crosswind	260	128	62	240	111	54
	crosswind	299	205	119	353	183	99
16	upwind	165	140	52	205	135	44
	downwind	294	171	90	359	159	84
	crosswind	249	239	93	262	219	91
	crosswind	135	147	81	170	229	68

TABLE 10. SCALE LENGTHS OF ATMOSPHERIC TURBULENCE (ft).
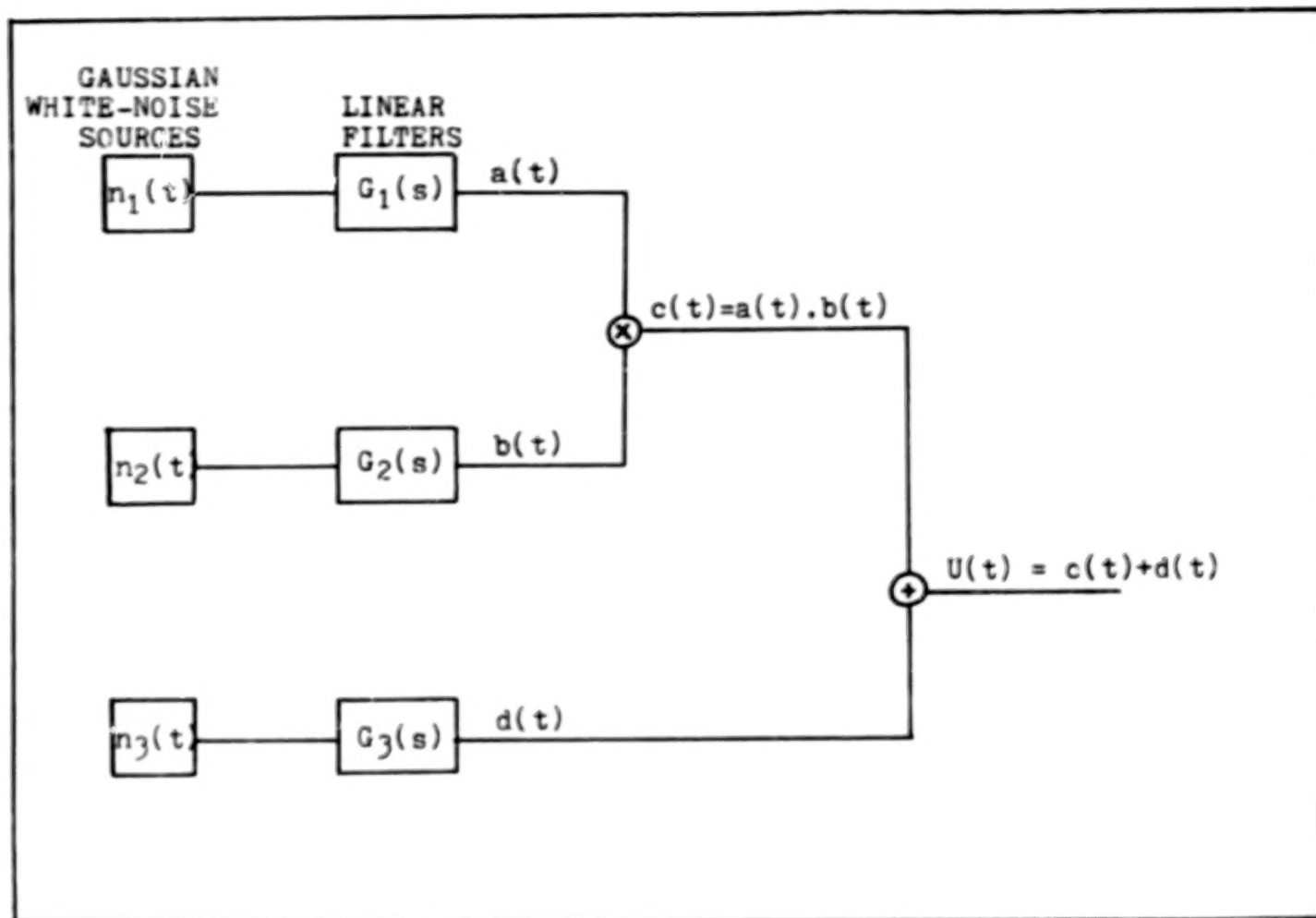
FIGURE 1.   THE NON-GAUSSIAN TURBULENCE SIMULATION MODEL

43

FIGURE 2.   THE TEST AIRCRAFT, BEECHCRAFT D-18 S, N-4545
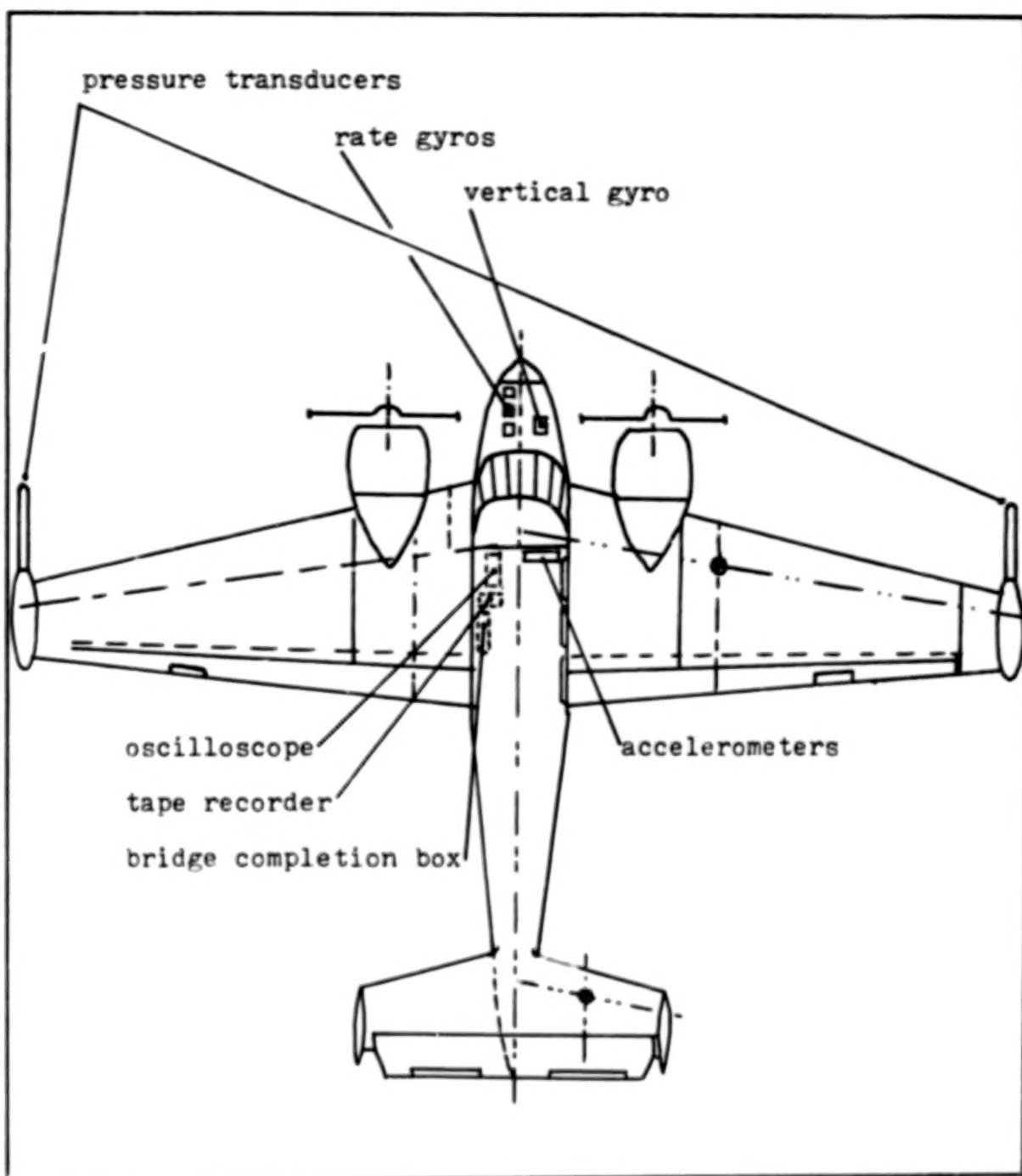
FIGURE 3.   INSTRUMENTATION
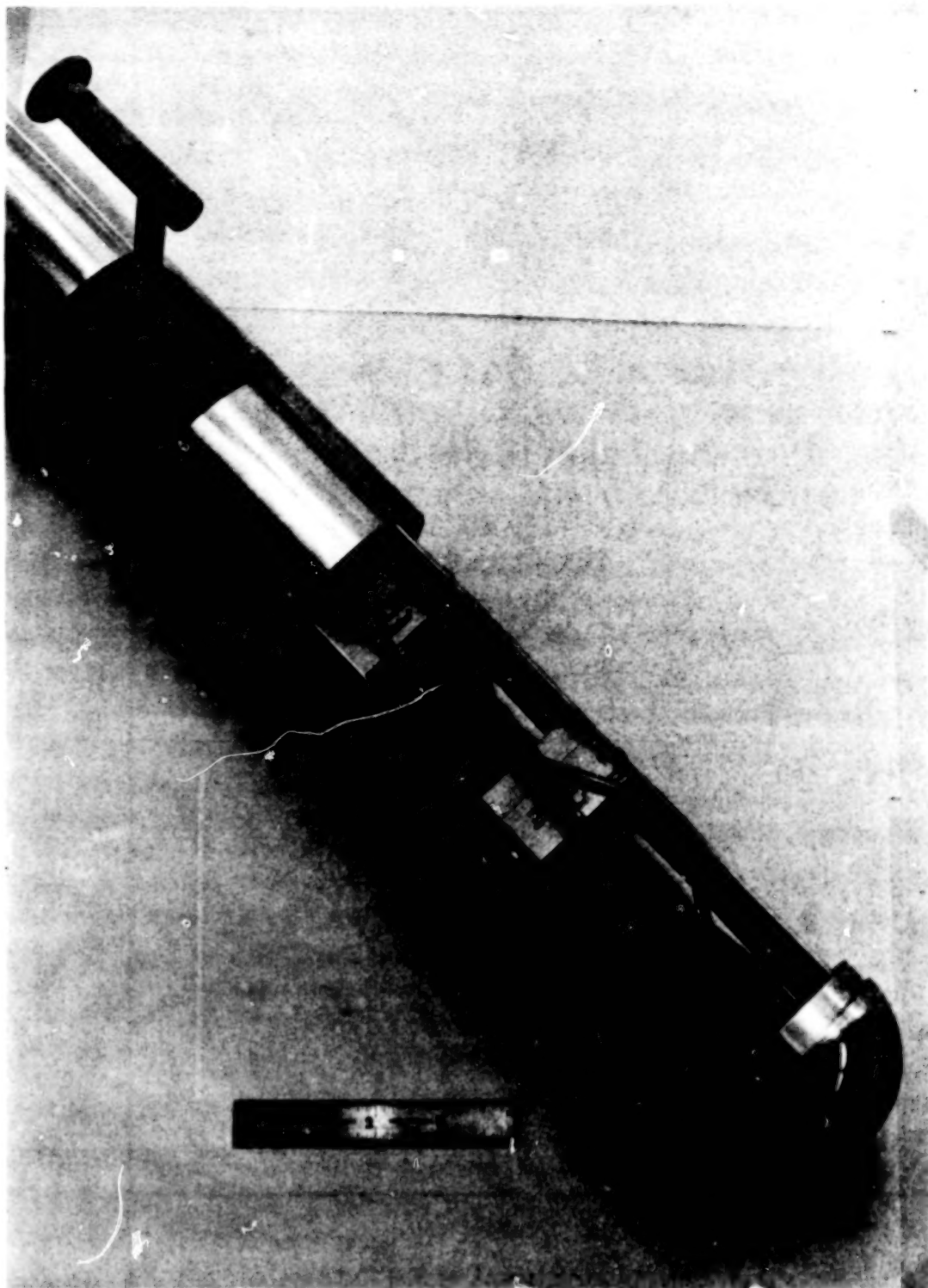
FIGURE   4.   PROBEHEAD WITH PRESSURE TRANSDUCERS
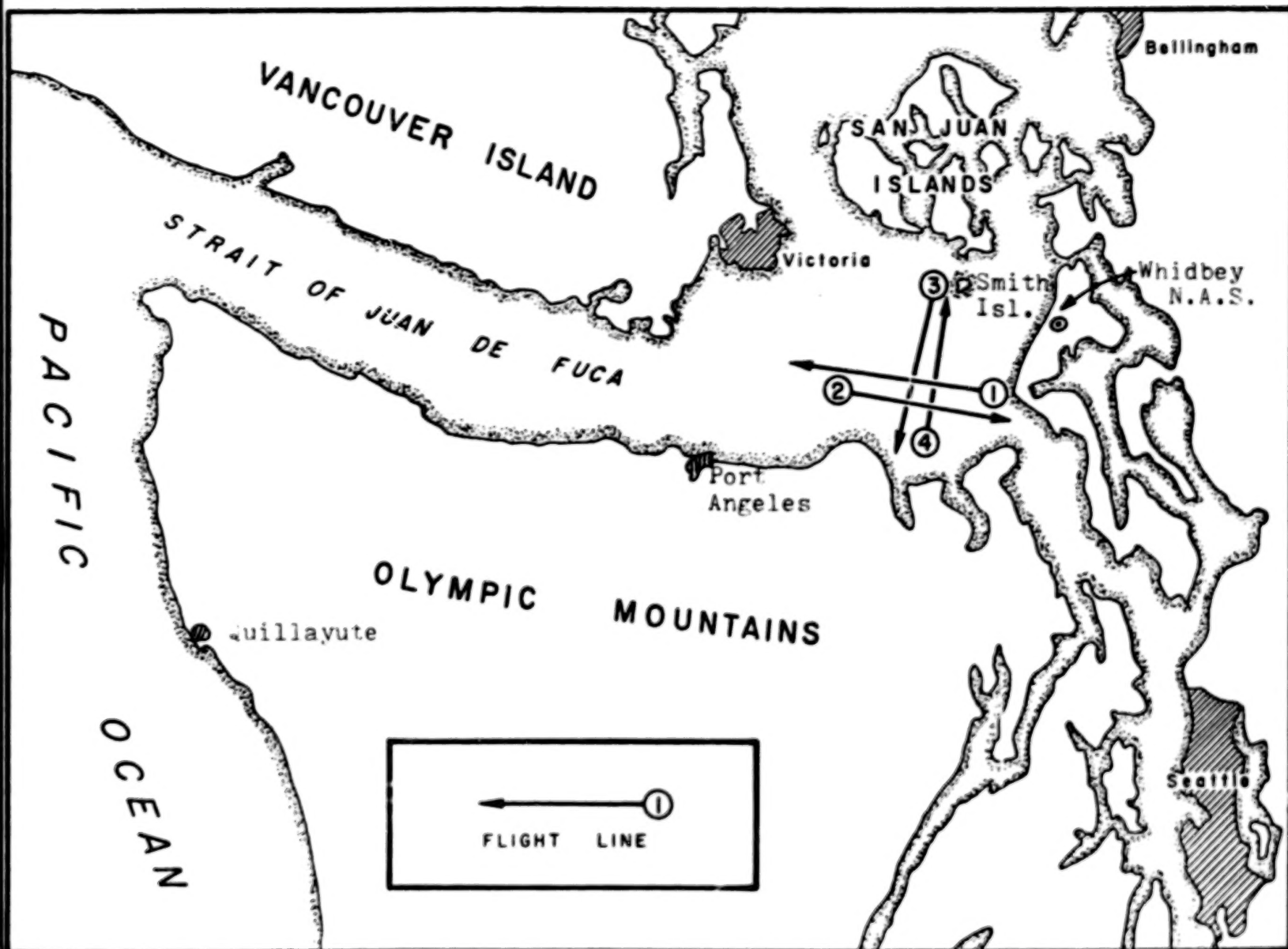
FIGURE 5. GENERAL TEST AREA FOR ATMOSPHERIC TURBULENCE DATA FLIGHTS

47

San Juan Islands

290/8

Victoria

③

Smith Island
270/20

Whidbey
⊙ N.A.S.
260/9

②   ①

④

270/14

Port Angeles

2000

4000

OLYMPIC

MTS.

4000

6000

2000
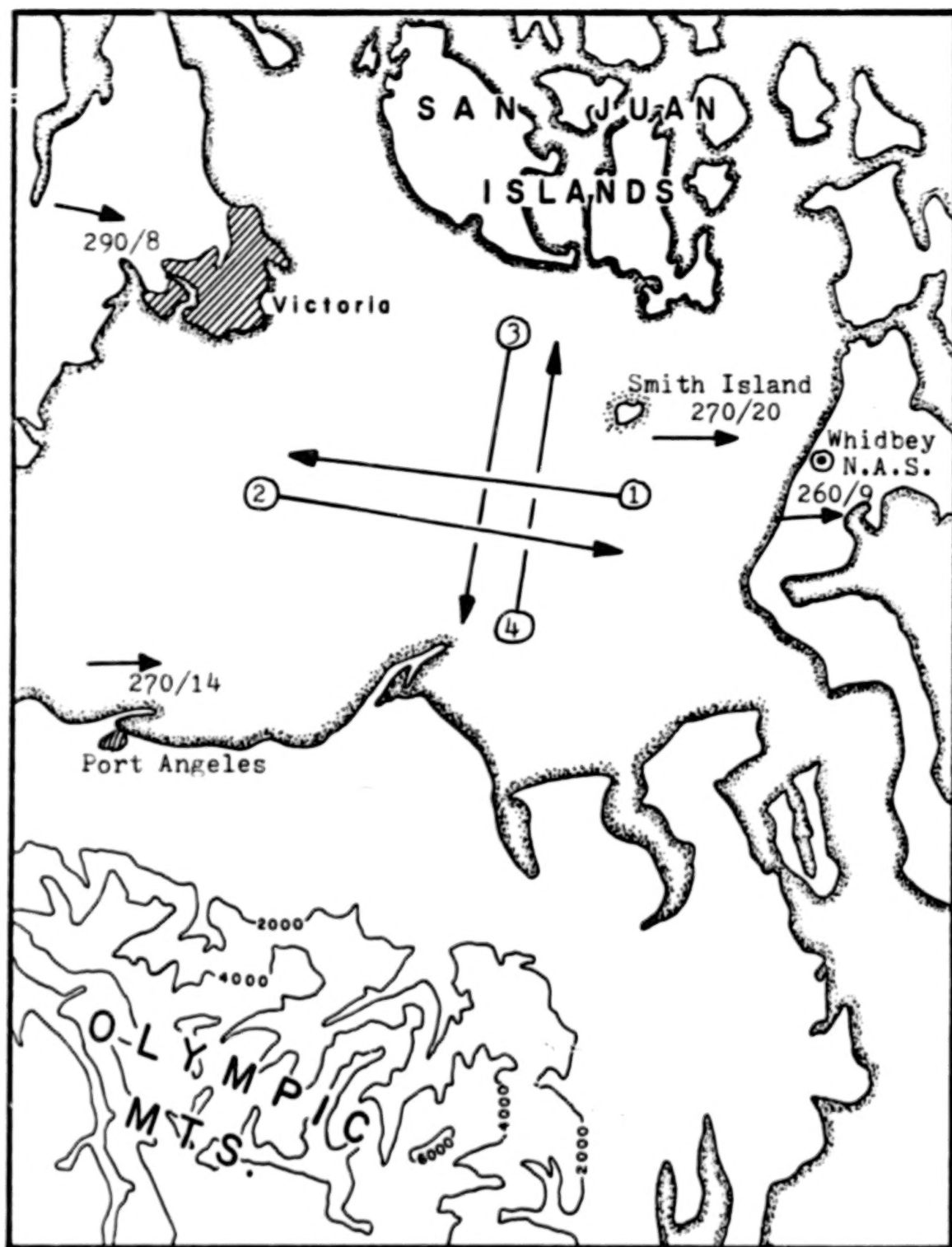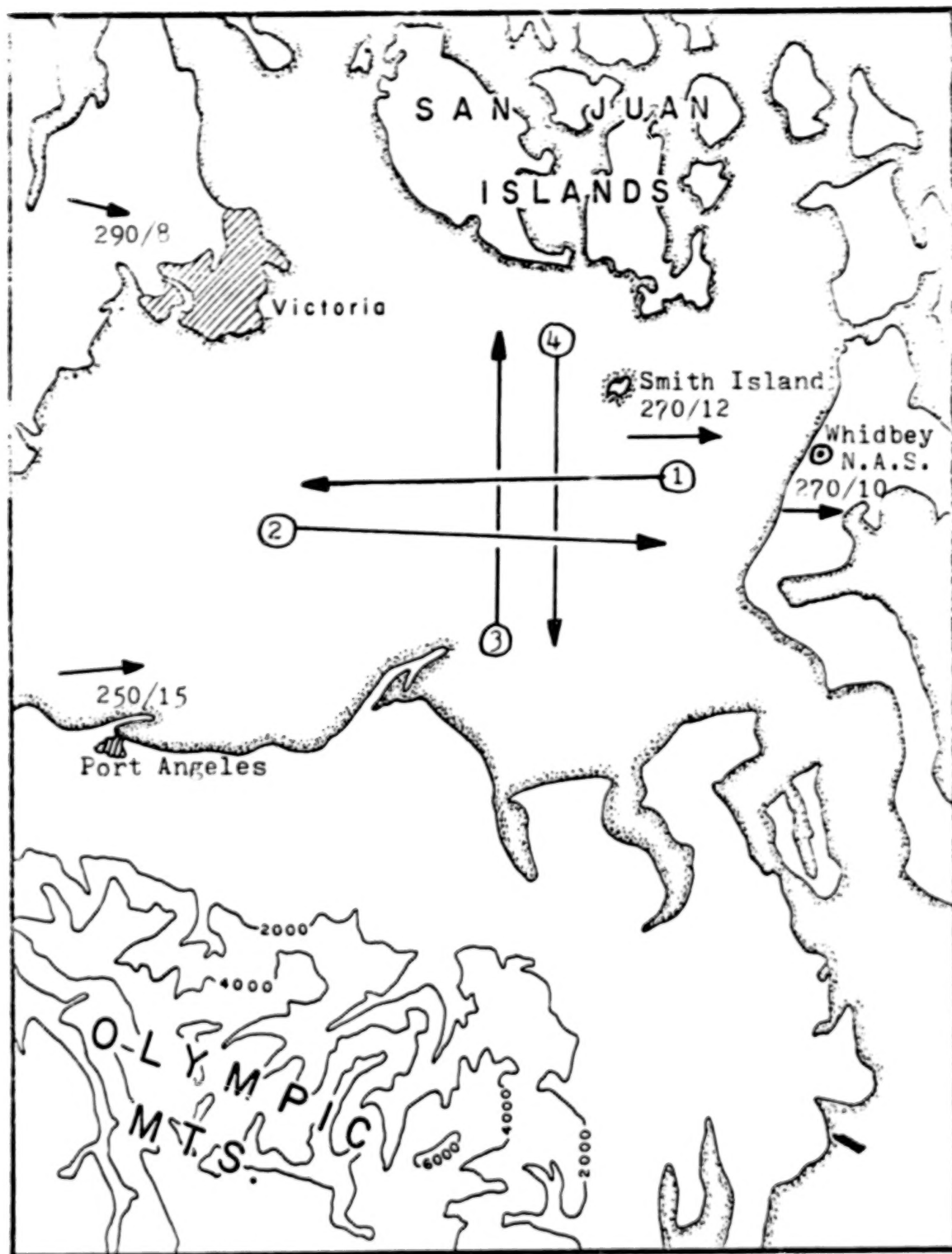
FIGURE 7.   FLIGHT PATTERN AND WIND DATA, FLIGHT 16
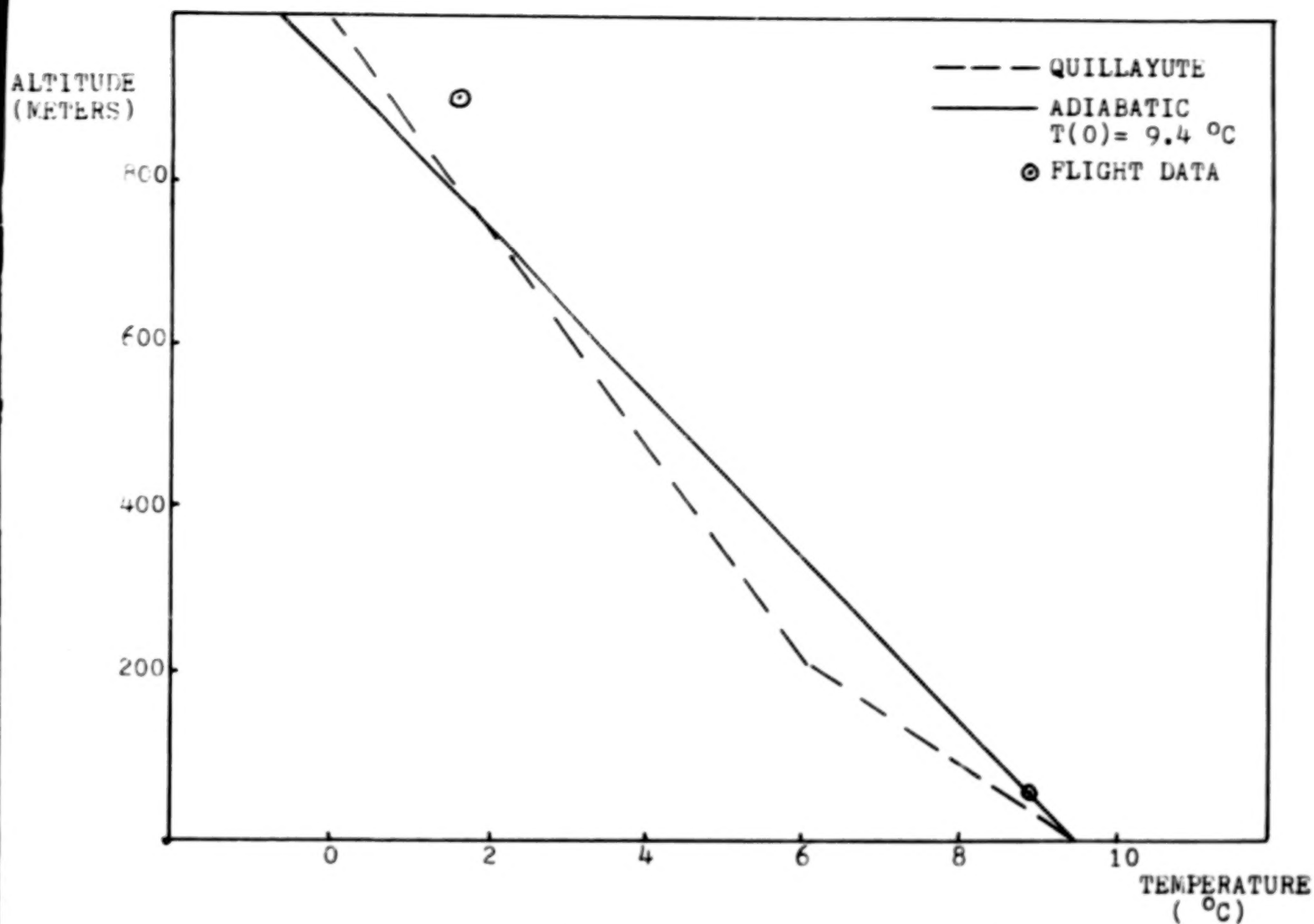
FIGURE 8. TEMPERATURE VS. ALTITUDE, FLIGHT 15

50
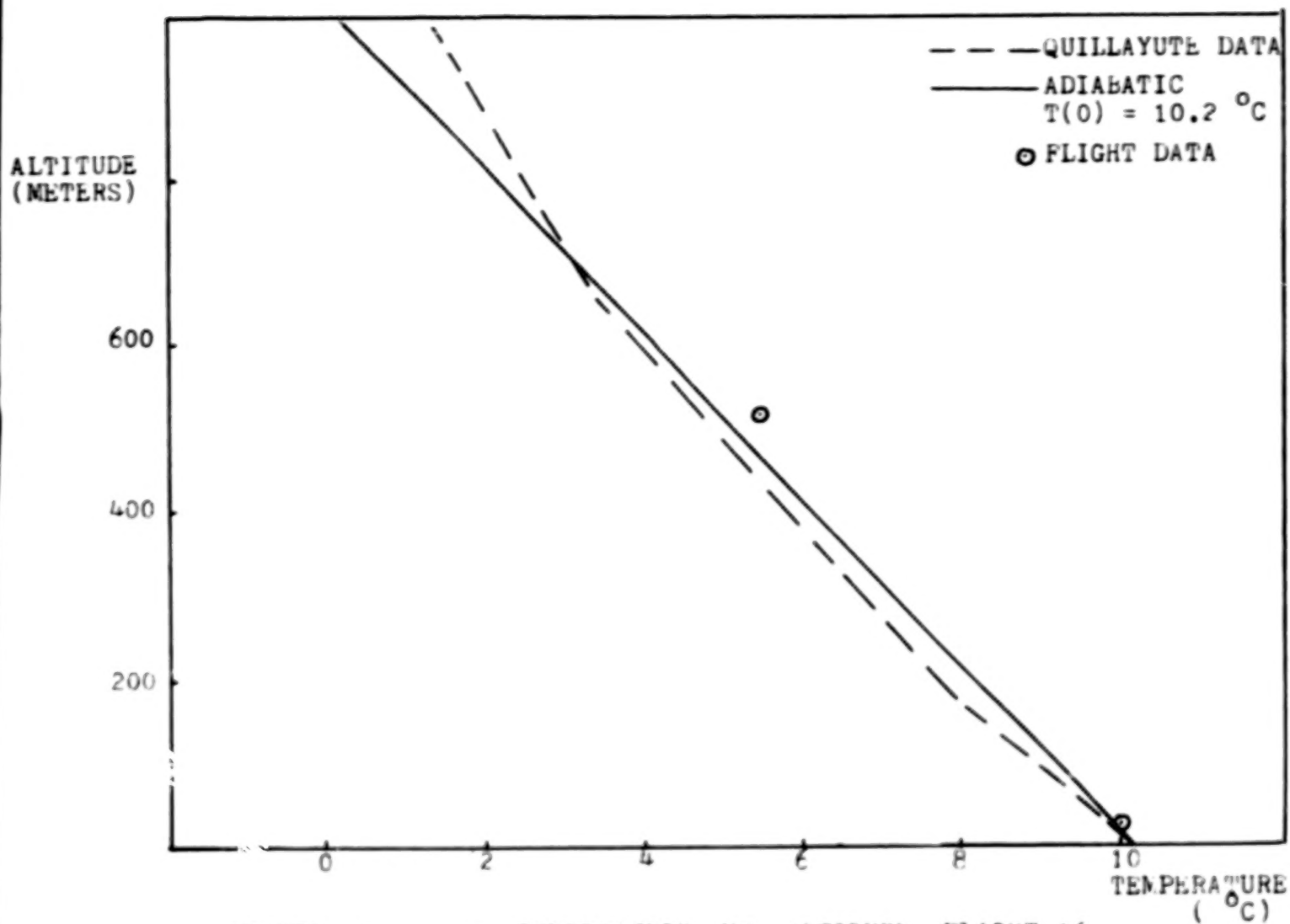
FIGURE 5.   : TEMPERATURE VS. ALTITUDE, FLIGHT 16

51
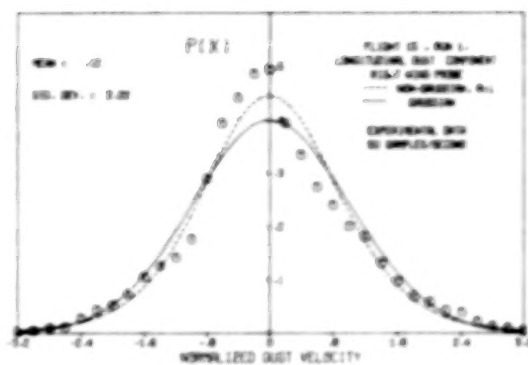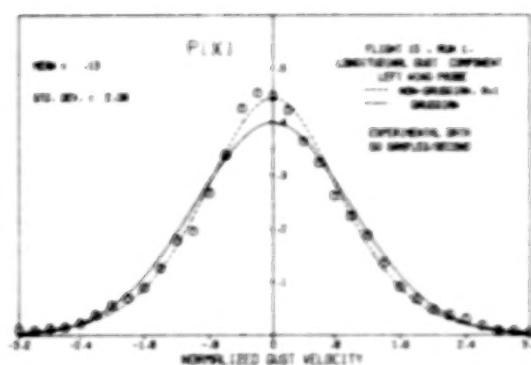
a) LONGITUDINAL COMPONENTS
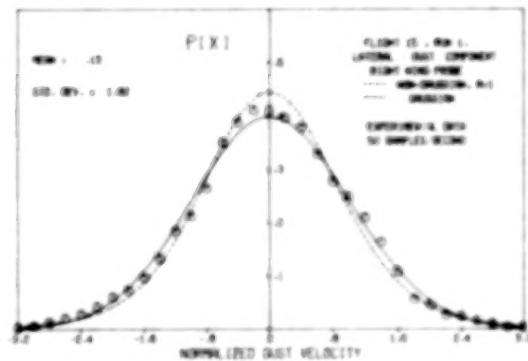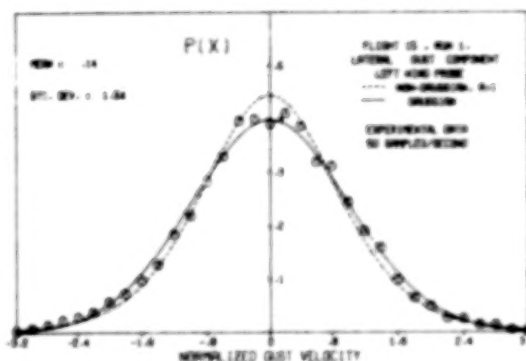
b) LATERAL COMPONENTS
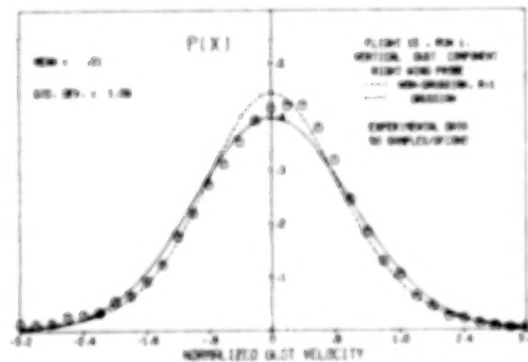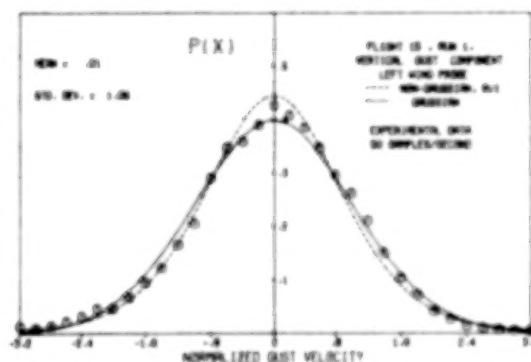
c) VERTICAL COMPONENTS

FIGURE 10. PROBABILITY DENSITY
DISTRIBUTION. FLIGHT 15 RUN I

a) LONGITUDINAL COMPONENTS

b) LATERAL COMPONENTS

c) VERTICAL COMPONENTS

FIGURE II. PROBABILITY DENSITY
DISTRIBUTION. FLIGHT I5 RUN 2
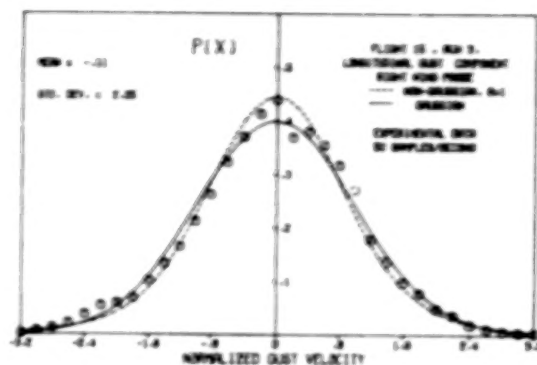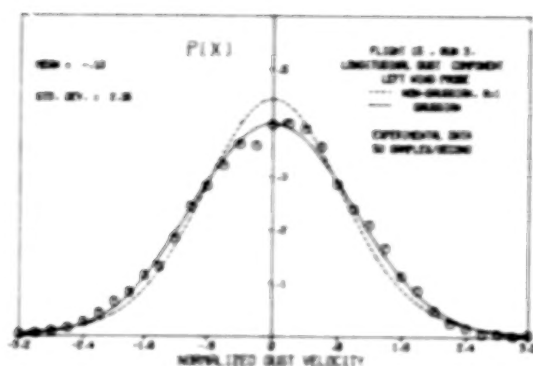
a) LONGITUDINAL COMPONENTS

b) LATERAL COMPONENTS

c) VERTICAL COMPONENTS

FIGURE 12. PROBABILITY DENSITY
DISTRIBUTION. FLIGHT 15 RUN 3
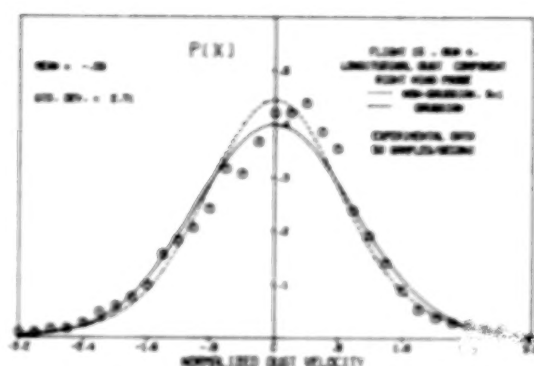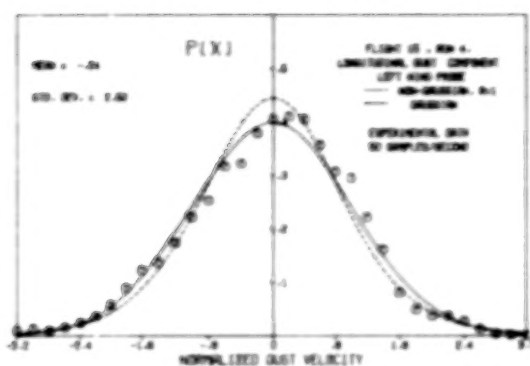
a) LONGITUDINAL COMPONENTS
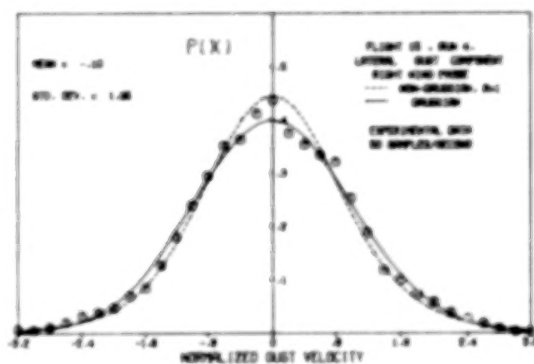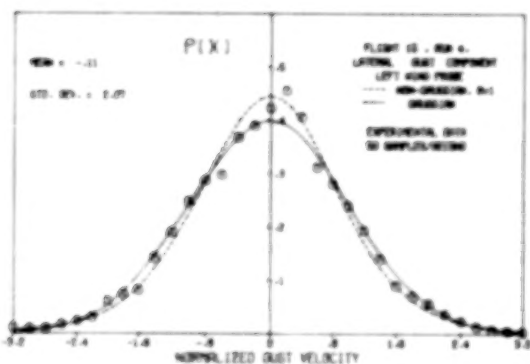
b) LATERAL COMPONENTS
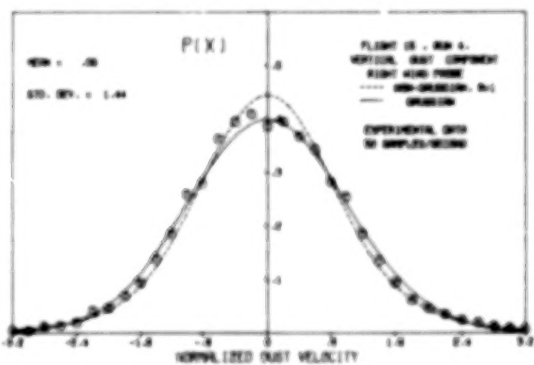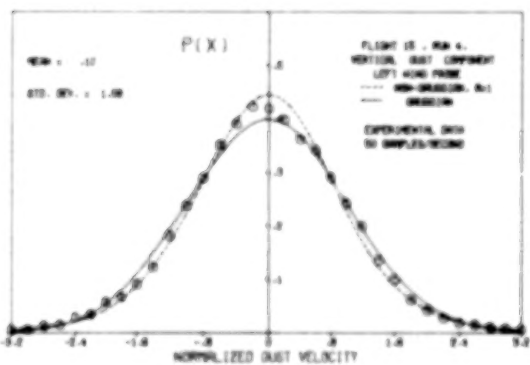
c) VERTICAL COMPONENTS

FIGURE 13. PROBABILITY DENSITY
DISTRIBUTION. FLIGHT 15 RUN 4
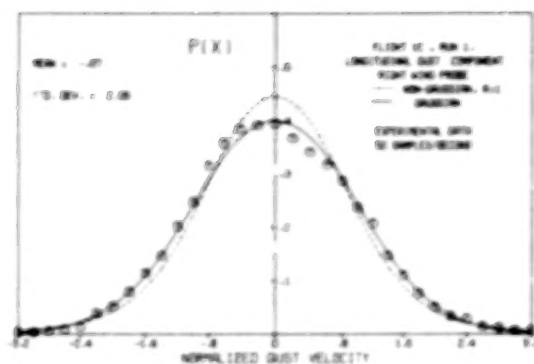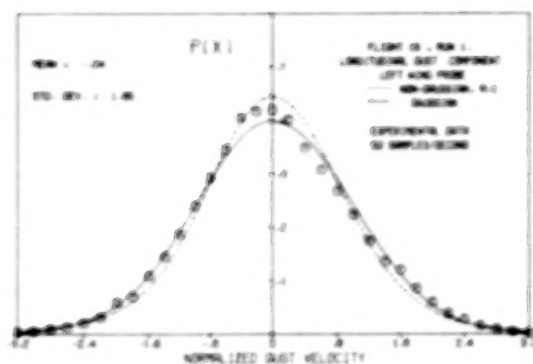
a) LONGITUDINAL COMPONENTS
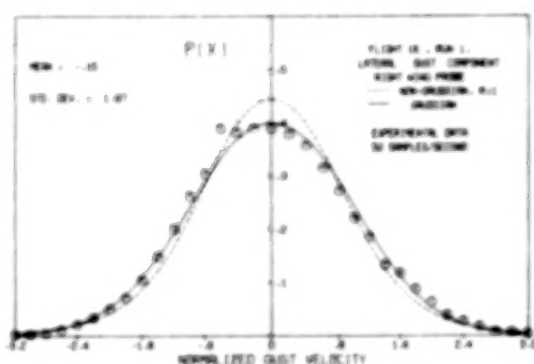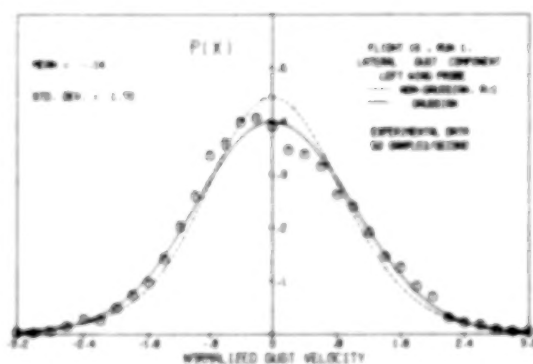
b) LATERAL COMPONENTS
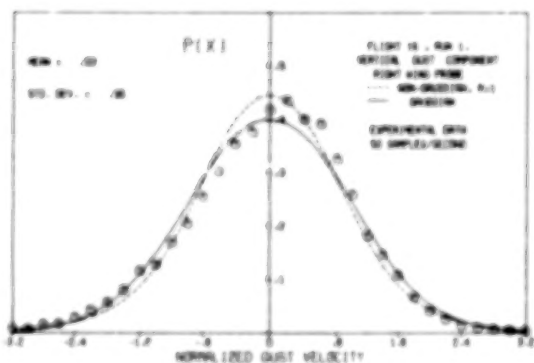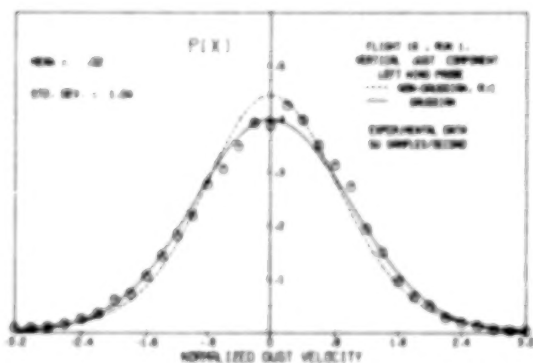
c) VERTICAL COMPONENTS

FIGURE 14. PROBABILITY DENSITY
DISTRIBUTION. FLIGHT 16 RUN 1
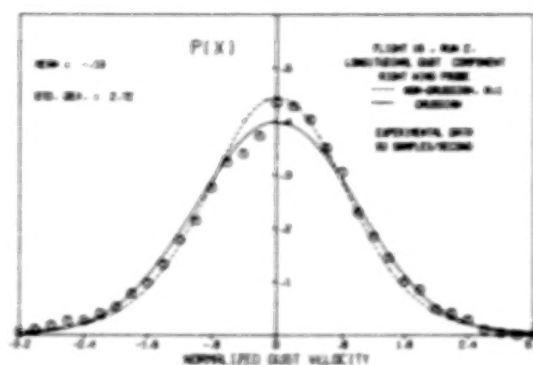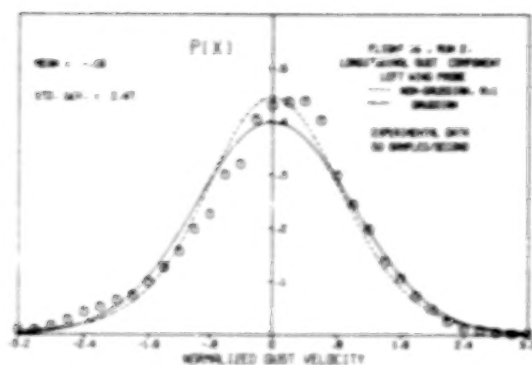
a) LONGITUDINAL COMPONENTS
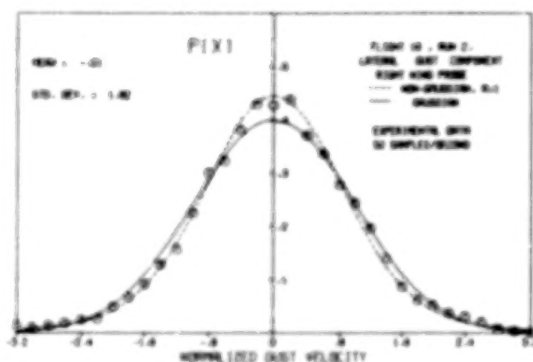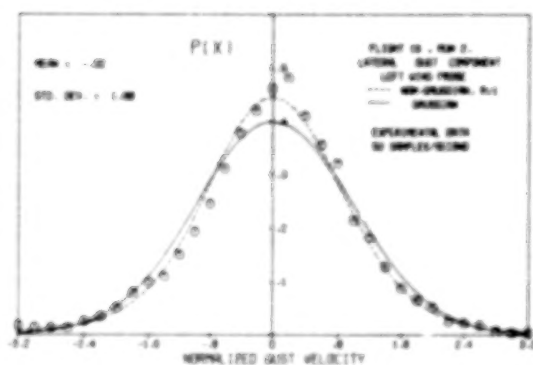
b) LATERAL COMPONENTS
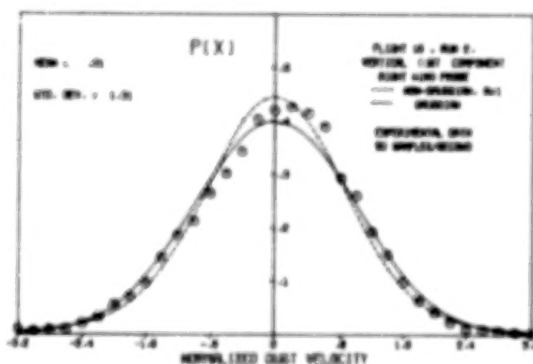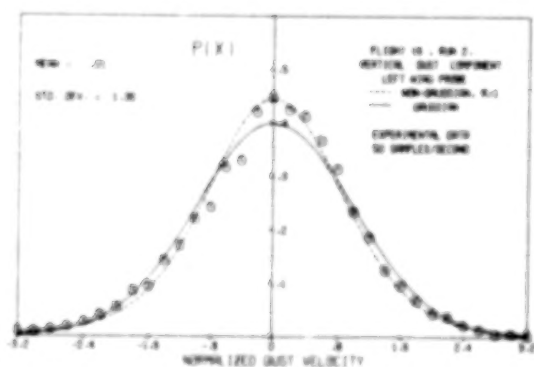
c) VERTICAL COMPONENTS

FIGURE 15. PROBABILITY DENSITY
DISTRIBUTION. FLIGHT 16 RUN 2
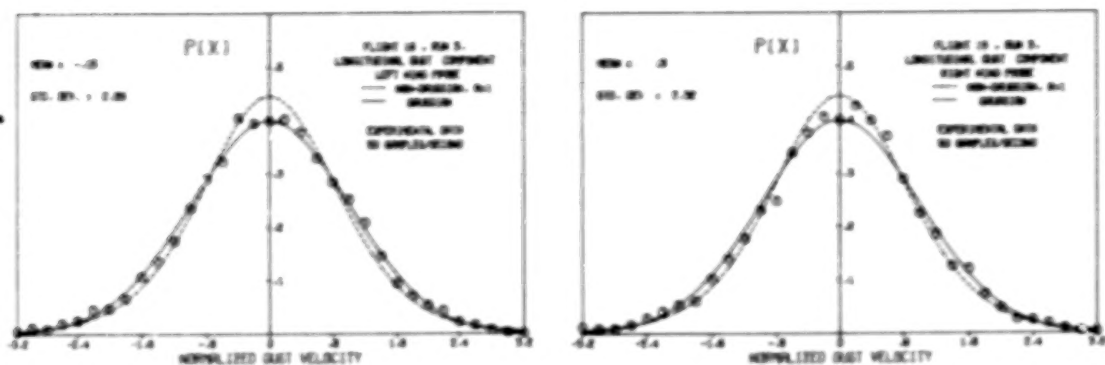
a) LONGITUDINAL COMPONENTS
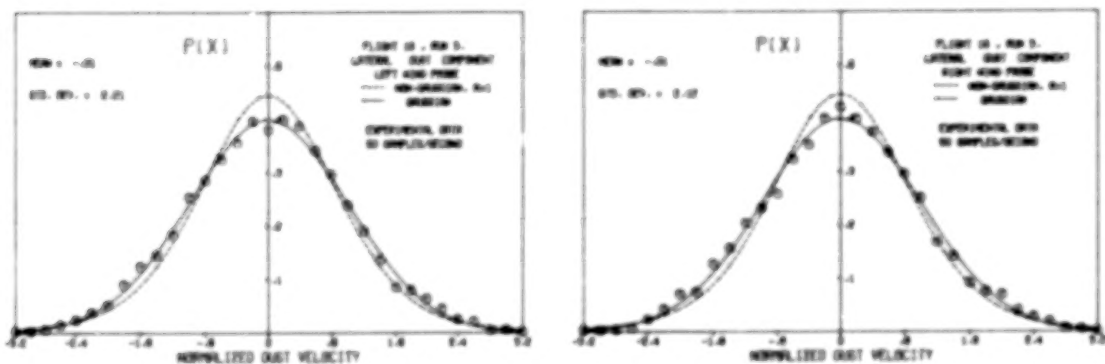
b) LATERAL COMPONENTS
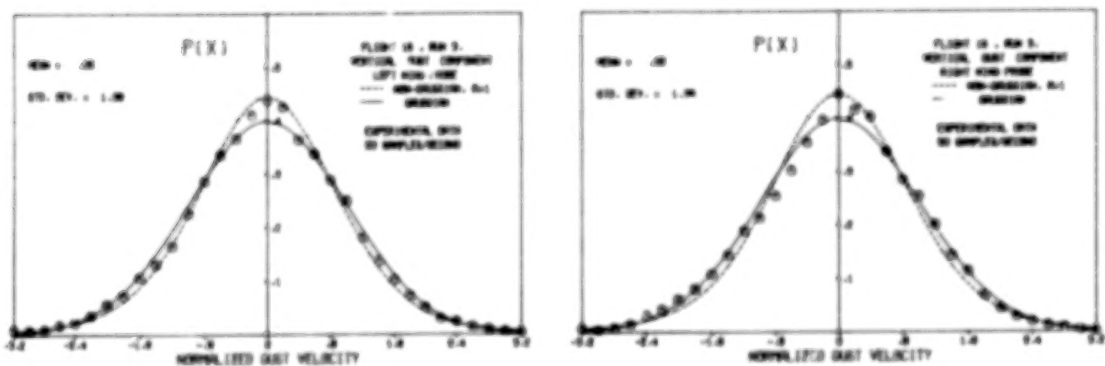
c) VERTICAL COMPONENTS

FIGURE 16. PROBABILITY DENSITY
DISTRIBUTION. FLIGHT 16 RUN 3
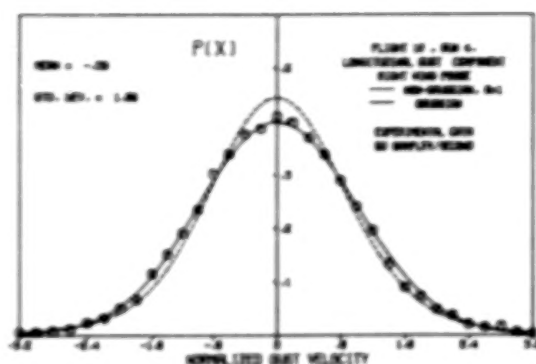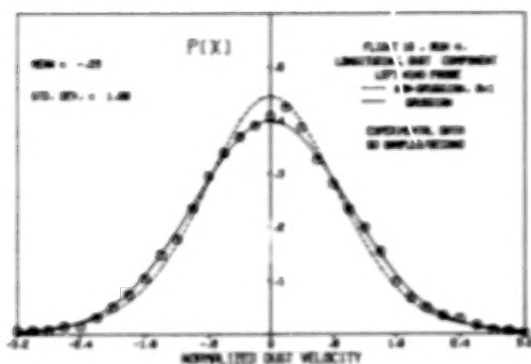
a) LONGITUDINAL COMPONENTS
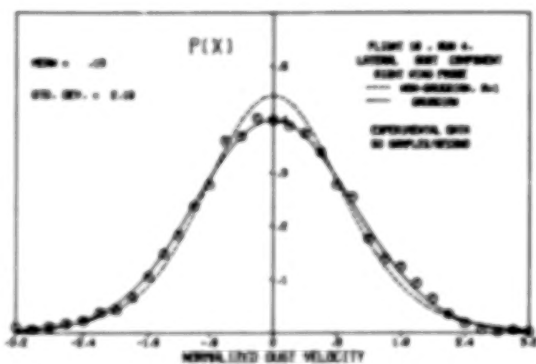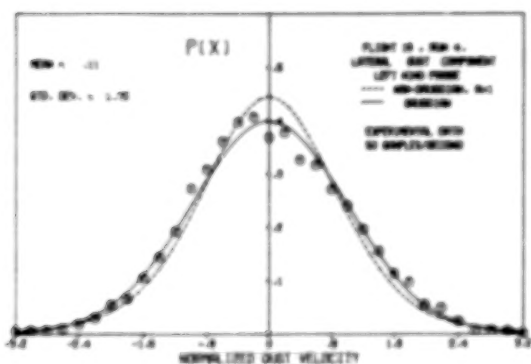
b) LATERAL COMPONENTS
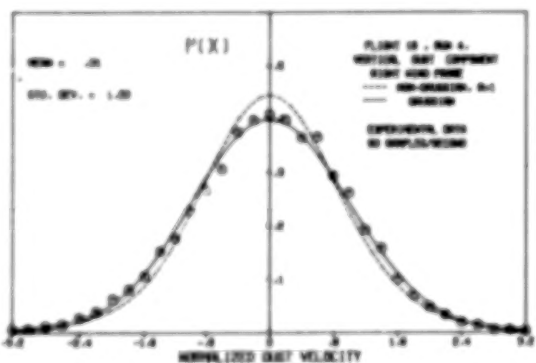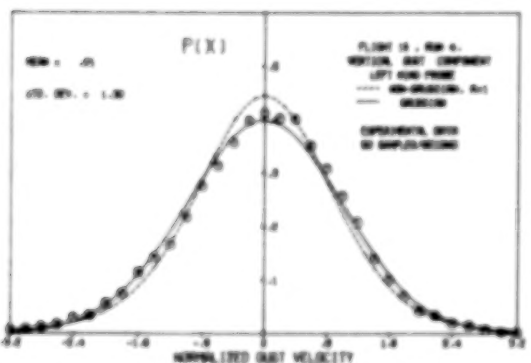
c) VERTICAL COMPONENTS

FIGURE 17. PROBABILITY DENSITY
DISTRIBUTION. FLIGHT 16 RUN 4

59
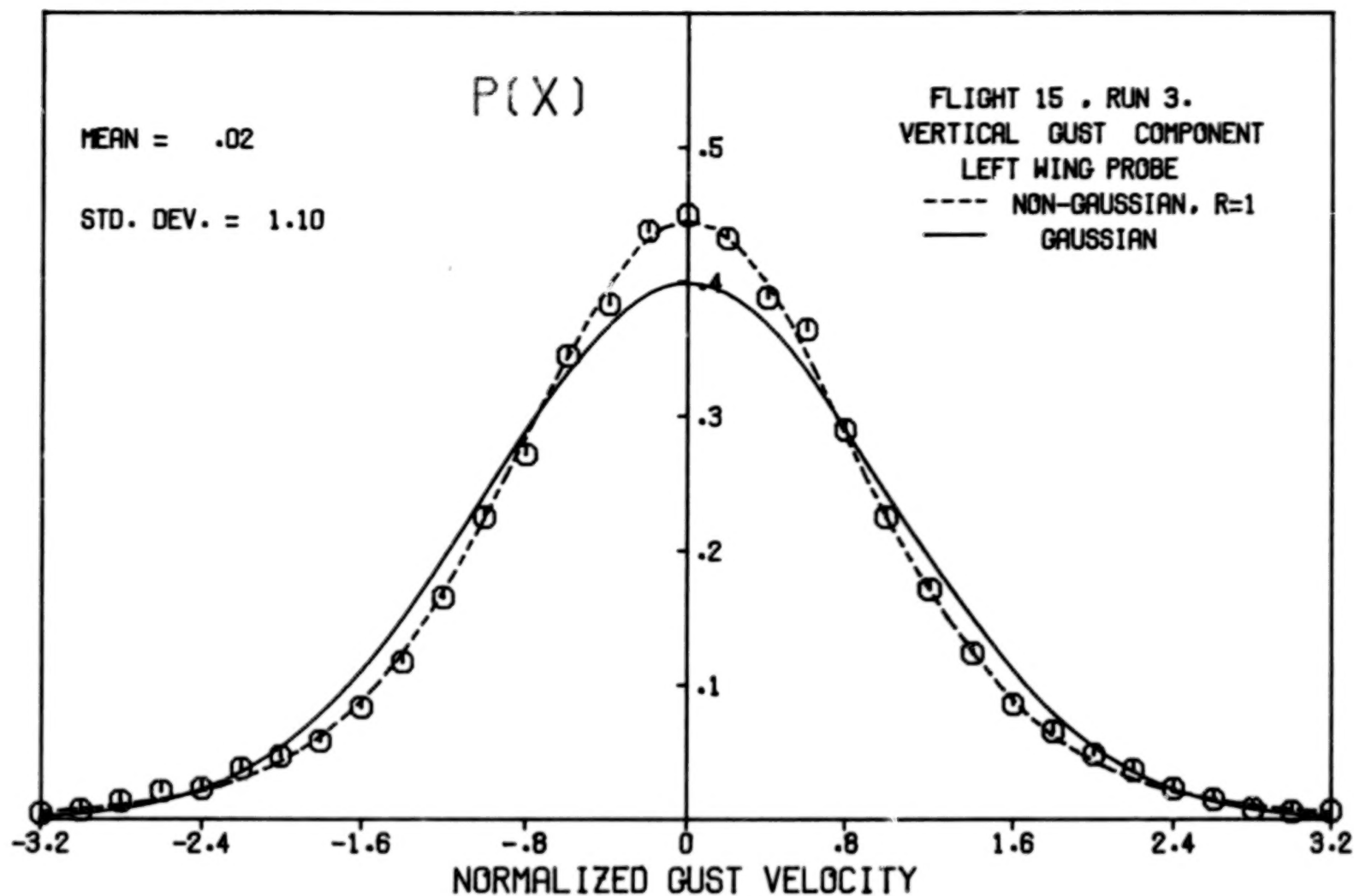
FIGURE 18   PROBABILITY DENSITY DISTRIBUTION
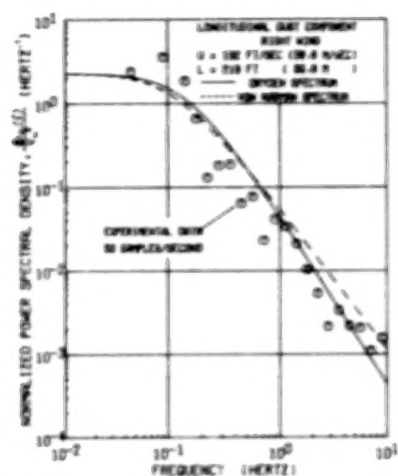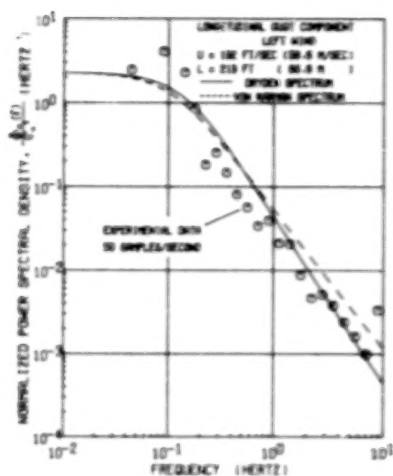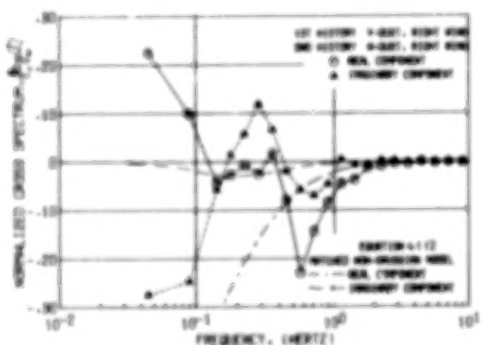
a) LONGITUDINAL COMPONENTS
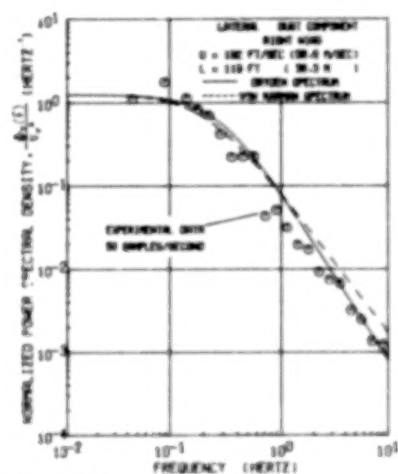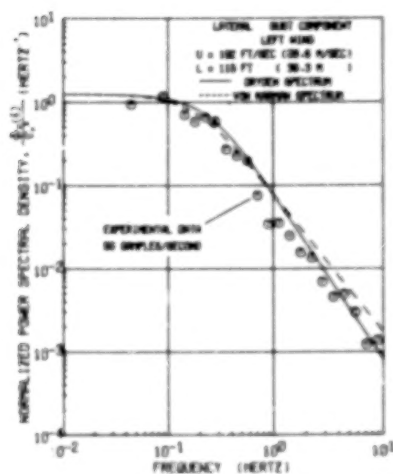
b) LATERAL COMPONENTS
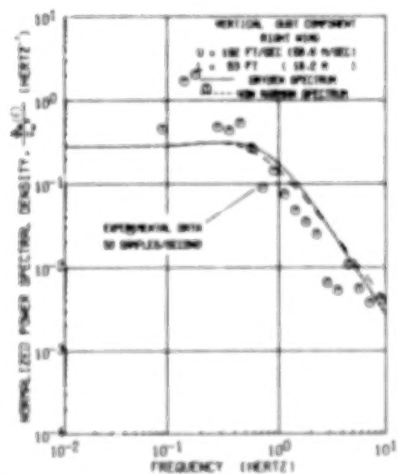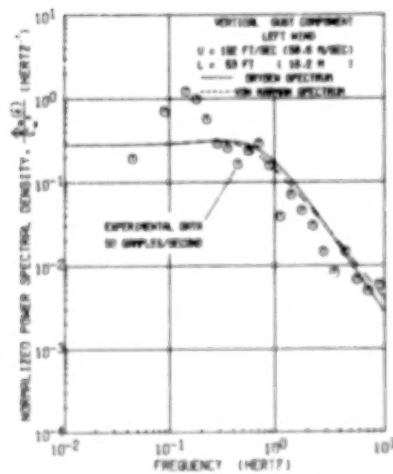
c) VERTICAL COMPONENTS

FIGURE 19. POWER SPECTRAL
DENSITY. FLIGHT 15 RUN I
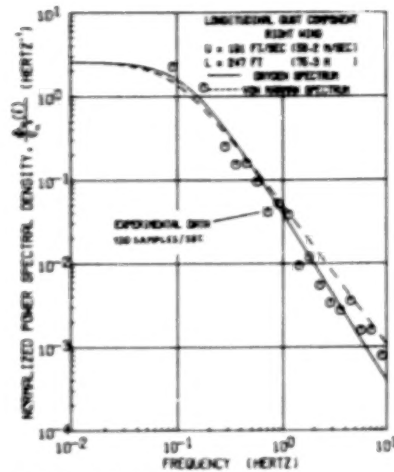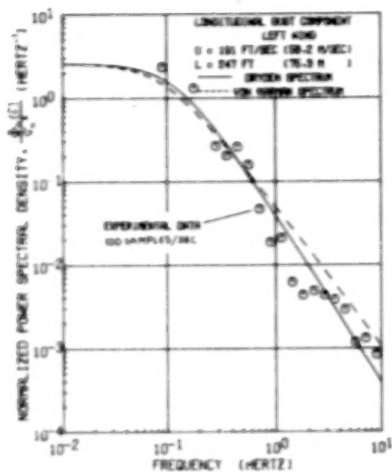
a) LONGITUDINAL COMPONENTS
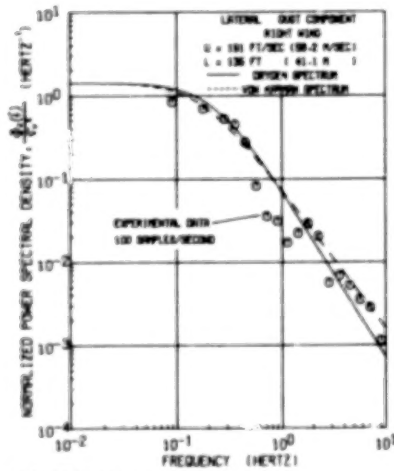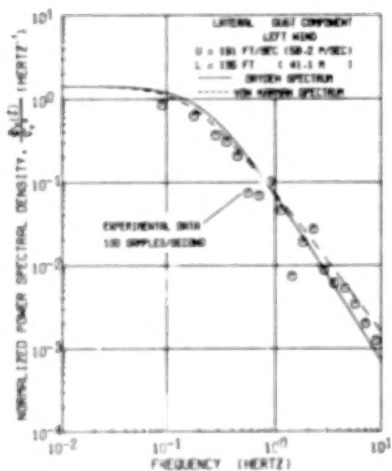
b) LATERAL COMPONENTS
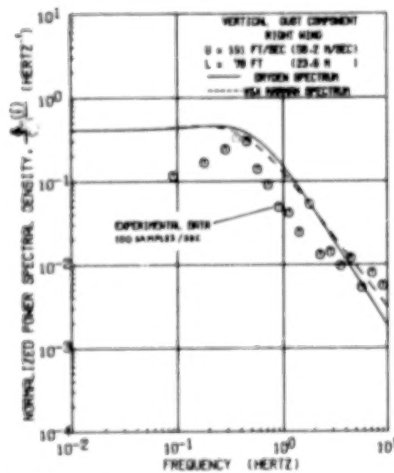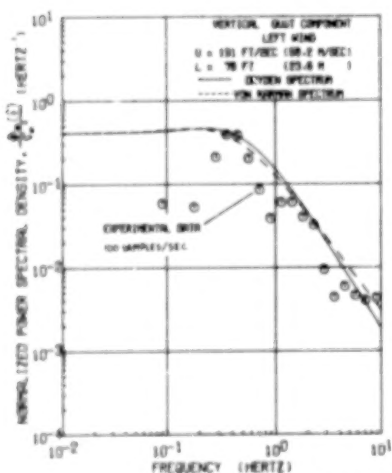
c) VERTICAL COMPONENTS

FIGURE 20. POWER SPECTRAL
DENSITY. FLIGHT 15 RUN 2
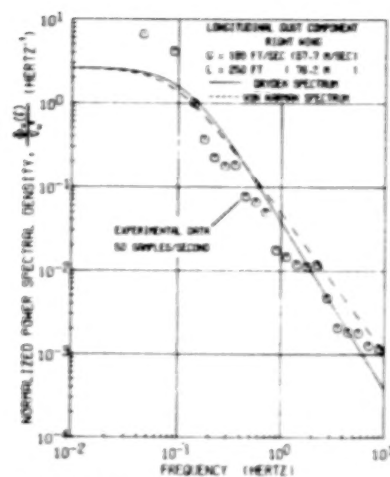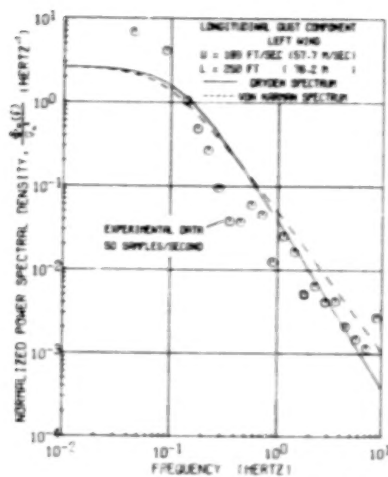
a) LONGITUDINAL COMPONENTS
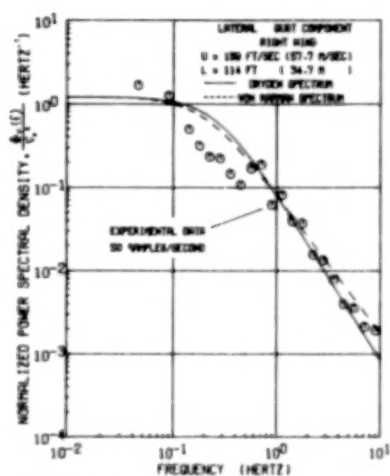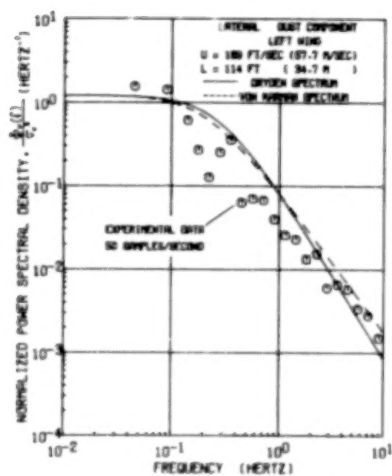
b) LATERAL COMPONENTS
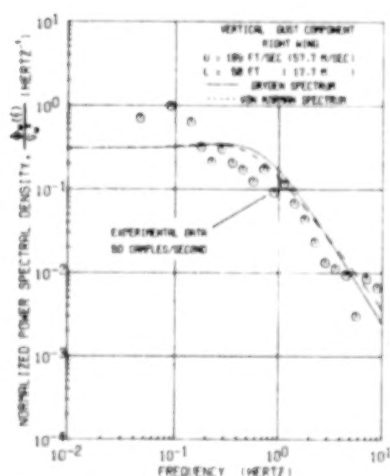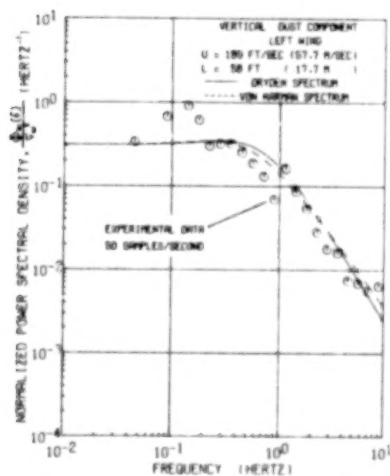
c) VERTICAL COMPONENTS

FIGURE 21. POWER SPECTRAL
DENSITY. FLIGHT 15 RUN 3
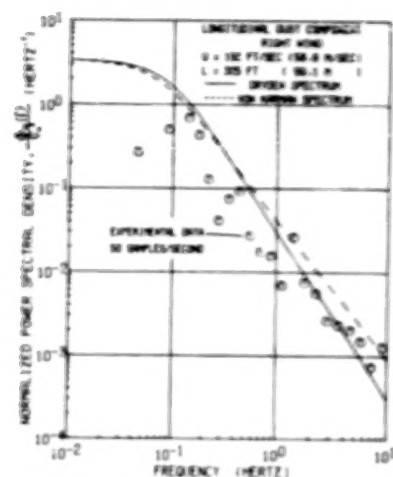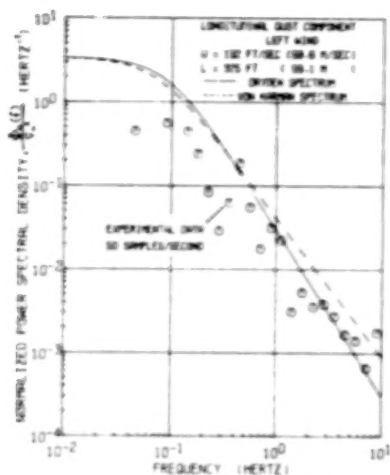
a) LONGITUDINAL COMPONENTS
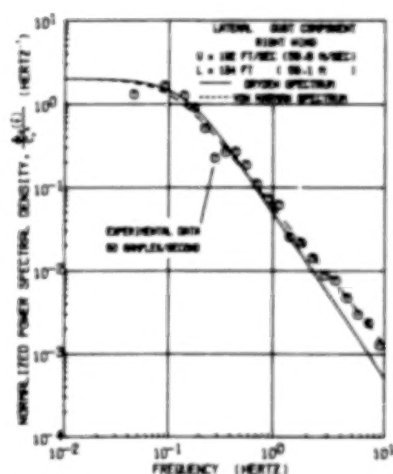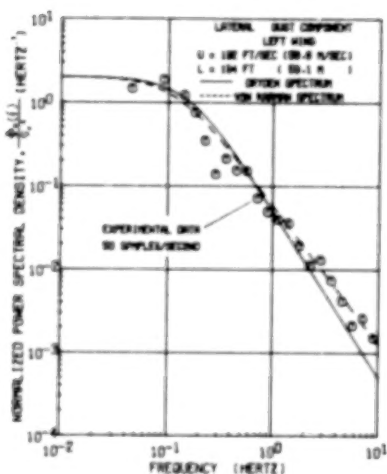
b) LATERAL COMPONENTS
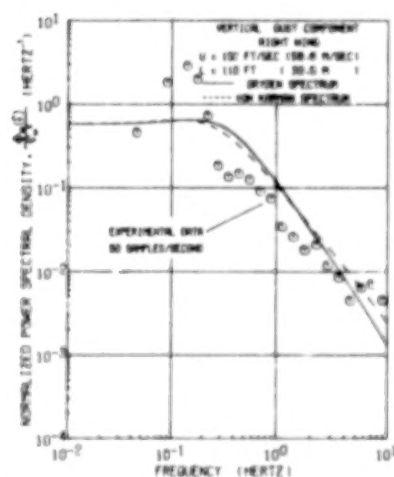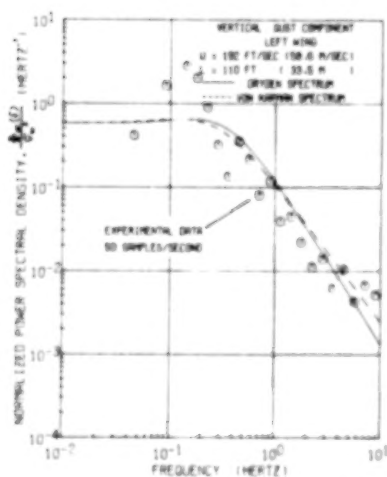
c) VERTICAL COMPONENTS

FIGURE 22. POWER SPECTRAL
DENSITY. FLIGHT 15 RUN 4
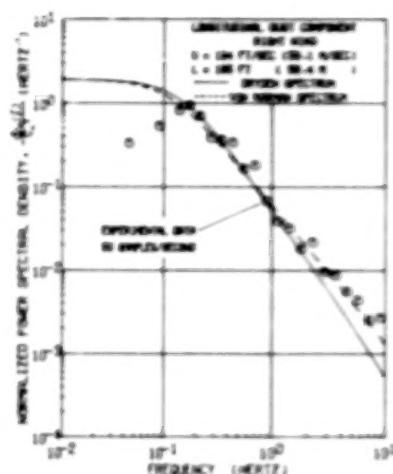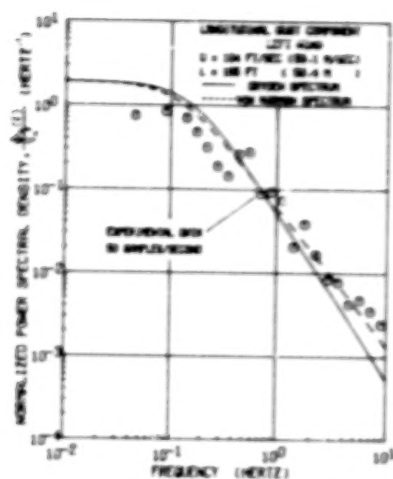
a) LONGITUDINAL COMPONENTS
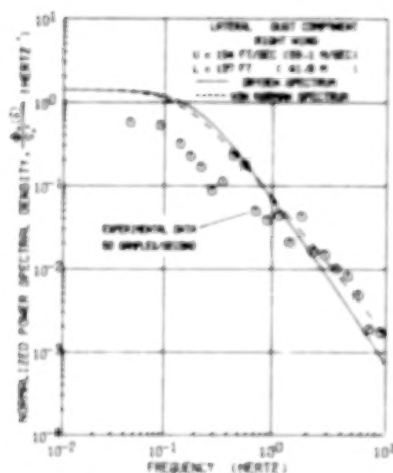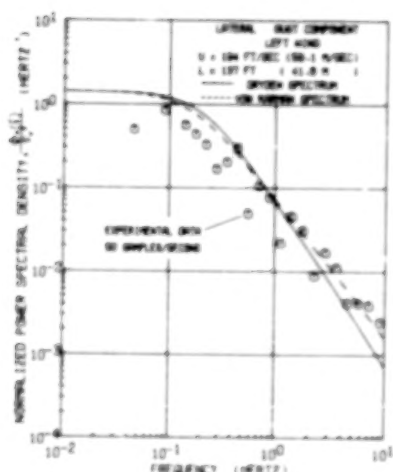
b) LATERAL COMPONENTS
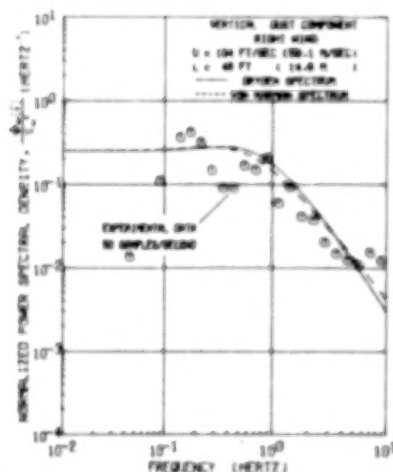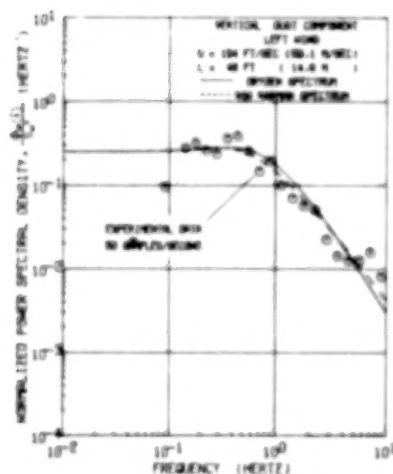
c) VERTICAL COMPONENTS

FIGURE 23. POWER SPECTRAL
DENSITY. FLIGHT 16 RUN 1
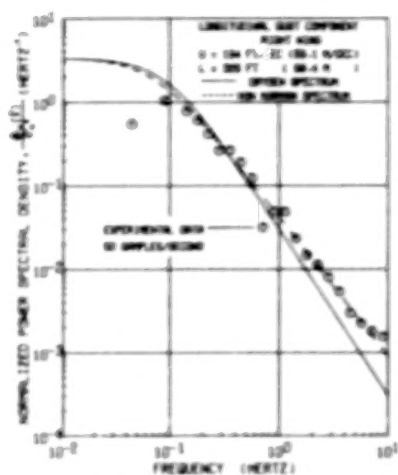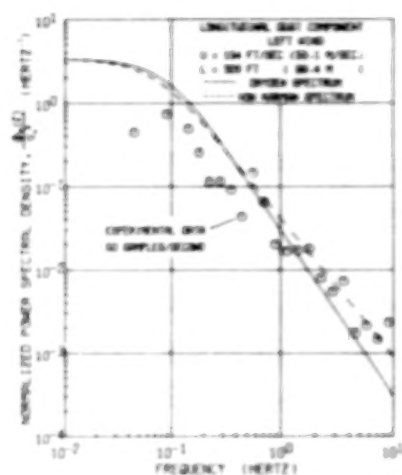
a) LONGITUDINAL COMPONENTS
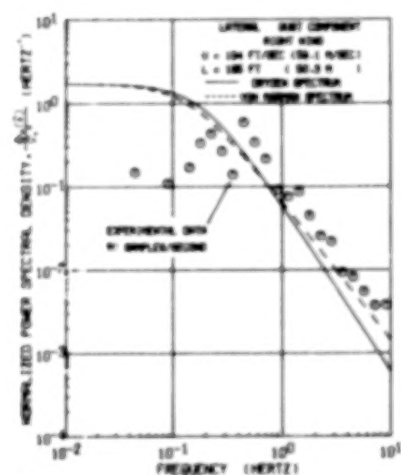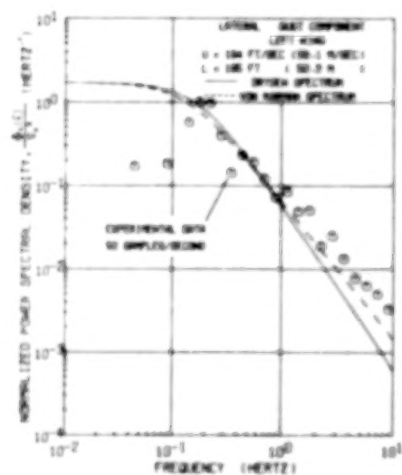
b) LATERAL COMPONENTS
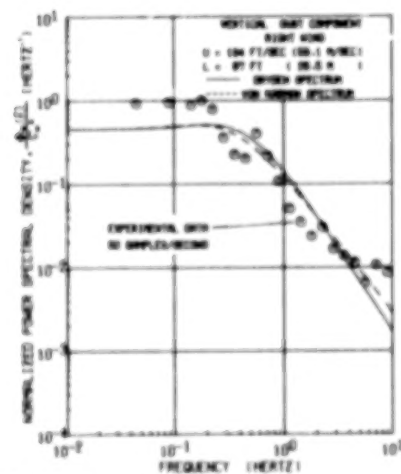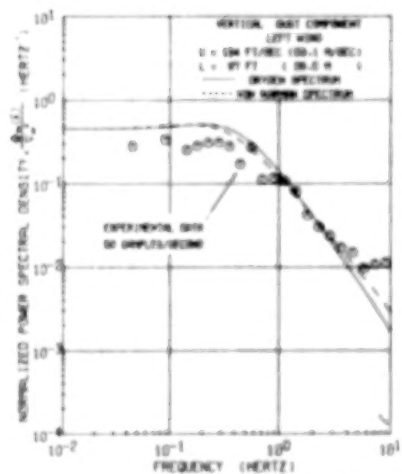
c) VERTICAL COMPONENTS

FIGURE 24. POWER SPECTRAL
DENSITY. FLIGHT 16 RUN 2
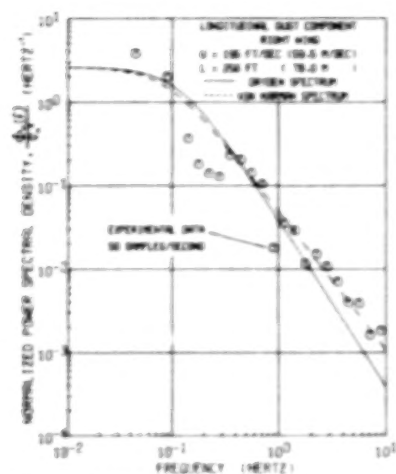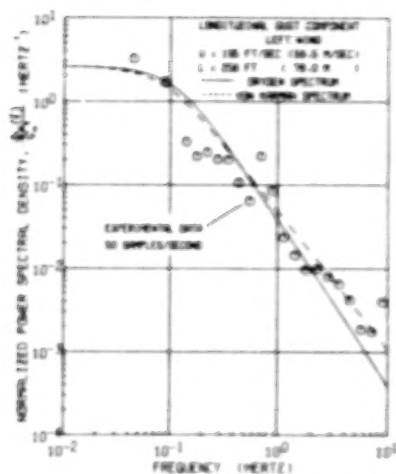
a) LONGITUDINAL COMPONENTS
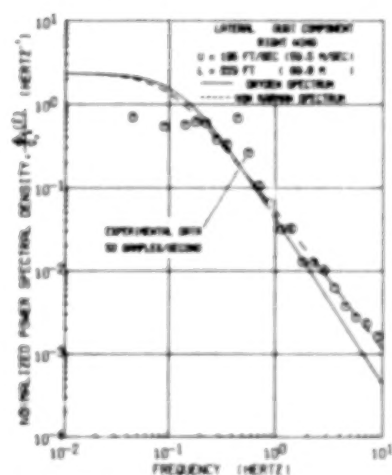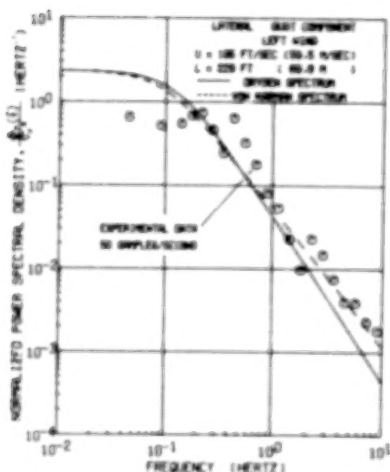
b) LATERAL COMPONENTS
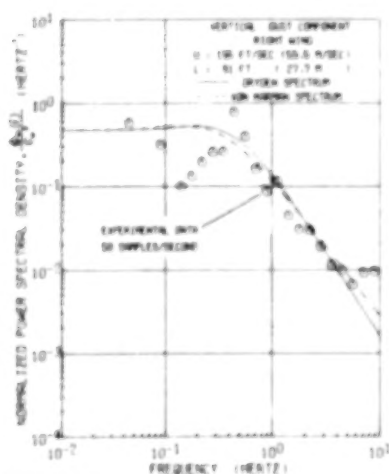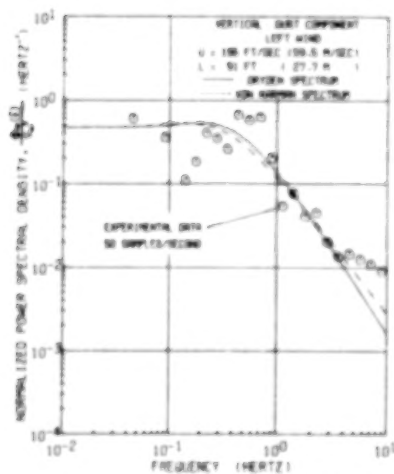
c) VERTICAL COMPONENTS

FIGURE 25. POWER SPECTRAL
DENSITY. FLIGHT 16 RUN 3
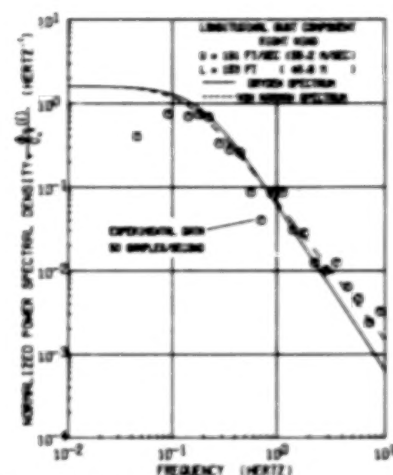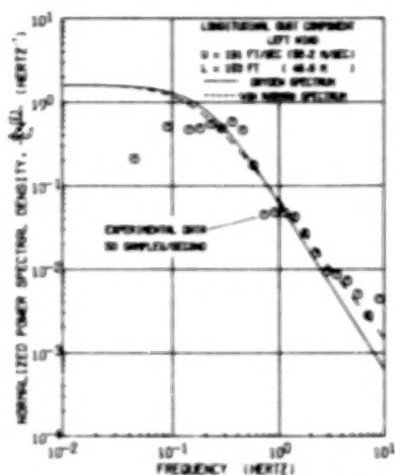
a) LONGITUDINAL COMPONENTS
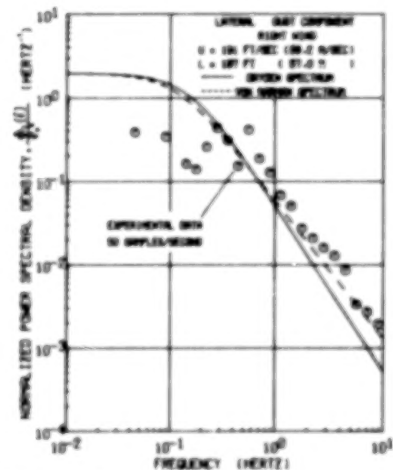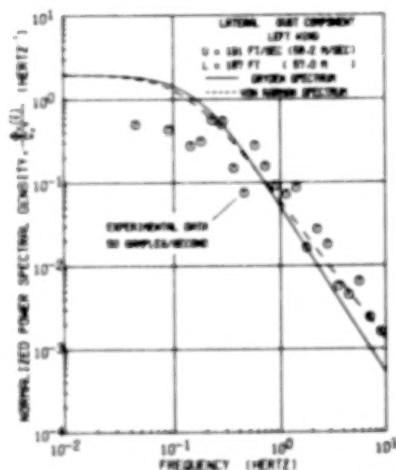
b) LATERAL COMPONENTS
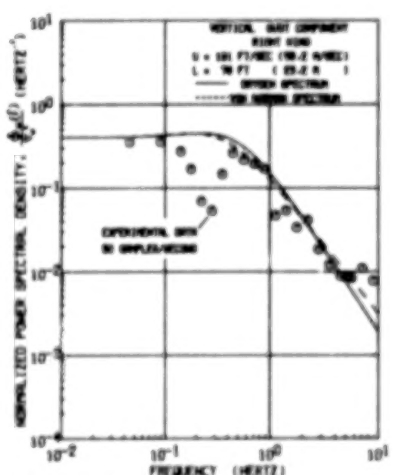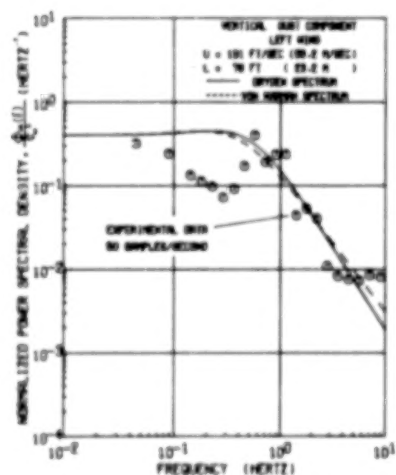
c) VERTICAL COMPONENTS

FIGURE 26. POWER SPECTRAL
DENSITY. FLIGHT 16 RUN 4
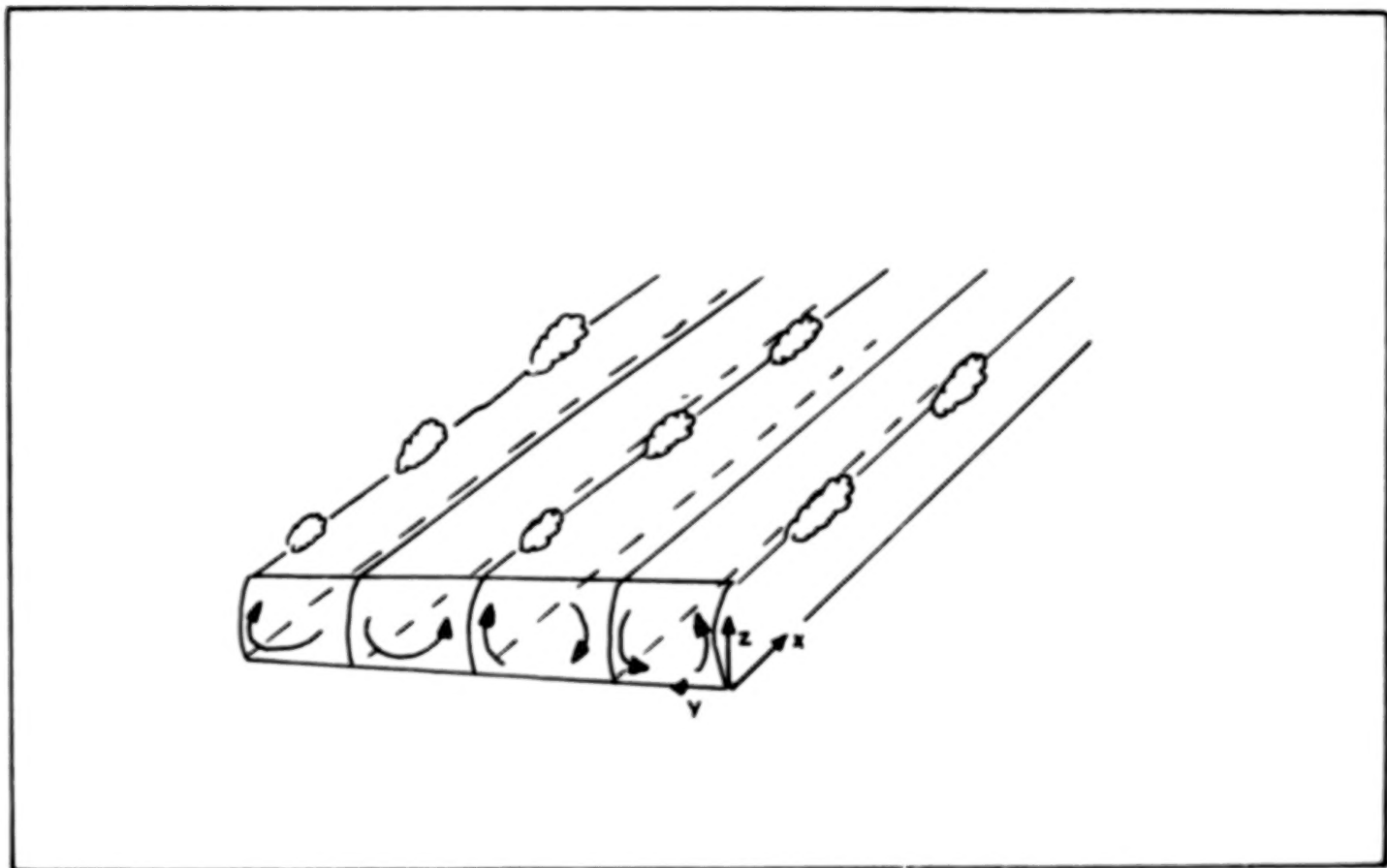
FIGURE 27.   FLOW MODEL OF THE HELICAL FLOW PATTERN

a) RUN 1

b) RUN 2

c) RUN 3

d) RUN 4

FIGURE 28. CROSS SPECTRAL DENSITY. FLIGHT 15   70
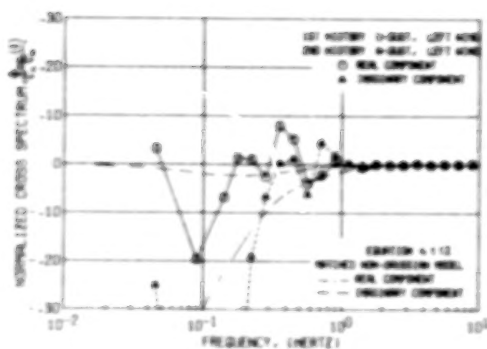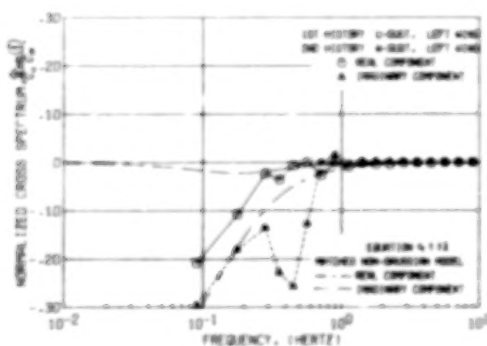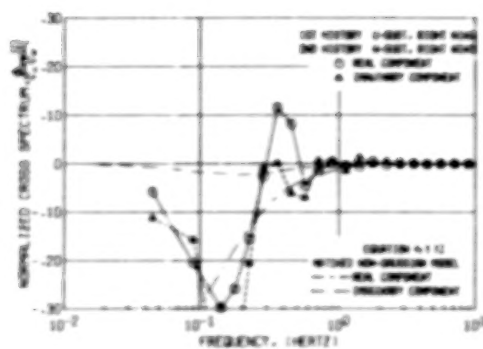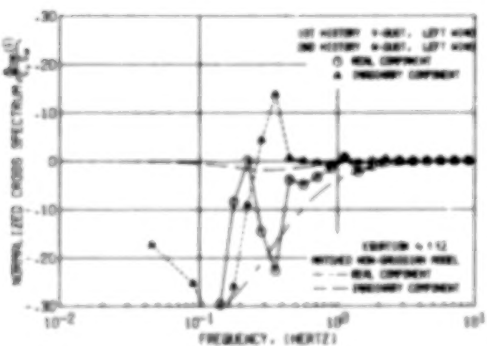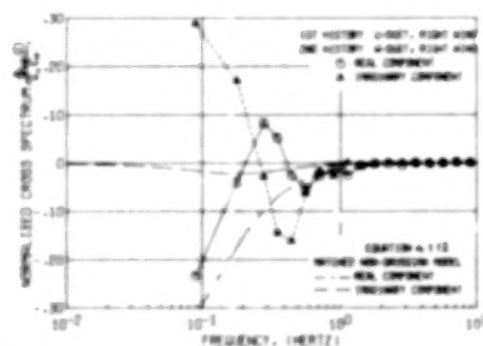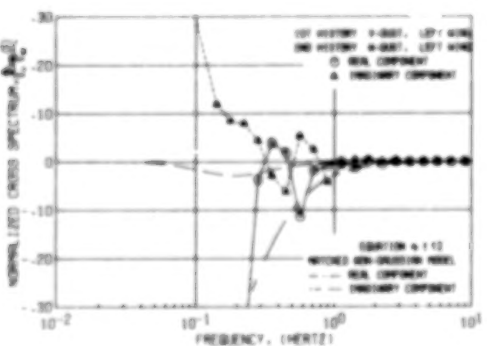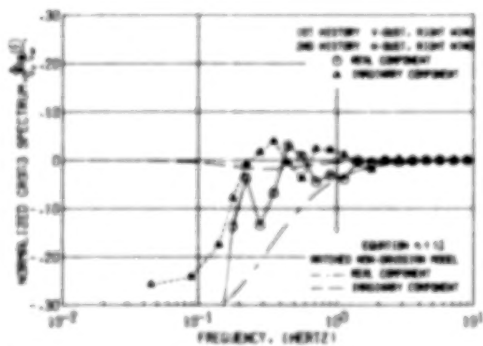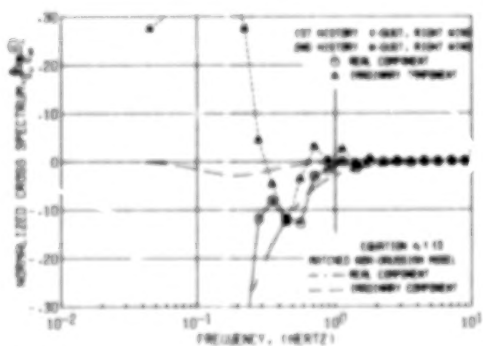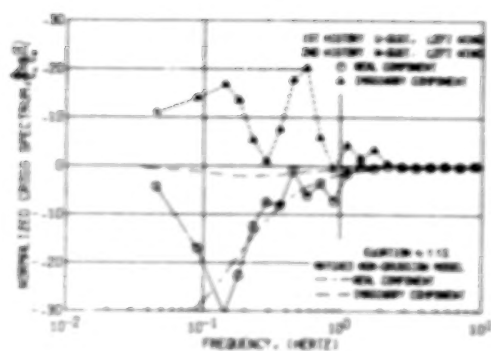
a) RUN 1
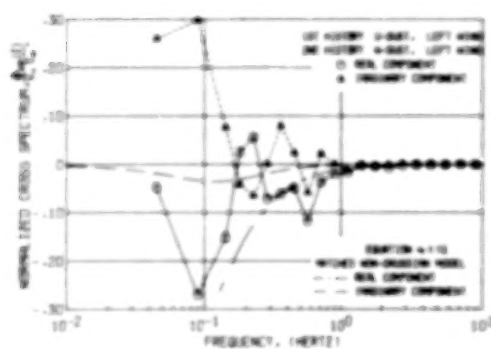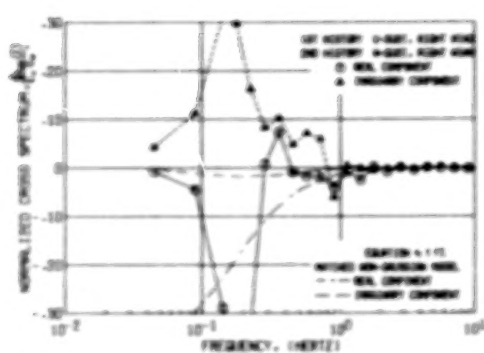
b) RUN 2
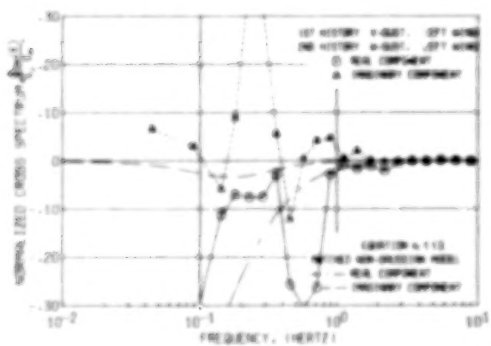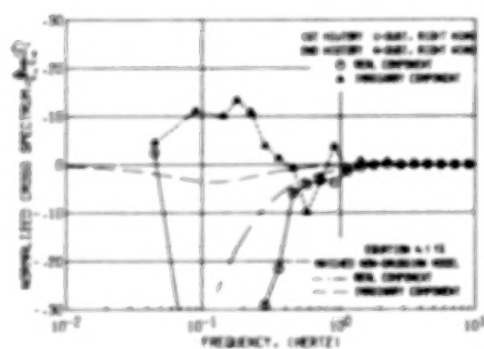
c) RUN 3
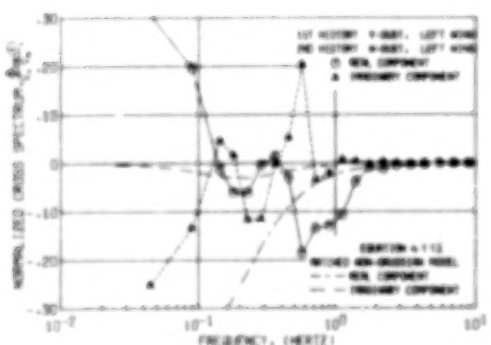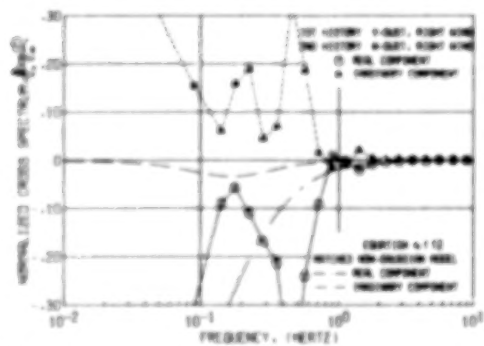
d) RUN 4

FIGURE 29. CROSS SPECTRAL DENSITY. FLIGHT 16
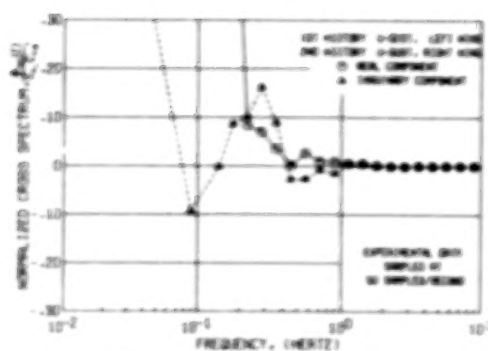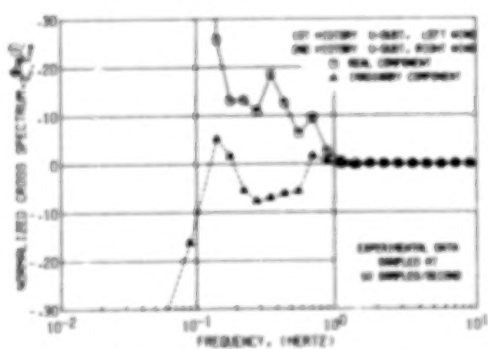
a) FLIGHT 15 RUN 1
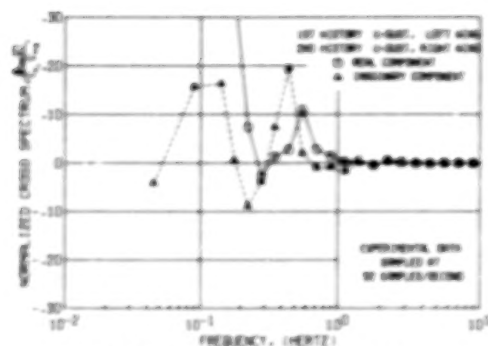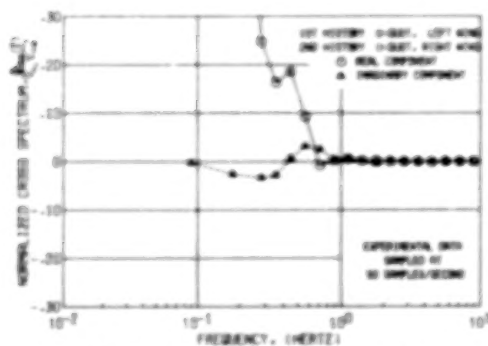
b) FLIGHT 15 RUN 2
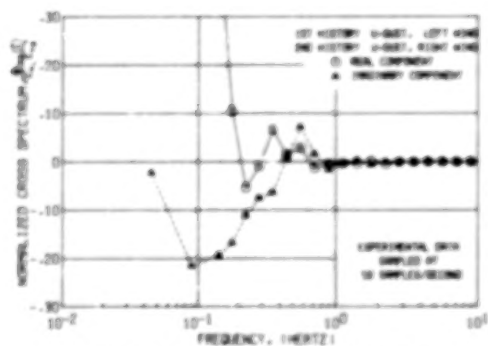
c) FLIGHT 15 RUN 3
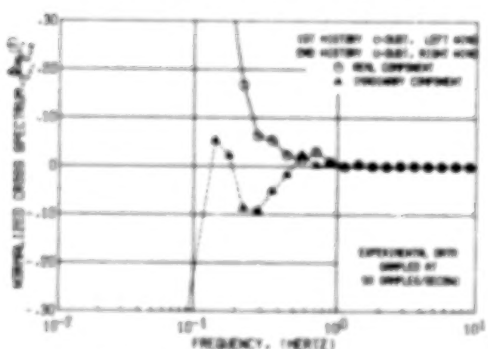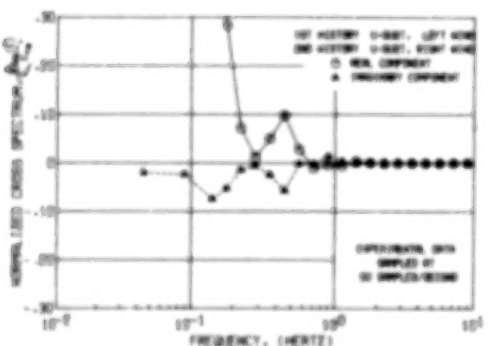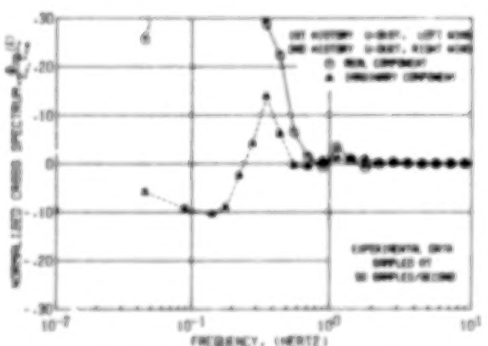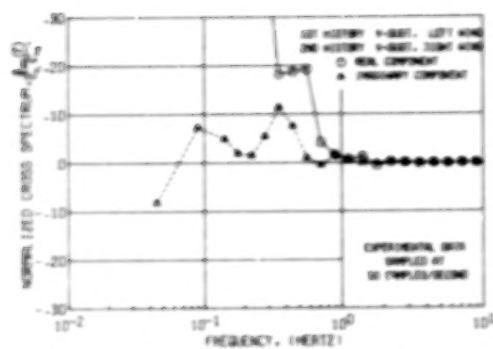
d) FLIGHT 15 RUN 4

e) FLIGHT 16 RUN 1

f) FLIGHT 16 RUN 2

g) FLIGHT 16 RUN 3

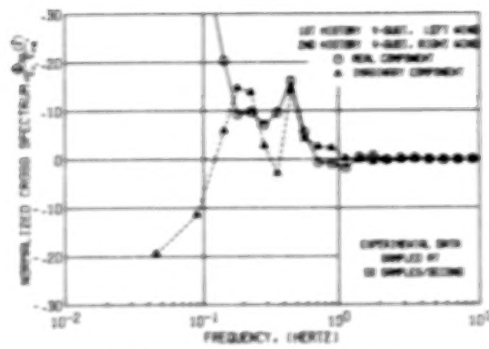h) FLIGHT 16 RUN 4

FIGURE 30. CROSS SPECTRAL DENSITY.
LONGITUDINAL COMPONENTS.

a) FLIGHT 15 RUN 1

b) FLIGHT 15 RUN 2

c) FLIGHT 15 RUN 3

d) FLIGHT 15 RUN 4

e) FLIGHT 16 RUN 1

f) FLIGHT 16 RUN 2

g) FLIGHT 16 RUN 3

h) FLIGHT 16 RUN 4

FIGURE 31. CROSS SPECTRAL DENSITY.
LATERAL COMPONENTS.

a) FLIGHT 15 RUN 1

b) FLIGHT 15 RUN 2

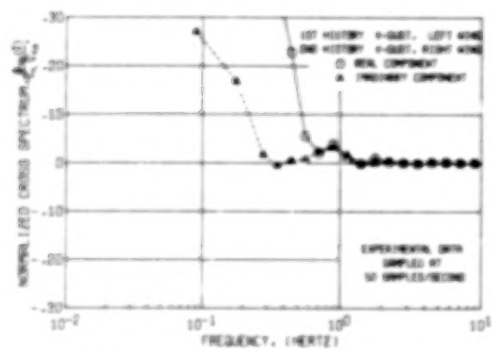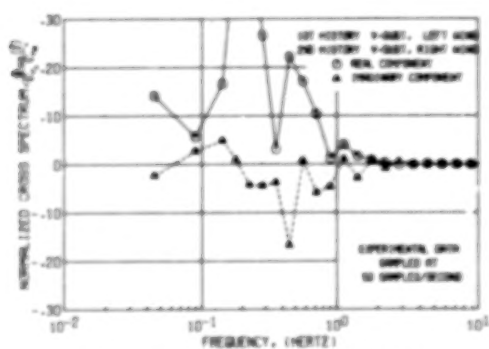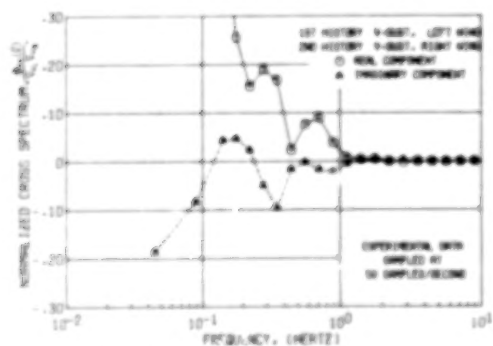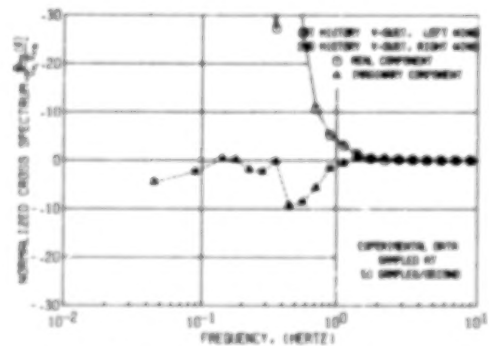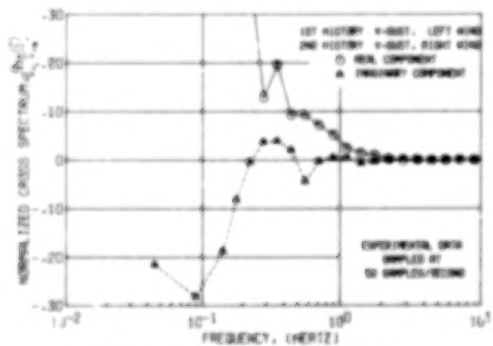c) FLIGHT 15 RUN 3

d) FLIGHT 15 RUN 4

e) FLIGHT 16 RUN 1

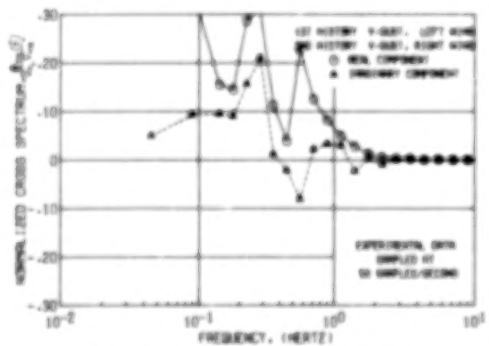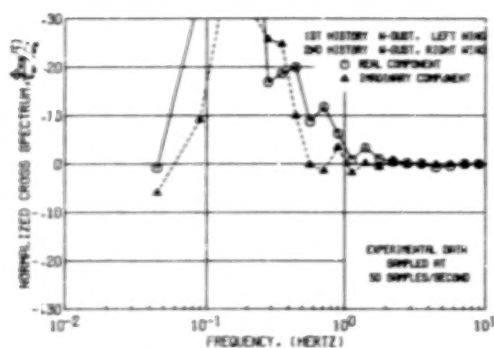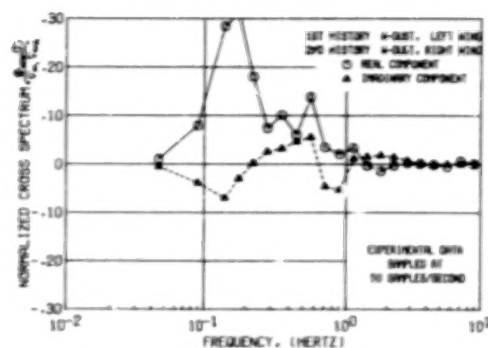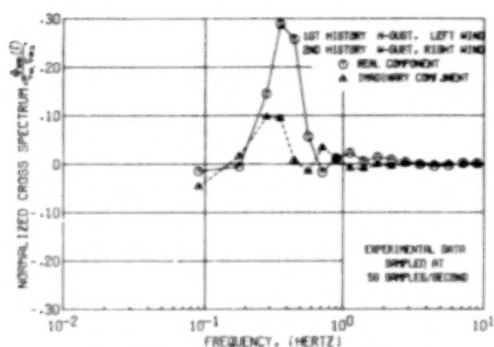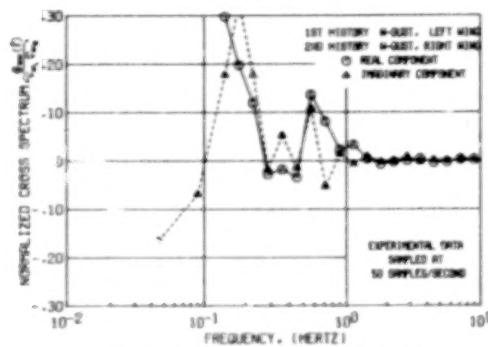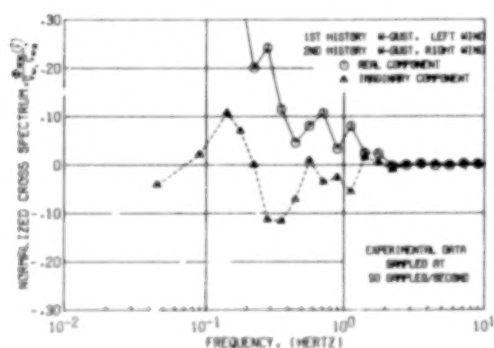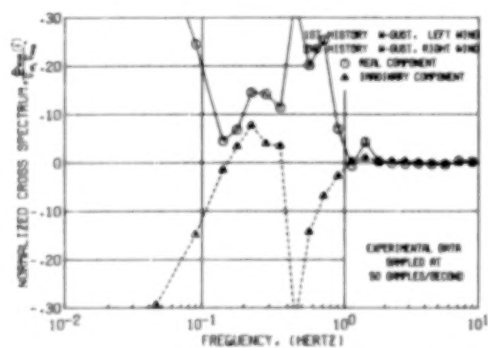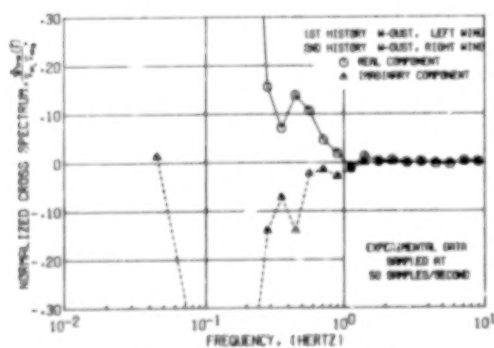f) FLIGHT 16 RUN 2
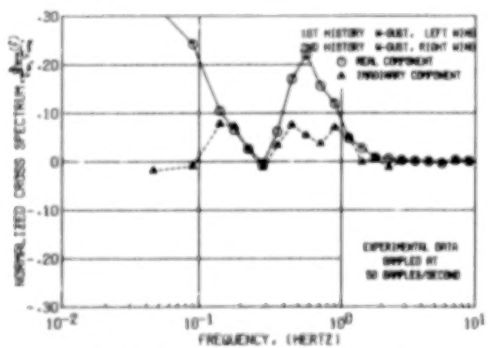
g) FLIGHT 16 RUN 3

h) FLIGHT 16 RUN 4

FIGURE 32. CROSS SPECTRAL DENSITY.
VERTICAL COMPONENTS.

APPENDIX   A

INSTRUMENTATION

This appendix presents a description of the instrumen-
tation system used in this research, as well as of the methods
of calibration for the different instruments. A separate sec-
tion, A.3, gives special attention to the problem of measuring
gusts in the direction of flight, as this proved to be a major
problem in this research program.

A.1   Description of the Data Instruments

In table Al   a summary of the data instruments with
their most important characteristics is given.

The Pressure Transducers.-Statham Instruments Inc. model
PM 283TC, were selected particularly because of their low
sensitivity to acceleration. This feature is important because
of the positioning of the transducers in the probeheads at the
two wingtips of the aircraft, where any motion of the aircraft
is most pronounced.

The approximate natural frequency of the pressure trans-
ducers is given by the manufacturers as $2,000\ Hz$, which is
well above the region of interest in this research program.

The Rate Gyros.-Honeywell model JG7005A-11, were located
in the nose bay of the aircraft. All three were positioned
on a single platform, each with the sensitive axis in the
appropriate direction. The entire package could be removed
for easy maintenance.

The Accelerometers.-These were located behind the instru-
ment panel in the right front corner of the cabin, against the
bulkhead dividing the cockpit and the cabin. Both accelero-
meters were manufactured by Statham Laboratories, Inc. The
lateral accelerometer was a model A 301TC-1-350-12425, with
a range of $\pm\ 1g$, while the vertical accelerometer was a model

NA1 D47-T-30, with a range ± *3g* .

Both accelerometers were fixed on a platform, which could
be tilted and rotated, so that the platform could be brought
to a level position for calibration purposes.

The Vertical Gyro.-This was also located in the nose bay
of the aircraft, and was used to measure the roll angle of
the aircraft. This gyro was manufactured by Honeywell, model
number JG 7044A-17. The platform on which the gyro was fixed
could be tilted for calibration of the gyro.

A.2   Calibration of the Data Instruments

The data instruments were calibrated by subjecting the
instruments to a known physical input and then adjusting the
output voltages to a value that would give sufficient sensi-
tivity during the data runs, but at the same time would not
result in peaked-out signals during motions of the aircraft
or in high gusts.

The Pressure Transducers.-These were calibrated in a test
set-up as shown in Fig. A1.   The pressure in the enclosed
volume was changed by moving the neoprene piston in the plastic
cylinder. The magnitude of the pressure was measured by the
manometer which was set at an angle of 28.8° so that 1"
difference in fluid level on the manometer would correspond
to 2 psi differential pressure.

The calibrations were performed by first putting a pres-
sure load on the pressure transducer and measuring the cor-
responding output. The pressure would then be returned to
zero level and by pushing the calibration button the normally
open switch (Fig. A1) would be closed, shifting the balance
of the bridge, which resulted in a jump in the output voltage.
This voltage then corresponded to the calibration value for
that channel. The calibration values used for flight #15
and #16 are given in table A2.

The Rate Gyros.-These were calibrated by positioning
them on a rocker table, which oscillated. The angle traversed

by the rocker table was measured accurately. Its value,
14° 35' would then correspond to the area under the rate vs.
time curve. This curve was obtained by plotting the output
voltage of the rate gyro on mm graph paper. From this the
physical equivalent of $1 mm$ would be known and thus the
equivalent of the calibration jump could be calculated in
rad/sec. Table A 2 presents the values that were used for
the calibration jumps of the rate gyros.

The Accelerometers.-These were calibrated by first bring-
ing the platform on which they were fixed, to a level position.
In this position the lateral accelerometer would sense zero
acceleration while the vertical accelerometer would be subject-
ed to $1 g$. The output voltages of the accelerometers were
zeroed in this position.

The platform was then rotated over a prescribed angle
α($\pm$ $10°$ for the lateral accelerometer and $\pm$ $45°$ for the verti-
cal accelerometer). The component of the gravitational
acceleration in the sensitive direction of the accelerometers at
these angles could be calculated from the following relations:

$$a_y = g\ sin\ \alpha$$

$$a_z = g(1 - cos\ \alpha)$$

These accelerations, with the accelerometers at the respective
calibration angles, would then correspond to the output voltages
measured at the output of the accelerometers. These relations
were then used to calculate the accelerations which would cor-
respond to the voltage outputs which occurred when the calibra-
tion button was pushed.

The Vertical Gyro.-This was calibrated by rotating the
platform on which it was fixed over a $10°$ angle about an
angle parallel to the aircraft roll axis. The value for the
calibration jump that resulted from this calibration is given
in table A 2 .

77

A.3 Measurement of the Longitudinal Gusts

The measurement of the longitudinal gusts (gusts in the direction of flight) posed a major problem in this research program. The initial concept was to measure the difference between the static and the total head pressures on the probehead, which in essence is the dynamic pressure

$$q = \frac{1}{2} \rho \, V^2$$

From this the instantaneous longitudinal velocity of the flow w.r.t. the probehead could be calculated. Subtracting the average airspeed of the aircraft from this instantaneous velocity would give the gust velocity in longitudinal direction. This set-up poses a problem when the aircraft undergoes slight changes in altitude, e.g. a decrease in altitude, which means an increase in density, is usually accompanied by an increase in velocity of the aircraft. Such a maneuver would then be registered as a gust, while in actuality no gust had taken place.

First it was attempted to solve this problem by setting up a system as shown in Fig. A 2 . Pressure port #1, connected to the front side of the pressure transducer, measures the pressure from which the gust velocity would be calculated. Pressure port #2, connected via a cavity to the back side of the pressure transducer, provides a reference pressure which, through proper dimensioning of the cavity size, would vary with altitude changes of the aircraft. The variations of the pressure at pressure port #2 which have frequencies higher than the altitude variations of the aircraft, would be damped out in the cavity. Calculations showed however, that this type of physical filter does not have a cut-off that would be adequately sharp to filter out the atmospheric turbulence frequencies, while letting the frequencies in the range of the change of altitude of the aircraft through.

The second possible solution for this problem was based on the following concept. A venturi probe can be dimensioned so the following relation is valid:

$$p_2 = p_1 - \frac{1}{2} \rho \, u_1^2$$

This venturi probe is connected to the front side of the pressure transducer, while the back side of the transducer is connected, via a valve, to a similar venturi probe (Fig. A 3). At the beginning of each data run the valve is closed. In this arrangement the pressure transducer measures

$$\Delta p = \rho \, u_o \left[u_{gust}(t) - u_{gust}(0) \right]$$

where u_o is the velocity of the aircraft w.r.t. the uniform flow field.

This system was built, extensively tested in the Venturi windtunnel of the Department of Aeronautics and Astronautics of the University of Washington, and installed on the probe-heads (Fig. A 4). Several flights were made with this set-up. The system worked well insofar as change in aircraft altitude did not affect the signal level. However, the flow through the venturi probes generated noise in the signal, which could not be filtered out as some of the noise was very close to the frequency range of interest in this research program.

The system eventually used for the measurement of the longitudinal gusts rests on the following principle.

The front side of the pressure transducer was connected to the total head pressure port on the hemispherical probe-head. The back side of the transducer was connected via a valve to another total head pressure port (Fig. A5). When the valve is closed, the pressure transducer measures

$$\Delta p = - \rho \, u_o \left[u_{gust}(t) - u_{gust}(0) \right]$$

The valves were closed after the aircraft had been established on a course and was maintaining the altitude selected for this flight accurately. After closure of the valves, the data recording equipment was started.

Ch. No.	Measured Variable	Instrument	Make	Model	Range
1	$\Delta p_{x \text{ Left}}$	diff. pressure transducer	Statham	PM283TC	± .15 psid
2	$\Delta p_{y \text{ Left}}$	diff. pressure transducer	Statham	PM283TC	± .15 psid
3	$\Delta p_{z \text{ Left}}$	diff. pressure transducer	Statham	PM283TC	± .15 psid
4	$\Delta p_{x \text{ Right}}$	diff. pressure transducer	Statham	PM283TC	± .15 psid
5	$\Delta p_{y \text{ Right}}$	diff. pressure transducer	Statham	PM283TC	± .15 psid
6	$\Delta p_{z \text{ Right}}$	diff. pressure transducer	Statham	PM283TC	± .15 psid
7	roll rate p	rate gyro	Honeywell	JG7005A-11	± 6 deg/sec
8	pitch rate q	rate gyro	Honeywell	JG7005A-11	± 6 deg/sec
9	yaw rate r	rate gyro	Honeywell	JG7005A-11	± 6 deg/sec
10	lateral acceleration a_y	accelerometer	Statham	A301TC	± 1 g
11	vertical acceleration a_z	accelerometer	Statham	NA1 D47	± 3g
12	roll angle ϕ	vertical gyro	Honeywell	JG7044A-17	± 85°

TABLE A1.   CHARACTERISTICS OF THE DATA INSTRUMENTS

Chan-nel	Instru-ment	Ground Calibration		Bridge Voltage	
		Physical Calibration	Signal Voltage	Signal Voltage	Calibration Value
1	pressure trans-ducer	6 psf	.5	.5	6 psf
2	"	9 psf	.55	.55	9 psf
3	"	9 psf	.5	.5	9 psf
4	"	6 psf	.5	.5	6 psf
5	"	9 psf	.5	.5	9 psf
6	"	9 psf	.55	.52	8.5 psf
7	rate gyro	.084 rad/sec	.41	.56	.115 rad/sec
8	"	.084 rad/sec	1.0	.5	.042 rad/sec
9	"	.084 rad/sec	.66	.55	.07 rad/sec
10	accelero meter	5.59 ft/sec^2	.975	.48	2.75 ft/sec^2
11	"	9.45 ft/sec^2	.65	.72	10.47 ft/sec^2
12	vertical gyro	.174 rad	.5	.65	.236 rad

TABLE A2.   CALIBRATION OF THE DATA INSTRUMENTS

Pressure transducer

Manometer

Probehead

Pressure transducer

+

−

Output voltage

N.O.

Piston and cylinder

Bridge completion box
in the aircraft
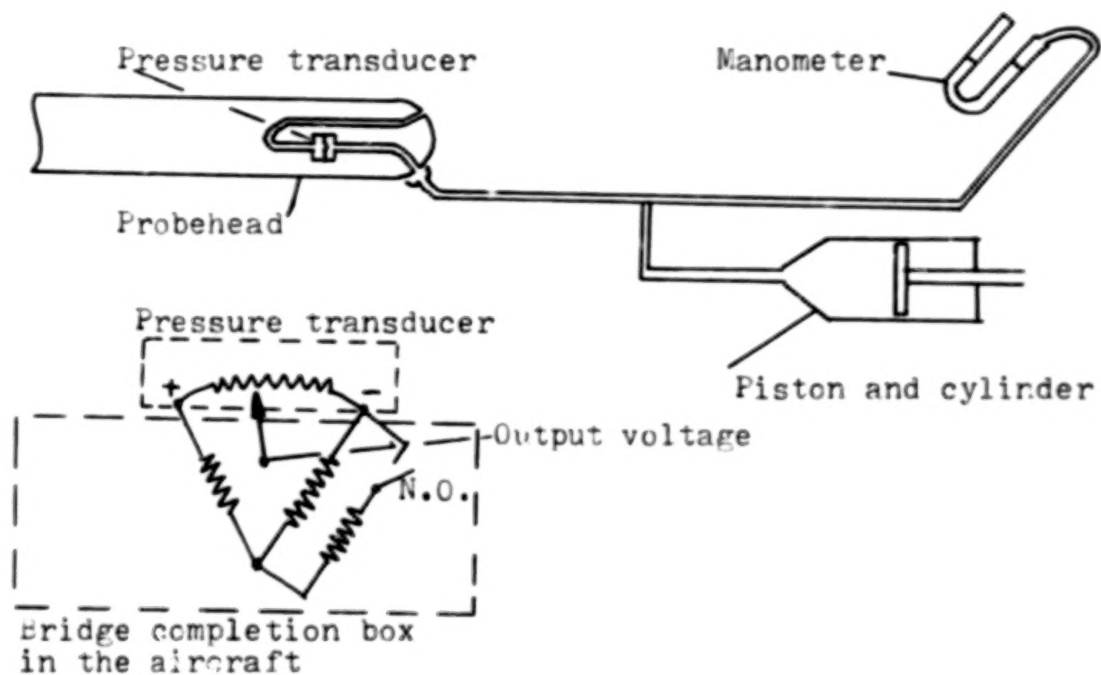
FIGURE A1.   CALIBRATION OF THE PRESSURE TRANSDUCERS

82
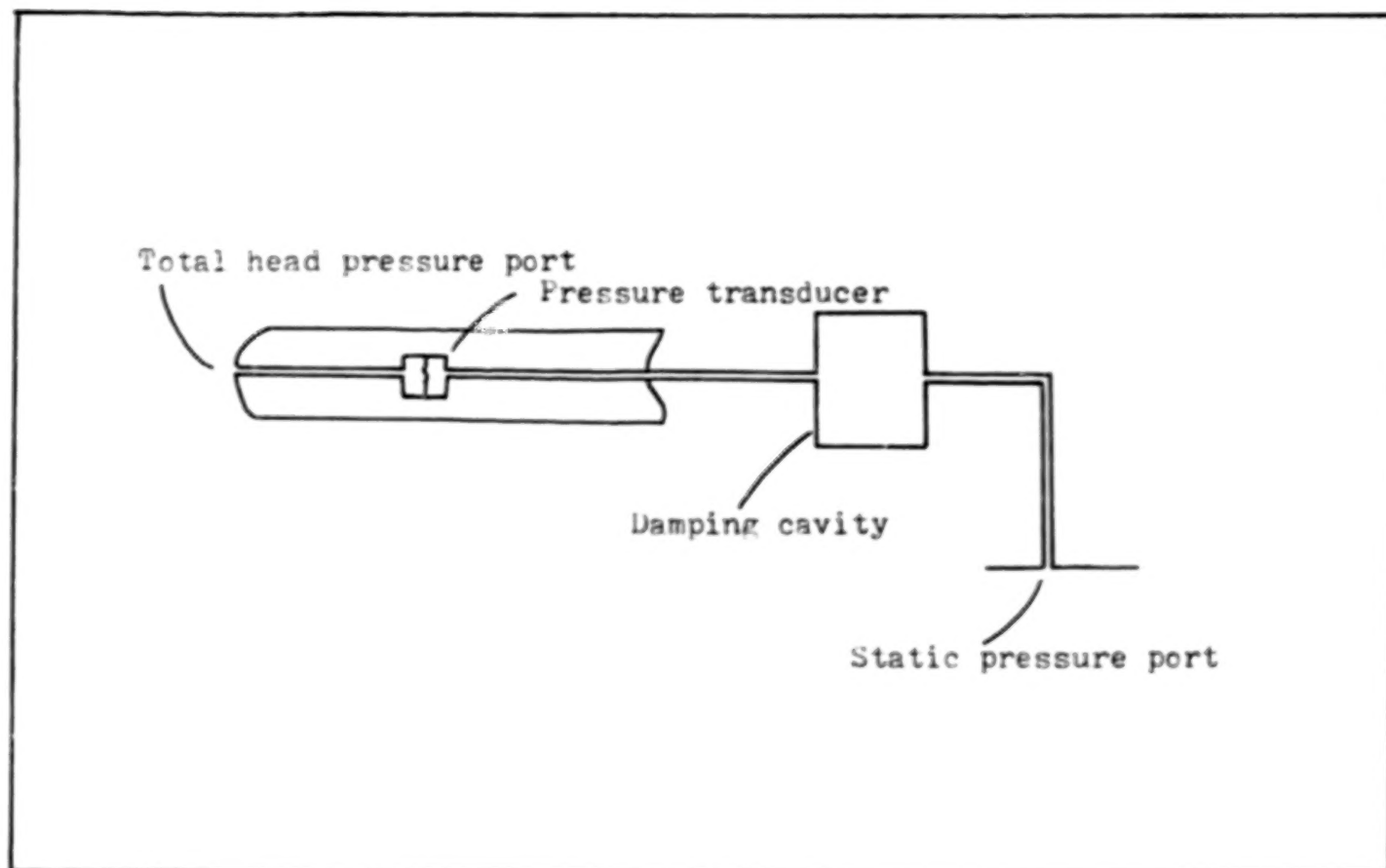
FIGURE A2.   SYSTEM WITH DAMPING CAVITY FOR MEASUREMENT
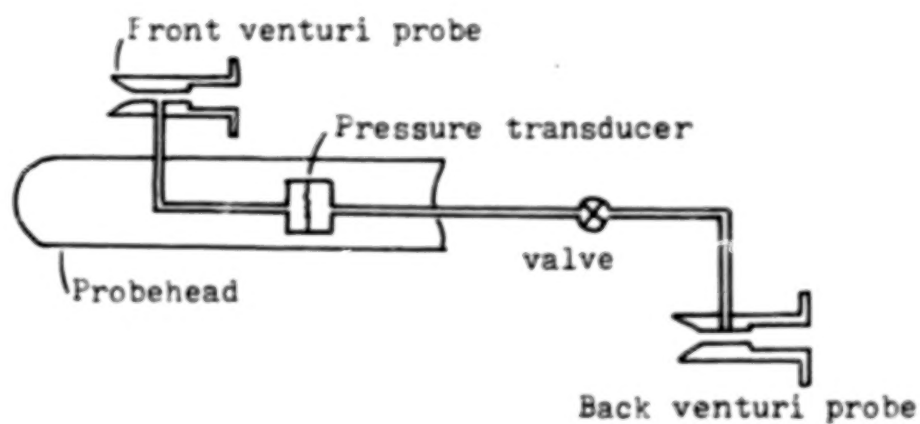   OF LONGITUDINAL GUSTS

Front venturi probe

Pressure transducer

Probehead

valve

Back venturi probe

FIGURE   A3.   SYSTEM WITH TWO VENTURI PROBES FOR MEASUREMENT
                   OF LONGITUDINAL GUSTS
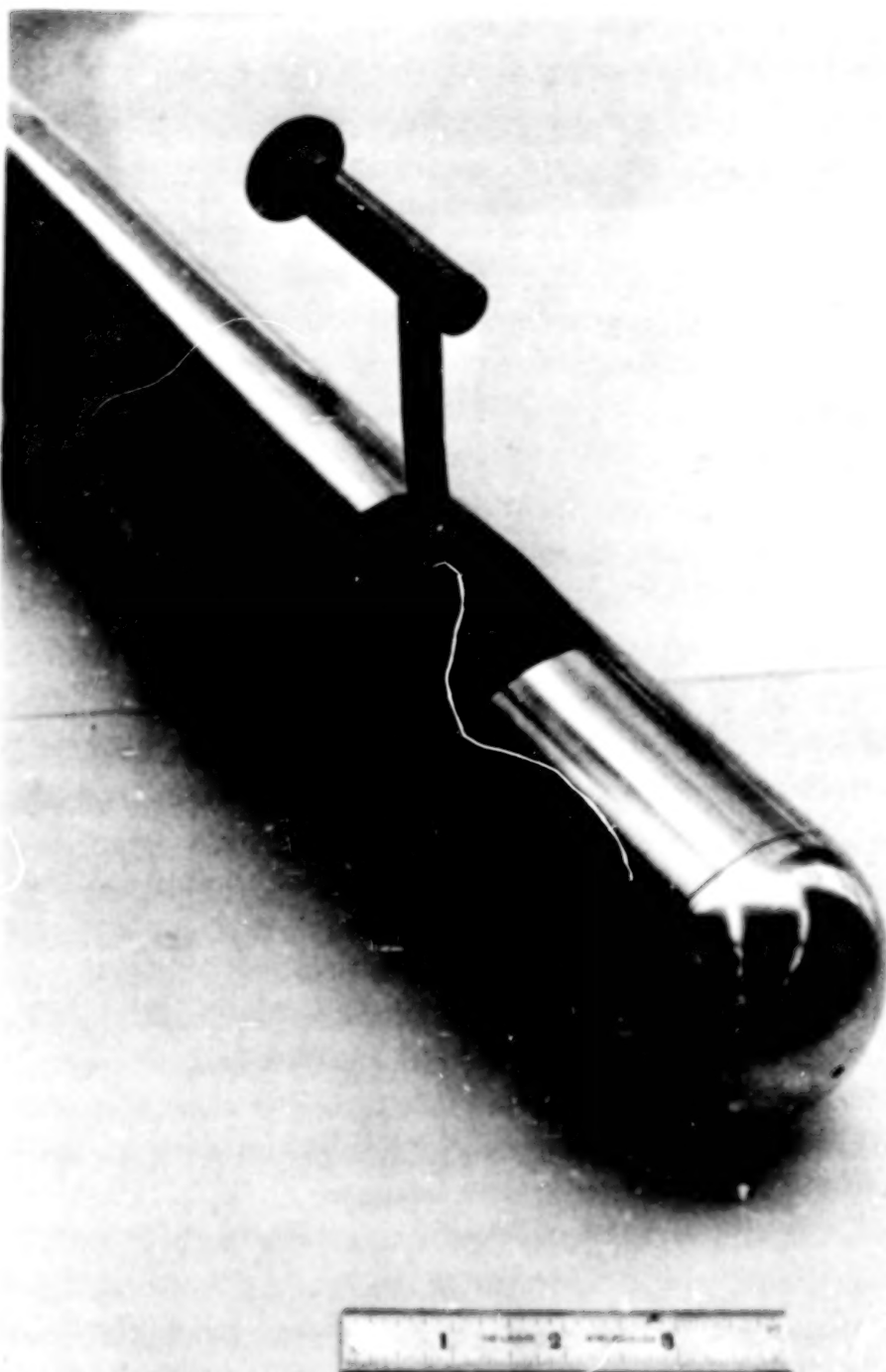
FIGURE A4.   VENTURI PROBE MOUNTED ON A

PROBEHEAD   85
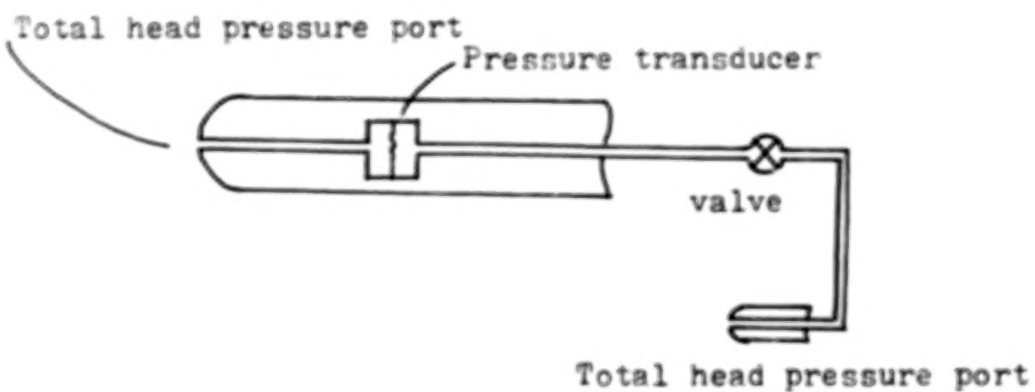
FIGURE A5.   SYSTEM WITH TWO TOTAL HEAD PRESSURE PROBES

FOR MEASUREMENT OF LONGITUDINAL GUSTS

86

APPENDIX B

DATA REDUCTION

This appendix presents a description of the computations
that were performed to obtain spectral properties from the
data as measured in flight and recorded on the analog tapes.

B.1 Evaluation of Raw Data

After each flight the data were checked by playing the
analog tapes back and recording the signals on a chart recorder.
This chart could be checked to see that all channels had
continuous data. If any instrument failures had occurred dur-
ing the flight, this could be detected immediately.

From the recordings made during the motions at altitude it
could be determined whether any signals had peaked out in severe
gusts. The analog records were also used in checking the cali-
bration values of the signals from the transducers.

B.2 Digitizing

After it was determined that the analog records of a
flight contained no errors, the data were digitized. Digitizing
was performed on the Varian 620f digitizer of the Department
of Geophysics of the University of Washington.

The data were played back on the Ampex FR 1300 analog
taperecorder on which these data were recorded in flight. The
digitizer sampled the 12 channels of data at a sampling rate
of 100 samples per second. The data points (1200 per second)
were written onto the digital tape in blocks of 996 data
points, giving .83 seconds of data per block.

Each flight consisted of a "motions at altitude" run and
four data runs. Each run was digitized according to the fol-
lowing format:

- First a short file containing the calibration data for
    the run.

TABLE OF CONTENTS

LIST OF TABLES

LIST OF FIGURES

NOTATION AND SYMBOLS

a	random function of time
a_y	lateral acceleration (right, positive), ft/sec^2
a_z	vertical acceleration (down, positive), ft/sec^2
b	wingspan, ft; also a random function of time
c	wing chord, ft; also a random function of time
C_{uu}	autocorrelation of random process $u(t)$
$\tilde{C}_{uu}$	$= \dfrac{C_{uu}}{\sigma_u^2}$, normalized autocorrelation
C_{uv}	cross correlation of random processes $u(t)$ and $v(t)$
$\tilde{C}_{uv}$	$= \dfrac{C_{uv}}{\sigma_u \sigma_v}$, normalized cross correlation
d	random function of time
f	frequency, hertz
g	standard acceleration, ft/sec^2
K_o	modified Bessel function of second type, order zero
L	scale-length of atmospheric turbulence, ft
n	integer
p	roll rate (right wing down, positive), rad/sec
Δp	differential pressure, psi
P	probability density function
q	pitch rate, (nose-up, positive), rad/sec also dynamic pressure
r	yaw rate, (nose right, positive), rad/sec

R	$\left(= \dfrac{\sigma_c}{\sigma_d}\right)$, ratio of standard deviations
s	Laplace transform variable
S	wing area, ft^2
t	time, sec
T	total time history length, sec. also temperature in the atmosphere, °F
$\bar{U}$	velocity of the mean wind ft/sec
u_o	reference flight speed, ft/sec
(u, v, w)	x, y and z-components of aircraft velocity with respect to still air, ft/sec
(u_m, v_m, w_m)	x, y and z-components of the gust velocities measured at the probeheads, ft/sec
(u_p, v_p, w_p)	x, y and z-components of the velocity of the probehead with respect to an aircraft centered inertial axis system, ft/sec
x , y	distances of the probeheads to the aircraft center of gravity, ft
x, y, z	aerodynamic forces on the aircraft in x, y and z direction.
z	height above sealevel
α	aircraft angle of attack, rad
α_p	probe angle of attack, rad
β	aircraft sideslip angle, rad
β_p	probe sideslip angle, rad
γ	$\left(= -\dfrac{dT}{dz}\right)$, lapse rate, °F/1000 ft

Γ adiabatic lapse rate, °F/1000 ft

η Gaussian white noise

σ standard deviation

ρ atmospheric density

ϕ aircraft roll angle, rad

τ time lag, sec

$\Phi_i(f)$ power spectral density of the variable i, in (units of the variable $i)^2$/hertz

$\Phi_{ij}(f)$ cross spectral density of the variables i and j, in (units of variable i) (units of variable j)/hertz

SUBSCRIPTS

u,v,w denotes u, v, or w gust component

$(\quad)_o$ = value at reference flight condition

- Followed by an end-of-file mark.

- In turn followed by a file containing the data of the run.

- Another end-of-file mark.

After digitizing had been performed the quality of the digitized data was checked by plotting the data on a digital plotter and visually examining the records.

Figure B1 presents a digital record of all 12 channels for the calibration of flight #7, Motions at Altitude. As can be seen the signal of channel 11, the vertical accelerometer, contained noise. It was determined that this noise had a frequency of approximately $32\ Hz$, and was probably the result of engine vibrations in the sensitive direction of the accelerometer.

It was decided to filter out this noise through a z-filter with a cornerfrequency at $25\ Hz$. This filtering was also performed on the Varian digitizer.

B.3 Computation of Gust Time Histories

After completion of the digitizing process the data were in the proper format for use in the computation of the gust time histories. This computation was performed on the CDC 6400 computer of the University of Washington Computer Center.

Inputs to the computation process were 12 channels of data in digitized form, in blocks of .83 seconds on the digital tapes. Outputs from the process were 6 channels of gust time histories, written in blocks of .83 seconds on digital tapes.

Program GUST was written to execute these computations. The main computations of this program were based on the following relations. As shown in section 2.3 of this report the relation between the differential pressure and the angle of attack is given as

$$\alpha = \frac{\Delta p}{PHC \ast q} \tag{B.3.1}$$

where *PHC* is the probehead constant as determined in wind-tunnel testing and q is the dynamic pressure. The angle of attack and the sidewash angle for the two probeheads on Beechcraft D-18S N4545 are then

$$\alpha_p = \frac{\Delta p_z}{5.45 * q} \qquad (B.3.2)$$

$$\beta_p = \frac{\Delta p_y}{4.7 * q} \qquad (B.3.3)$$

It is then possible to calculate the velocity of the air w.r.t. the probehead. These measured velocities are designated as v_m and w_m

$$v_m = \beta_p * (u_p + u_{c.g.}) \qquad (B.3.4)$$

$$w_m = \alpha_p * (u_p + u_{c.g.}) \qquad (B.3.5)$$

where $u_{c.g.}$ is the velocity of the center of gravity of the aircraft w.r.t. a wind-fixed coordinate system. u_p is the velocity of the probehead w.r.t. an aircraft-fixed inertial coordinate system. u_p is obtained from the yaw rate signal in the following manner

$$u_{p_{left}} = r * y$$

$$\qquad (B.3.6)$$

$$u_{p_{right}} = - r * y$$

where r is the yaw rate and y is the distance between the centerline of the probe and the center of gravity of the aircraft.

The velocity of the air w.r.t. the probeheads in the longitudinal direction of the aircraft is measured with a system as described in appendix A.3. The relation between the differential pressure and the measured velocity in x-direction is for this system

$$u_m = \frac{\Delta p_x}{\rho * u_{c.g.}} \tag{B.3.7}$$

where ρ is the density of the atmosphere.

In order to compute the gusts that actually occurred in the atmosphere, the velocity of the air w.r.t. the probeheads due to the motions of the aircraft had to be removed from the measured velocities u_m, v_m and w_m. The motions of the probes were computed in the following manner.

First the velocity components of the center of gravity of the aircraft were computed from the general equations of motion for aircraft. These equations are

$$\frac{X}{m} - g \sin \theta = \dot{u} + qw - rv$$

$$\frac{Y}{m} + g \cos \theta \sin \phi = \dot{v} + ru - pw \tag{B.3.8}$$

$$\frac{Z}{m} + g \cos \theta \cos \phi = \dot{w} + pv - qu$$

where X, Y and Z are the aerodynamic forces on the aircraft,

θ and ϕ are the pitch and roll angles,

p, q and r are the roll, pitch and yaw rates and

u, v and w are the velocities of the $c.g.$ of the aircraft in x, y and z direction.

As the angles are small the above equations can be linearized as follows

$$\dot{u}_{c.g.} = 0$$

$$\dot{v}_{c.g.} = a_y + g \cdot \phi - r \cdot u_{c.g.} + p \cdot w_{c.g.} \qquad \text{(B.3.9)}$$

$$\dot{w}_{c.g.} = (a_z + g) + q \cdot u_{c.g.} - p \cdot v_{c.g.}$$

The velocity components of the center of gravity of the aircraft in y and z direction are then obtained from Eq. B.3.9 by trapezoid integration. The longitudinal velocity of the aircraft is computed in a little different manner. The initial value is taken from the hand-taken data and changes only if both the left and right probe measure an increase or decrease of forward velocity.

The velocity components of the probes are then computed with the following relations

$$v_{P_{left}} = v_{c.g.} + r \cdot x$$

$$v_{P_{right}} = v_{c.g.} + r \cdot x \qquad \text{(B.3.10)}$$

$$w_{P_{left}} = w_{c.g.} - p \cdot y - q \cdot x$$

$$\omega_{p_{right}} = \omega_{c.g.} + p * y - q * z$$

The gusts actually occurring in the atmosphere are then found by subtracting the velocities measured by the probes from the probe motion velocities.

B.4   Data Filtering for Drift Removal

The output of program GUST was checked by plotting the gust time histories vs. time. It was discovered that excessive drift occurred in the gusts, particularly in the lateral and vertical direction, although the longitudinal gusts also showed some drift.

For the longitudinal gusts this drift was traced to a slow change in pressure in the closed-off volume between the pressure transducer and the valve. Appendix A.3 presents a full description of this system. The change in pressure occurred due to equalization of temperature in and outside the tubing. Insulation of the tubing partly solved this problem. Filtering of the data still was deemed necessary.

The drift in the lateral and vertical gust time histories was traced to the integration procedure in program GUST. The velocities of the center of gravity of the aircraft were obtained by integration of rate gyro and accelerometer signals over time. These instruments had been zeroed as accurately as possible, but a slight deviation from the true zero in time integrated to a large value.

It was decided to set up a filtering procedure similar to that used in program LO-LOCAT Phase III and described in [12].

According to this procedure the data are first filtered through a preliminary low pass filter, the Ormsby filter, with characteristics as shown in Fig. B2 .   The following values were selected:

cut off frequency f = .2 cy/sec

92

roll off frequency interval $\Delta f = 1.66$ cy/sec

number of filter weights $N = 50$

The sampling frequency of the data was already determined as
100 samples/sec. The output of the Ormsby filter was an
array of weighted data points with a rate of 2 samples per
second.

This output was then used as input for the secondary low
pass filter, the Martin-Graham filter, which had character-
istics as shown in Fig. B3 .   The following were the values
selected for this filter:

cut off frequency $f_c = .01$ cy/sec

roll off frequency interval $\Delta f = .036$ cy/sec

sampling frequency 2 $samples/sec$

number of filter weights 70

The output of the Martin-Graham filter consisted of the
weighted average of the original data, which was then sub-
tracted from the original data. Fig. B4   , B5   and   B6
present filtered gust time histories of the longitudinal,
lateral and vertical gust components.

Computer program NODRIFT performed these computations. A
printout of this program is given at the end of this section.

B.5 Computation of the Spectral Properties

The filtered gust time histories, output of program
NODRIFT, were used in the computation of the spectral properties
of the atmospheric turbulence. The computer program used to
compute the spectral properties was developed by P.M. Reeves.
Some minor changes were made in this computer program, program
ANALIZ, to account for the difference in the format of the data.
A printou: of the main program of computer program ANALIZ is
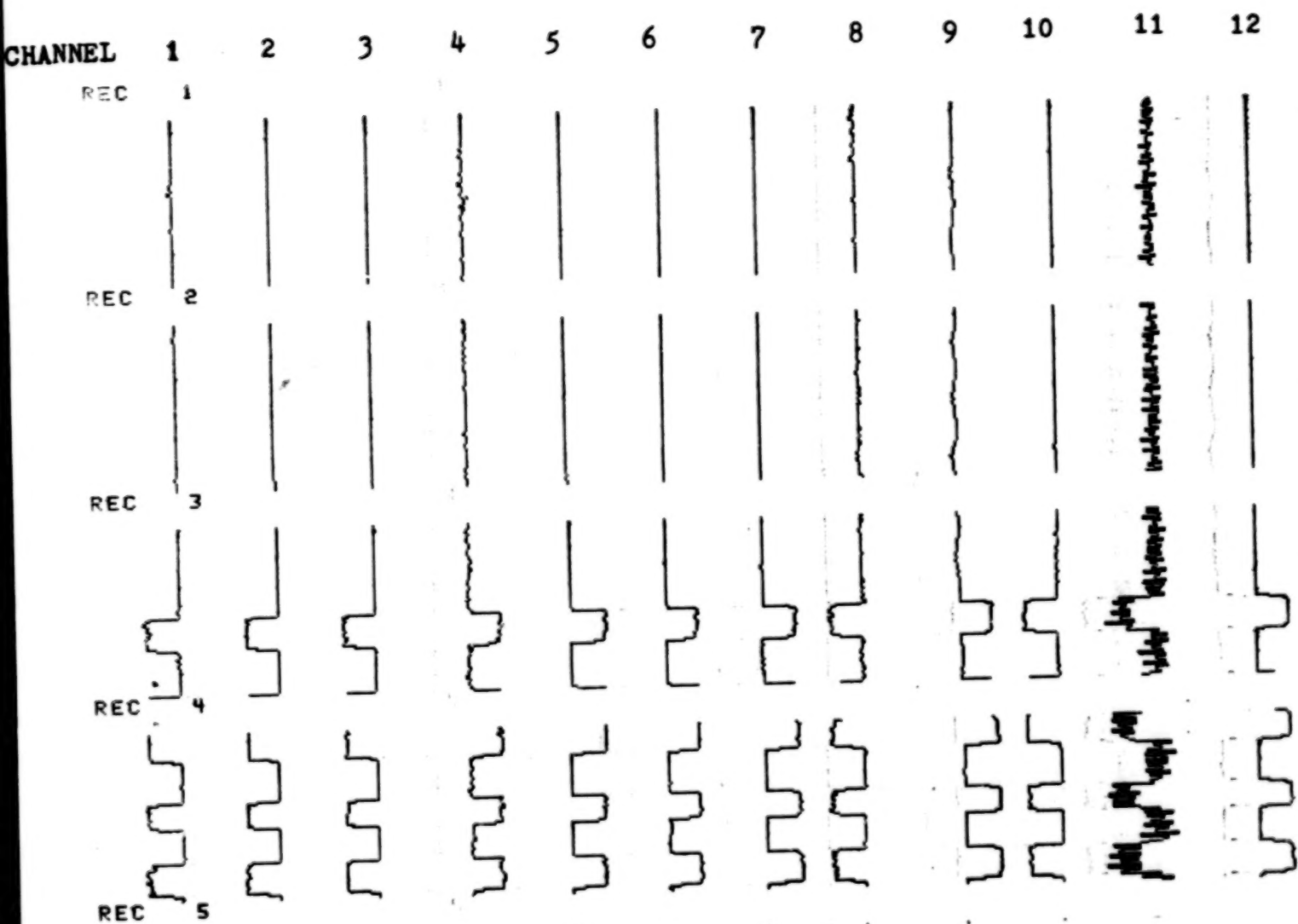given at the end of this section.

93

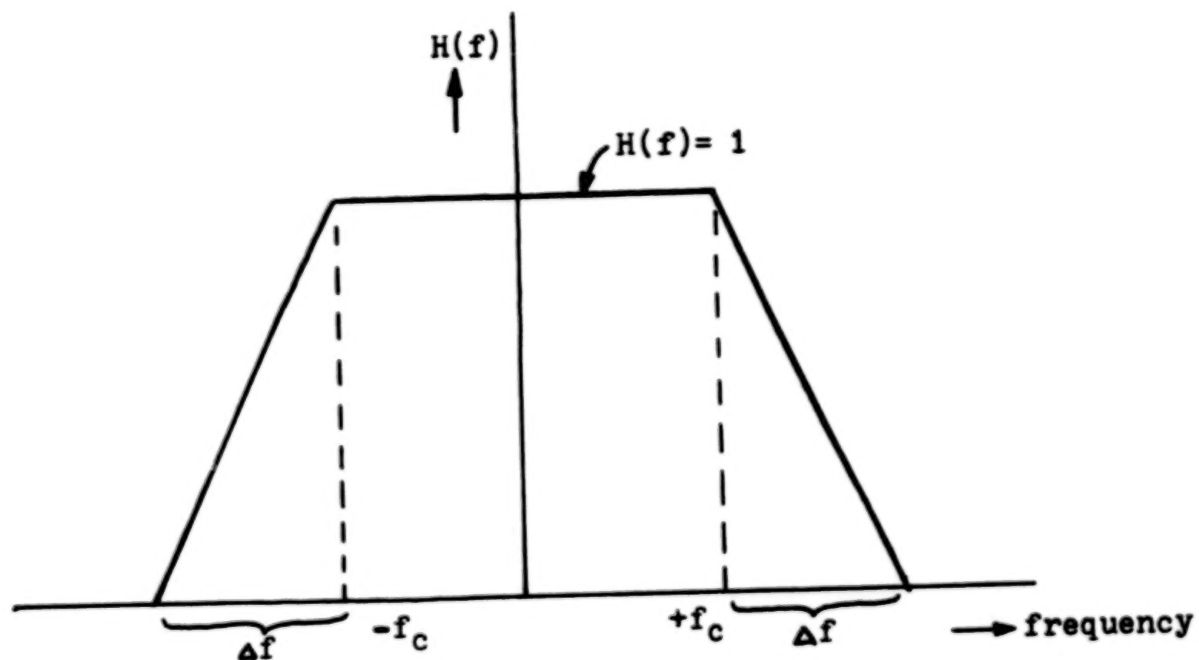FIGURE B1.   DIGITAL RECORDS, FLIGHT # 7, CALIBRATION SIGNALS
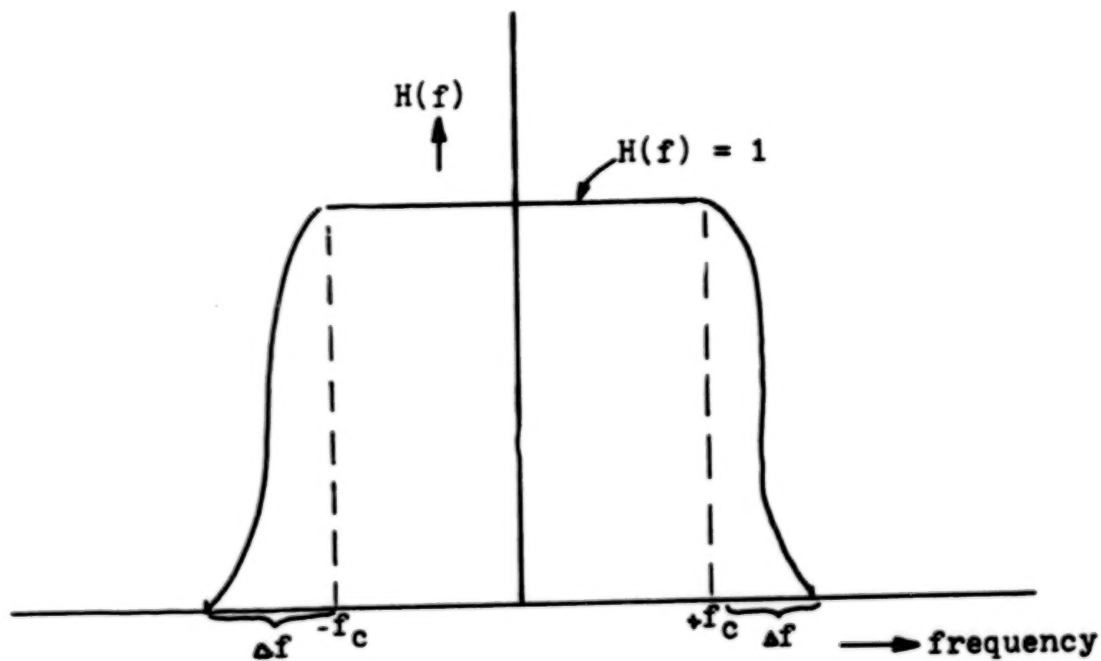
94

FIGURE B2.   ORMSBY FILTER CHARACTERISTICS

95

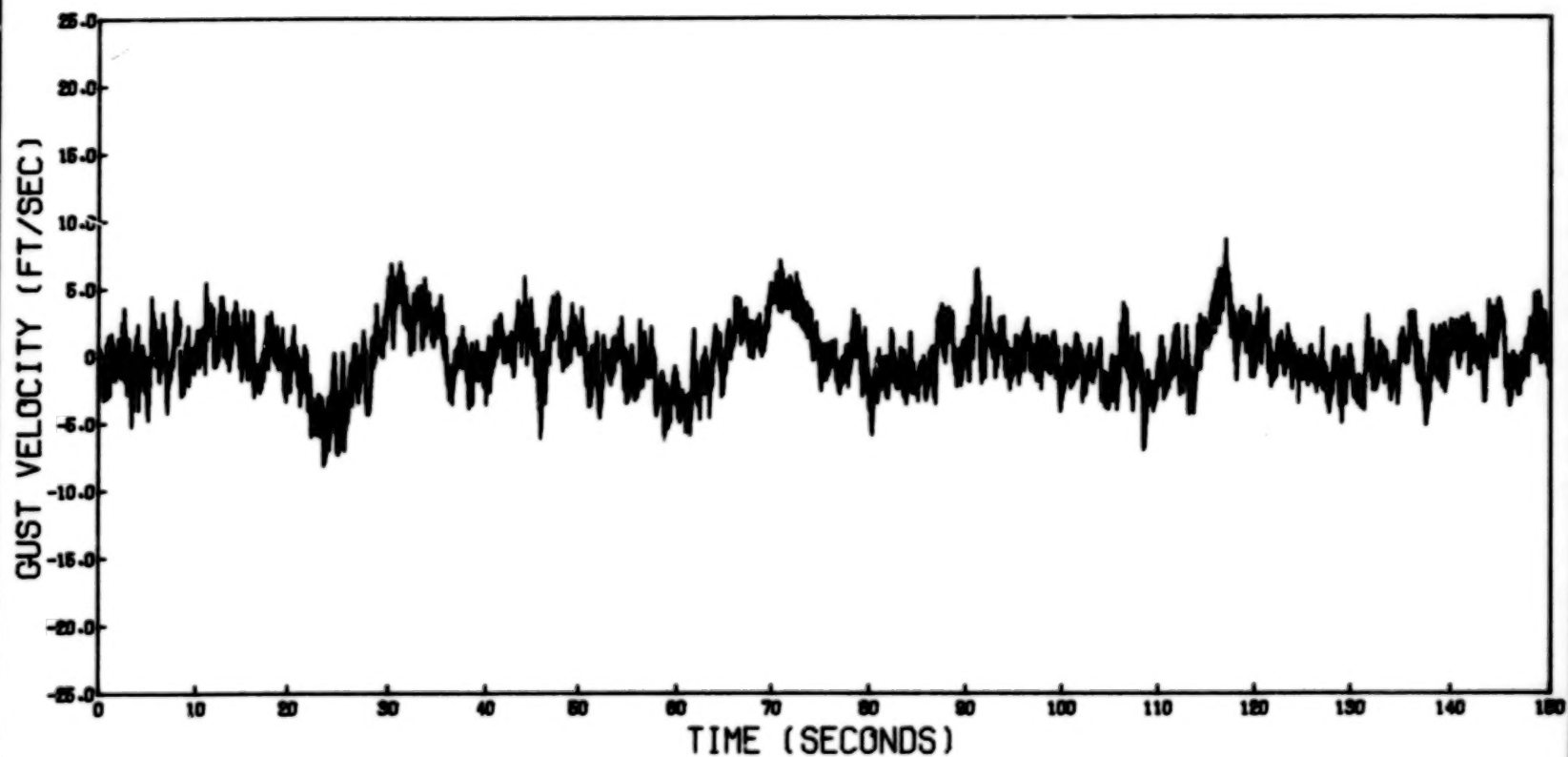FIGURE B3.   MARTIN-GRAHAM FILTER CHARACTERISTICS

96

FIGURE B 4.   GUST TIME HISTORY, CHANNEL NO. 1
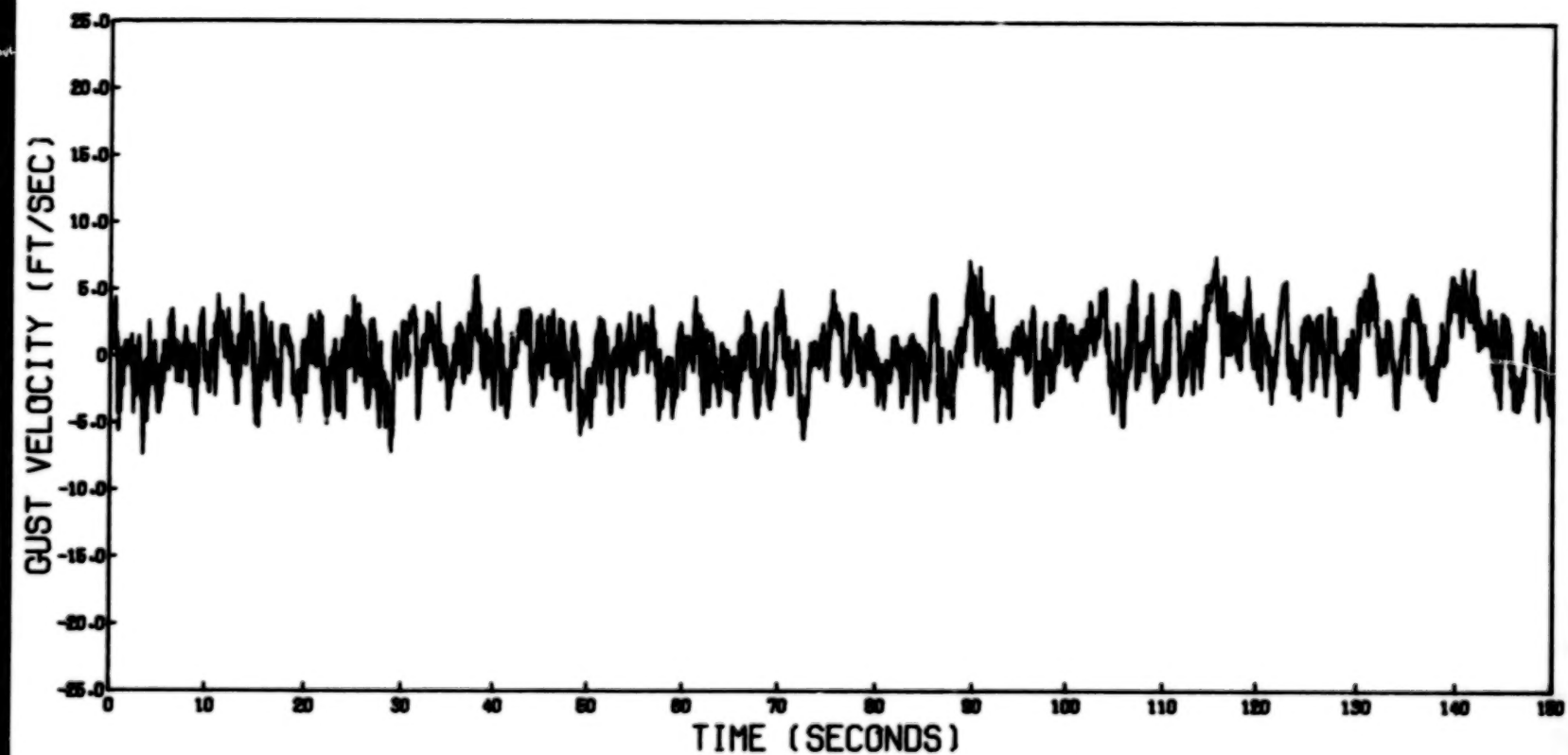FLIGHT 16 , RUN 3 .

97

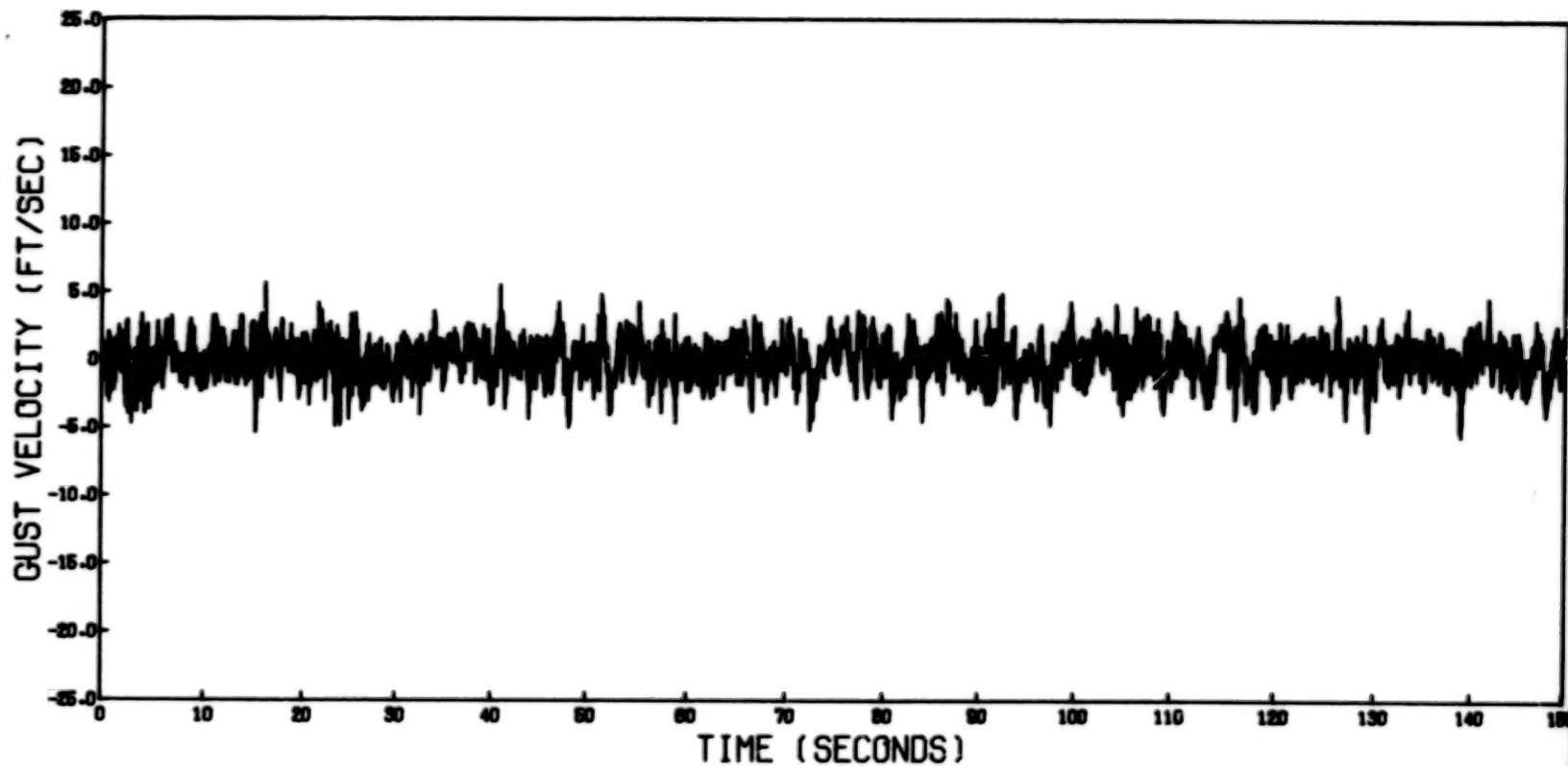FIGURE B 5.   GUST TIME HISTORY, CHANNEL NO. 2
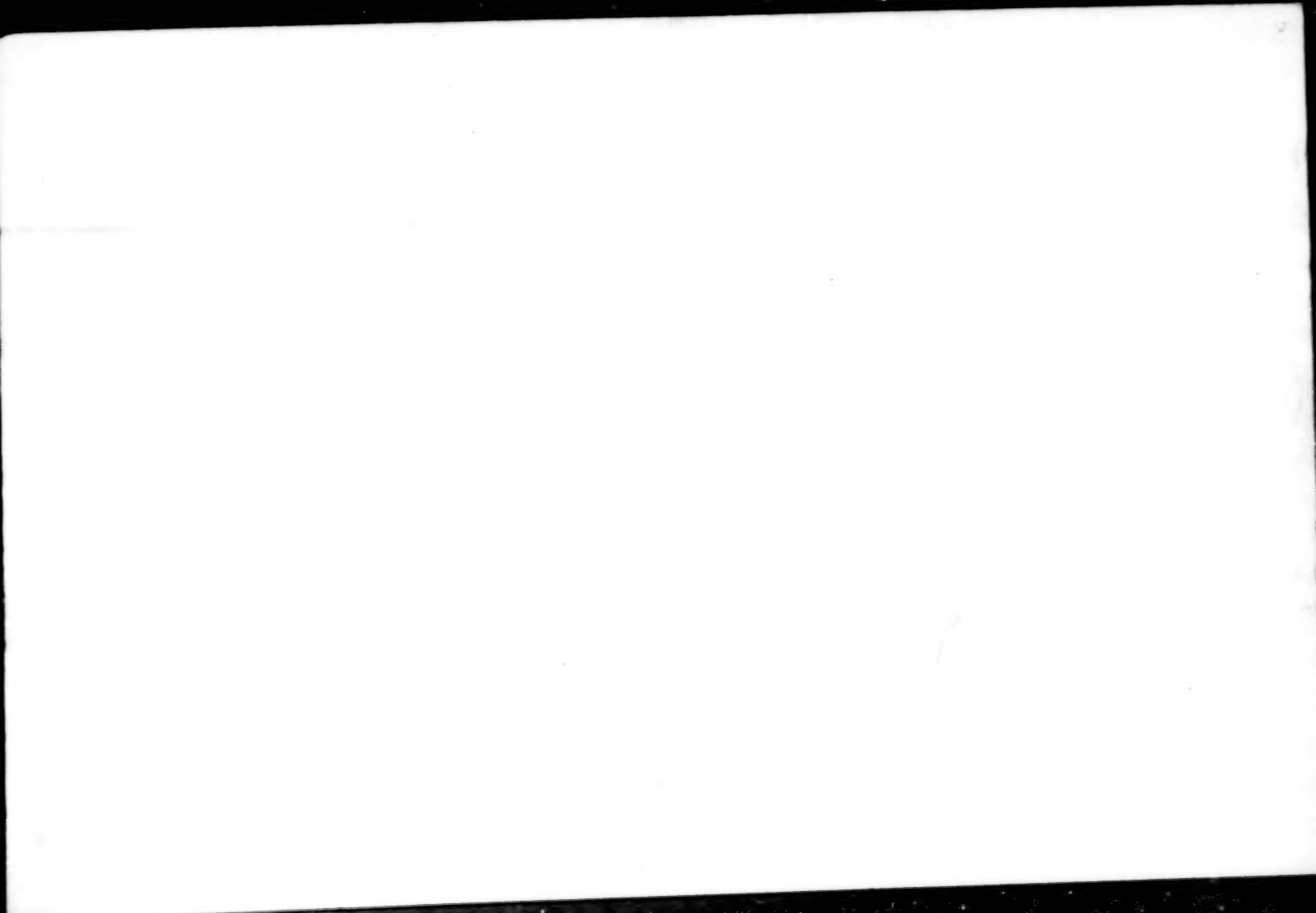FLIGHT 16 , RUN 3 .

FIGURE B6.   GUST TIME HISTORY, CHANNEL NO. 3
FLIGHT 16 , RUN 3 .

99

END
4.19.78